Master of Science Thesis

A Computational Study of Combination Therapies in Growing Tumors: Combination of Chemotherapy and Radiotherapy

National Technical University of Athens

Computational Mechanics

Joint Postgraduate Course

Marina Koutsi
Supervisor: Kavousanakis Mihalis

February 2023, Athens

Acknowledgments

The present master of science thesis drew up in the framework of the Joint Postgraduate Studies Program of Computational Mechanics of the National Technical University of Athens.

I would like to take the opportunity to thank my thesis supervisor, Mihalis Kavousanakis, Assistant Professor of the School of Chemical Engineering at the National Technical University of Athens, for giving me the chance to work on this interesting subject. His advice and guidance through the process of this thesis were essential.

A special thanks also goes to Ioannis Lampropoulos, PhD student of the School of Chemical Engineering at the National Technical University of Athens, for his insightful direction on this thesis which contributed to my better understanding of various aspects concerning computational mechanics.

Finally, I want to thank all the course Professors of this Joint Postgraduate Studies Program of Computational Mechanics who offered me their knowledge and expertise in computational mechanics.

Dedication

To my parents for their unconditional love

Abstract

Cancer is a major public health problem worldwide, and it is a well-known killer of humans. Moreover, cancer is a highly complex disease, so it is urgent to be faced by the scientific community. Mathematical models and computer simulations have contributed to a great extent to the research on how to face cancer disease. The mathematical models make good use of the already existing data and predict the process of this disease under specific conditions. In essence, experiments are carried out through computer simulations (in silico) without compromising the safety of each patient.

The present master of science thesis deals with the computational study of combination therapies in growing tumors, especially the combination of chemotherapy and radiotherapy. In order to carry out this computational study, a two-dimensional, continuous mathematical model was developed and solved in the environment of COMSOL Multiphysics ®.

In the model mentioned above, radiotherapy and chemotherapy were applied to observe how these treatments affect the number of cancer cells and the number of blood vessels connected to these cancer cells. These treatments are applied, either separately or in combination, to the mathematical model. Therefore, combined chemoradiotherapy has resulted in the best results being observed both in terms of the cancer cells and the blood vessels connected to them. Blood vessels are linked to the possibility of cancer cells metastasizing. The chance of tumor metastasis is lower for a small number of blood vessels than for an increased number of vessels.

Given that combined chemoradiotherapy treats cancer more effectively, some additional simulations were performed. Combined chemoradiotherapy is applied in these simulations where the start time of both chemotherapy and radiotherapy varies in each therapeutic case. This resulted in the therapeutic efficacy varying depending on the therapeutic case but without substantial differences in the percentages of therapeutic efficacy. Regarding the number of blood vessels in cases where radiotherapy precedes chemotherapy, the number of blood vessels increases at a lower rate compared to cases where chemotherapy precedes radiotherapy. This implies that in the first case, the metastatic potential of the tumor is less compared to the second case of the therapeutic cases. Therefore, the chance of metastasis is also lower when cancer cells have access to fewer blood vessels.

In conclusion, the most important outcome that emerged through this study is computational models with radiotherapy and chemotherapy applied separately or a combination of these two treatments. Each model can be applied to a different type of radiotherapy, both in terms of the radiation's strength and how it is administered to the cancer cells in the tissue. Also, each computational model can be applied to a different cytotoxic drug in terms of its type and administration.

It is also established that these models conclude with logical results by applying the respective treatment. For instance, when chemoradiotherapy applied concurrently according to the clinical protocol [1] gives the biggest efficacy compared with the other therapeutic cases. It is worth noting that further study and improvements are required to obtain even more accurate simulations that will respond even more to the growth of a cancerous tumor within a tissue.

Περίληψη

Ο καρκίνος αποτελεί ένα από τα σημαντικότερα προβλήματα της δημόσιας υγείας. Τα υψηλά ποσοστά θνησιμότητας και η πολυπλοκότητα της ασθένειας αυτής καθιστά την αντιμετώπισή της από την επιστημονική κοινότητα ως απόλυτη προτεραιότητα. Στην έρευνα για τους τρόπους αντιμετώπισης του καρκίνου συμβάλλουν σε μεγάλο βαθμό τα μαθηματικά μοντέλα και οι υπολογιστικές προσομοιώσεις όπου αξιοποιούν τα ήδη υπάρχοντα δεδομένα και προβλέπουν την πορεία της ασθένειας αυτής κάτω από συγκεκριμένες συνθήκες. Στην ουσία πραγματοποιούνται πειράματα μέσω προσομοίωσης στον υπολογιστή (in silico) χωρίς να θέτουν σε κίνδυνο τον ασθενή.

Η παρούσα μεταπτυχιακή διπλωματική εργασία πραγματεύεται την υπολογιστική διερεύνηση συνδυαστικών θεραπειών και πιο συγκεκριμένα τη μελέτη συνδυαστικής δράσης Χημειοθεραπείας και Ακτινοθεραπείας, σε αναπτυσσόμενους καρκινικούς όγκους. Για να πραγματοποιηθεί η ανάλυση αυτή, χρησιμοποιήθηκε διδιάστατο, συνεχές μαθηματικό μοντέλο, το οποίο επιλύθηκε στο περιβάλλον του COMSOL Multiphysics ®.

Στο προαναφερόμενο μοντέλο, εφαρμόστηκε τόσο ακτινοθεραπεία όσο και χημειοθεραπεία για να παρατηρηθεί πώς οι θεραπείες αυτές επιδρούν στον αριθμό των καρκινικών κυττάρων και στον αριθμό των αιμοφόρων αγγείων που συνδέονται με τα καρκινικά κύτταρα. Οι θεραπείες αυτές εφαρμόζονται είτε ξεχωριστά είτε σε συνδυασμό. Από τους υπολογισμούς, προέκυψε ότι με συνδυαστική χημειοακτινοθεραπεία προκύπτουν τα καλύτερα αποτελέσματα τόσο ως προς τα καρκινικά κύτταρα όσο και ως προς τα αιμοφόρα αγγεία που συνδέονται μ΄ αυτά. Τα αιμοφόρα αγγεία συνδέονται με την πιθανότητα ο καρκίνος να κάνει μετάσταση. Για μικρό αριθμό αιμοφόρων αγγείων η πιθανότητα για μετάσταση είναι μικρότερη σε σύγκριση με τον αυξημένο αριθμό τους.

Με δεδομένο λοιπόν ότι η συνδυαστική χημειοακτινοθεραπεία αντιμετωπίζει αποτελεσματικότερα τον καρκίνο έγιναν κάποιες επιπλέον προσομοιώσεις. Στις προσομοιώσεις αυτές εφαρμόζεται συνδυασμένη χημειοακτινοθεραπεία όπου ο χρόνος έναρξης τόσο της χημειοθεραπείας όσο και της ακτινοθεραπείας διαφοροποιούνται σε κάθε θεραπευτικό σχήμα. Αυτό είχε σαν αποτέλεσμα να παρατηρηθούν διαφορές μεταξύ των διαφορετικών σχημάτων, όχι όμως τόσο μεγάλες στο ποσοστό της θεραπευτικής αποτελεσματικότητας. Ως προς τον αριθμό των αιμοφόρων αγγείων στις περιπτώσεις όπου η ακτινοθεραπεία προηγείται της χημειοθεραπείας ο αριθμός των αιμοφόρων αγγείων αυξάνεται με μικρότερο ρυθμό σε σχέση με τις περιπτώσεις όπου η χημειοθεραπεία προηγείται της ακτινοθεραπείας. Αυτό συνεπάγεται ότι στην πρώτη περίπτωση το μεταστατικό δυναμικό του καρκινικού όγκου είναι μικρότερο σε σύγκριση με τη δεύτερη περίπτωση των θεραπευτικών περιπτώσεων. Συνεπώς, και η πιθανότητα

να γίνει μετάσταση είναι μικρότερη όταν τα καρκινικά κύτταρα έχουν πρόσβαση σε λιγότερα αιμοφόρα αγγεία.

Εν κατακλείδι, το σημαντικότερο αποτέλεσμα που προέκυψε μέσω της μελέτης αυτής είναι υπολογιστικά μοντέλα που εφαρμόζουν τόσο την ακτινοθεραπεία όσο τη χημειοθεραπεία και το συνδυασμό αυτών των δύο θεραπειών. Κάθε μοντέλο μπορεί να εφαρμοστεί για διαφορετικό είδος ακτινοθεραπείας, τόσο ως προς την ισχύ της ακτινοβολίας, όσο και ως προς τον τρόπο χορήγησης αυτής στα καρκινικά κύτταρα του ιστού. Επίσης κάθε υπολογιστικό μοντέλο μπορεί να εφαρμοστεί για διαφορετικό κυτταροτοξικό φάρμακο και ως προς το είδος του αλλά και ως προς τον τρόπο χορήγησής του. Επιπλέον διαπιστώνεται ότι τα μοντέλα αυτά ανταποκρίνονται στις εκάστοτε προσδοκίες κρίνοντας από τα αποτελέσματα όπου προκύπτουν μέσω της εφαρμογής της εκάστοτε θεραπείας. Για παράδειγμα εφαρμόζοντας το ιατρικό πρωτόκολλο [1] προκύπτει ότι η συνδυασμένη χημειοακτινοθεραπεία έχει την υψηλότερη θεραπευτική αποτελεσματικότερη σε σχέση με τα υπόλοιπα θεραπευτικά σχήματα που εφαρμόστηκαν. Αξίζει να σημειωθεί ότι απαιτείται περαιτέρω μελέτη και βελτιώσεις, ώστε να προκύπτουν ακόμη πιο ακριβείς προσομοιώσεις οι οποίες θα ανταποκρίνονται ακόμη περισσότερο στην ανάπτυξη ενός καρκινικού όγκου μέσα σ΄ ένα ιστό.

Contents

1 Introduction **9**
- 1.1 The Cell Cycle and the Origins of Cancer . . . 9
- 1.2 Development Stages of a Tumor . . . 11
- 1.3 Basic Phenomena Involved in Tumor Evolution: tissue, cellular and sub-cellular level 13

2 Mathematical Models for Tumor Development **15**
- 2.1 The Types of Mathematical Tumor Models . . . 15
  - 2.1.1 Comparison Between Continuum and Discrete Models . . . 18
- 2.2 Model Development: Mathematical Formulation for Continuum Tumor Model . . . 18
- 2.3 The Mass Balance Equations . . . 19
  - 2.3.1 Source Terms for Healthy and Cancer Cell Phases (θ_1, θ_2) . . . 19
  - 2.3.2 The Blood Vessel Phase (θ_3) . . . 20
  - 2.3.3 The Extracellular Material Phase (θ_4) . . . 21
  - 2.3.4 Initial and Boundary Conditions . . . 22
- 2.4 The Momentum Balance Equations . . . 22
  - 2.4.1 Momentum Balance Equations for the Four Phases $(\theta_1, \theta_2, \theta_3, \theta_4)$ . . . 22
  - 2.4.2 Boundary Conditions . . . 23
- 2.5 Nutrient (Oxygen) . . . 24
  - 2.5.1 Mass Balance Equation for Nutrient (c) . . . 24
  - 2.5.2 Boundary Conditions . . . 24
- 2.6 Nondimensionalisation . . . 25
  - 2.6.1 Mass Balance Equations . . . 25
  - 2.6.2 Momentum Balance Equations . . . 26
  - 2.6.3 Reaction-Diffusion Equation for Nutrient . . . 27
- 2.7 Inserting the Mathematical Model into Comsol Multiphysics . . . 27

3 Cancer Treatments **31**
- 3.1 Radiotherapy . . . 31
  - 3.1.1 Radiation Therapy Effect on Cell Cycle . . . 31
  - 3.1.2 Types of Radiation Used to Treat Cancer . . . 33
  - 3.1.3 The Main Types of Radiation Therapy . . . 33
  - 3.1.4 Dosing and Treatment with External Beam Radiation . . . 34
- 3.2 Chemotherapy . . . 36
  - 3.2.1 Cytotoxic Drugs: Taxanes . . . 37
- 3.3 Combined Therapies . . . 38
  - 3.3.1 Chemoradiotherapy Treatment . . . 38

4 Radiotherapy Simulations **41**
4.1 Problem Statement . . . 41
4.2 The Linear-Quadratic Formula of Radiotherapy . . . 41
4.3 Parameters Fitting . . . 42
4.4 Inserting the Mathematical Model into Comsol Multiphysics . . . 44
4.5 Numerical Results . . . 47

5 Combined Chemoradiotherapy Simulations **50**
5.1 The Established Cancer Protocol . . . 50
5.2 Importing the Modeling of Cytotoxic Therapy in our Mathematical Model . . . 51
5.3 Nondimensionalisation . . . 53
5.4 Implementation of Cytotoxic Therapy Model into Comsol Multiphysics . . . 54
5.5 Numerical Results . . . 62

6 Different Schedules of Concurrent Chemoradiotherapy Simulations **70**
6.1 Examined Cases . . . 70
6.2 Numerical Results . . . 71

7 Conclusions and Discussion **80**
7.1 Conclusions . . . 80
7.2 Recommendations for Future Research . . . 82

Bibliography **84**

Chapter 1

Introduction

Cancer is a well-known killer of humans worldwide, a highly complex disease with myriad manifestations [2]. The reasons for this lie not only in the many types of different cells that exist in our bodies but also in the fact that populations of tumor cells often are highly heterogeneous and, overall, tumor growth depends on many aspects such as interactions with its microenvironment, especially immune response and tumor vasculature. At the same time, many commonalities exist across various types of cancer that allow for fundamental principles to apply [3].

1.1 The Cell Cycle and the Origins of Cancer

The building blocks of all life are cells, and cells constantly reproduce in the cell cycle through cell division, the primary mechanism of our body that governs growth and development. In the transition from cell birth to cell division, each cell passes through a complex and tightly regulated sequence of molecular events that are encoded in our DNA (deoxyribonucleic acid) and executed by proteins [3].

In the first growth phase **G1** (see Figure 1.1), mainly the synthesis of enzymes that are needed for DNA replication is carried out, and the cell grows in size. Various checkpoints (control mechanisms) are embedded in the cell cycle to verify that these processes have been adequately completed before the next phase of the cell cycle starts. One such checkpoint is located at the end of the G1 phase, where it is checked whether DNA was damaged in the process and whether environmental conditions (e.g., supply of oxygen and nutrients) are adequate for cell duplication. This phase lasts about 18 to 30 hours [4]. At this point, decisions are made on whether the cell should proceed with the cell cycle to division or delay division and enter a resting stage **G0**. The latter is a phase in the cell cycle where the cell neither divides nor prepares for division and is also called the quiescent state. Otherwise, if conditions are right, the cell enters phase **S** where DNA synthesis occurs. When it is complete, all of the chromosomes have been duplicated, and each chromosome has two copies, essentially doubling the amount of DNA in the cell. [3, 5]. This phase lasts about 18 to 20 hours [4].

After that, a second growth phase **G2** commences, in which the cell synthesizes other cellular components, such as microtubules that are needed for mitosis. At the end of the G2 phase, there is a second major checkpoint to ensure the cell is ready for mitosis. It lasts from 2 to 10 hours [4].

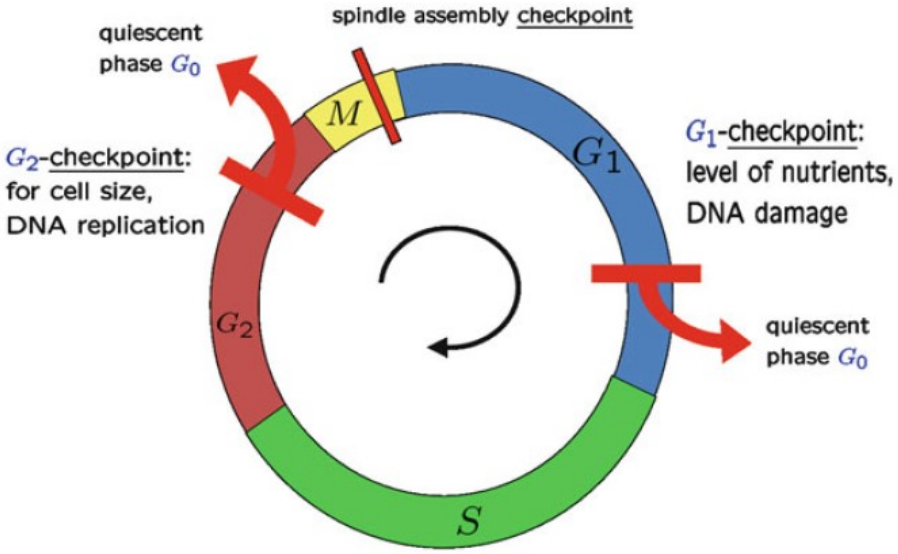

Figure 1.1: *Schematic representation of the cell cycle and its main checkpoints* [3].

If this checkpoint is passed, the cell enters phase **M**. Here cell growth stops, and mitosis occurs. This is the orderly division of the mother cell into two daughter cells containing roughly equal shares of the cellular components. It is a highly complex process consisting of various sub-phases. During an intermediate checkpoint in mitosis, the meta-phase checkpoint, it is verified that all the chromosomes are properly aligned on the mitotic spindle. If all checkpoints are passed, cell duplication starts. Ideally, the two daughter cells are genetically identical, and their parent cell [3]. This phase lasts only 30 to 60 minutes [4].

The general term "cancer" refers to an enormously large family of high-mortality diseases, widely differing from each other in their aspects and manifestations but all having in common a derangement of cellular proliferation that originated at some time in the past with mistakes in the process of cell duplication. Cell duplication is a tightly regulated molecular mechanism in which various types of proteins (the so-called cyclins) control the transitions through the phases of the cell cycle. Naturally, there exist many possibilities for things to go wrong in such a complex and lengthy chain of events, which happens regularly. But given the overall complexity of the process, life has developed many safeguard and rescue procedures specifically designed to deal with mistakes during cell duplication. In theory, only if conditions are suitable cells are allowed to pass from one phase into the next [3].

All in all, the regulation of the cell cycle includes numerous control mechanisms that detect and possibly repair genetic damage and are crucial for the survival of a cell. Many of these mechanisms are connected with the actions of a specific protein, p53, that, because of its importance as a suppressor gene in the cell cycle, has been labeled "the guardian of the genome." It is involved in various fundamental functions within the regulatory mechanisms of the cell cycle [3]. It activates DNA repair proteins when DNA has sustained damage; it induces cell arrest at the G1 checkpoint holding the cell so that DNA repair proteins are given time to fix the damage, and, if the DNA damage is too severe to be repaired, p53 can induce the cell to kill itself by undergoing a form of programmed cell death called apoptosis. If p53 is missing or defective, the unrestrained replication of damaged DNA leads to a high rate of mutation and the production of cells that tend to become

cancerous. In fact, mutations in the p53 gene are found in about half of all human cancers. Most human cancer cells harbor mutations in the p53 gene, allowing them to survive and divide even when their DNA is damaged [6].

Consequently, in many forms of cancer, the disease can be traced to a series of mutations that occurred in cell duplication and had the effect of inhibiting and disabling these regulatory pathways. While dysfunctional cells, produced in cell division, will be eliminated from our body under normal circumstances, in the case of a cancerous cell, these mechanisms become disabled, and, weirdly, the cell becomes "immortal." Typically a so-called cancer stem cell is not caused just by a single mutation but, by being genetically unstable, in a sequence of progressive genetic changes, which then enable these cells to undergo uncontrolled, abnormal mitosis and increase the total number of cancer cells at that location [3].

Yet, even if the cell cycle control mechanisms prove ineffective, this does not necessarily mean that the medical disease called cancer has to develop. Additional mechanisms exist outside the cell cycle and enable the body to deal with renegade cells [3]. One of these is the activation of the immune system. It has been hypothesized for a long time and backed up by medical evidence that the immune system can control cancerous cells in the early stages of the disease by immunosurveillance. But, as cancer cells are part of our body, there are also situations when the immune system does not react or when its reaction is inadequate to overcome the initial cancerous growth [7, 3]. Still, if for whatever reason cancer cells do not duplicate or grow so slowly that they never become a problem, the disease that generally is called cancer does not materialize [3].

To summarize, mistakes in cell duplication are common, but no harm is done if any of the body's inherent control mechanisms succeed in eliminating the initial dysfunctional cell. It is only if such a cancerous cell persists, starts to duplicate, eventually escapes regulatory mechanisms, and growth gets out of control that the disease called cancer occurs, i.e., the "uncontrolled growth of abnormal cells in the body [3]. In medical terms, cancer development stages are identified as sustaining proliferative signaling, evading growth suppressors, resisting cell death, enabling replicative immortality, inducing angiogenesis, activating invasion, and metastasis [8].

1.2 Development Stages of a Tumor

There exist hundreds of types of cancers which, in principle, all exhibit different characteristics and are very different diseases. Still, there are also common characteristics in their development. The word tumor (which is the Latin word for "being swollen" derived from tumere, "to swell") is commonly used for any abnormal growth of cells. Below are described the main phases of the development of a tumor. These are **avascular growth, tumor angiogenesis, and metastasis** [3].

Avascular growth is the first stage of tumor growth. As it develops, a tumor needs a steady supply of oxygen and nutrients for cell duplication. Initially, this supply is adequately provided by the surrounding environment through diffusion. At the onset of the disease, since tumor cells are dysfunctional and do not partake in any regular tasks, cells cluster together and form a coherent parasitical unit, often growing in a small spherical shape. Over time, cells toward the center become deprived of the necessary nutrients to divide further and develop a necrotic core of dead

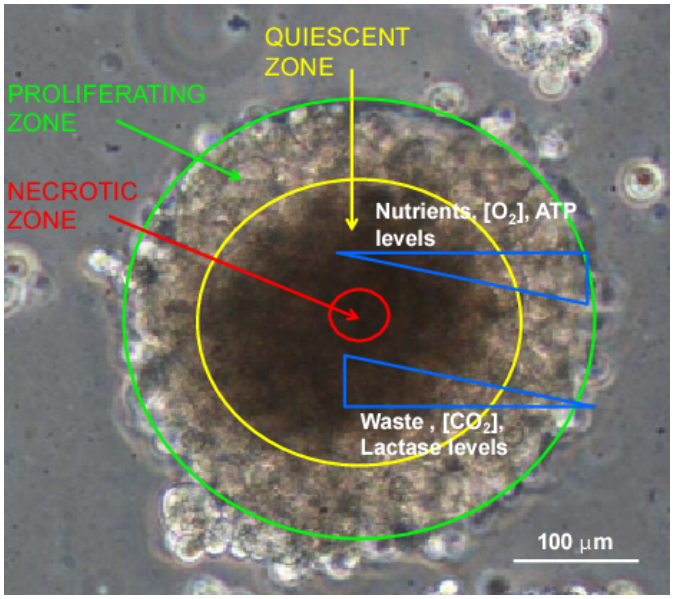

Figure 1.2: *Schematic of the necrotic, quiescent, and proliferative zones within a tumor spheroid* [11].

cells [9]. Proliferating cells generally are only found in the outermost cell layers (see Figure 1.2) with a band of quiescent cells lying between these two regions [3, 10].

Faced with a shortage of nutrients, tumor cells that enter the quiescent zone of the cell cycle trigger the release of vascular endothelial growth factor (VEGF) and other stimulating agents that promote the creation of a network of blood vessels and capillaries designed to provide the tumor with necessary nutrients, the tumor vasculature. It is generally recognized that primary tumors require such a network to grow beyond 2 mm^3 in volume. The creation of this vascular network is called **tumor angiogenesis**. Overall, this is a complex process characterized by both proangiogenic agents such as VEGF and antiangiogenic chemicals released by the tumor to modulate the growth of the vessel network. A tumor thus deploys a sophisticated strategy based on reciprocal signaling between endothelial cells (which form the lining of the newly formed vessels and capillaries) and tumor cells to control its growth through a balance of stimulatory and inhibitory mechanisms regulated through microenvironmental factors [12, 13]. Once the tumor succeeds in developing its vasculature, it has gained access to the needed supply of oxygen and nutrients via the bloodstream and undergoes vigorous growth.

In time, the size becomes large and incoherent enough that small parts of the tumor break off and travel through the bloodstream to other organs and parts of the body [3], in which case the tumor is said to be malignant. Malignant tumor cells with this invasive property often break loose from the primary tumor and enter the bloodstream or lymphatic vessels, where they form secondary tumors, or metastases, at other sites in the body (see Figure 1.3). The more widely cancer spreads, the harder it is to eradicate [6]. This last stage of tumor development is called **metastasis**.

Lastly, in the medical literature, the original tumor is called the primary tumor, while the newly formed secondary tumor is called a secondary or metastatic tumor. Since the type of cancer is defined by the type of cell it originated with, the type of cancer on the secondary site is the

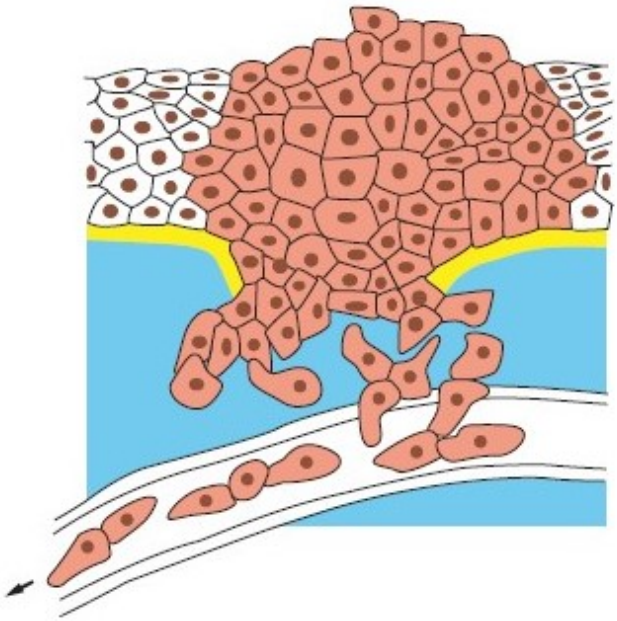

Figure 1.3: *Cancers invade surrounding tissues and often metastasize to distant sites* [6].

same as in the original one. Metastasis, along with increased cell duplications and invasiveness, is one of the main characteristics of a malignant tumor. In contrast, a tumor that does not grow uncontrollably, does not invade neighboring tissues, and does not spread throughout the body is called benign, and it can usually be removed cleanly and completely by surgery [3, 6].

1.3 Basic Phenomena Involved in Tumor Evolution: tissue, cellular and sub-cellular level

It should be noted that a tumor that successfully thrives in an organism is a bunch of surviving abnormal/mutated cells with the ability to outrival the inherent tumor-inhibiting mechanisms (e.g., tumor suppressor genes, immune response) in the body of that organism to a certain extent. Even though the exact mechanism that triggers the onset of cancer is still unknown, radiation, gene mutation, lifestyle, chemicals, etc., are identified as possible contributing factors [14].

Tumor evolution is a complex process involving many phenomena occurring at different scales. The phenomena occurring during the evolution of tumors using three natural viewpoints are the sub-cellular level, the cellular level, and the tissue level. From the modeling point of view, a connection can be approximately drawn between the description levels above and the microscopic, mesoscopic, and macroscopic scales (see Figure 1.4) [15].

The microscopic scale refers to those phenomena that occur at the sub-cellular level and, therefore, to activities that take place within the cell or at the cell membrane, e.g., DNA synthesis and degradation, gene expression, alteration mechanisms of the cell cycle, absorption of vital nutrients,

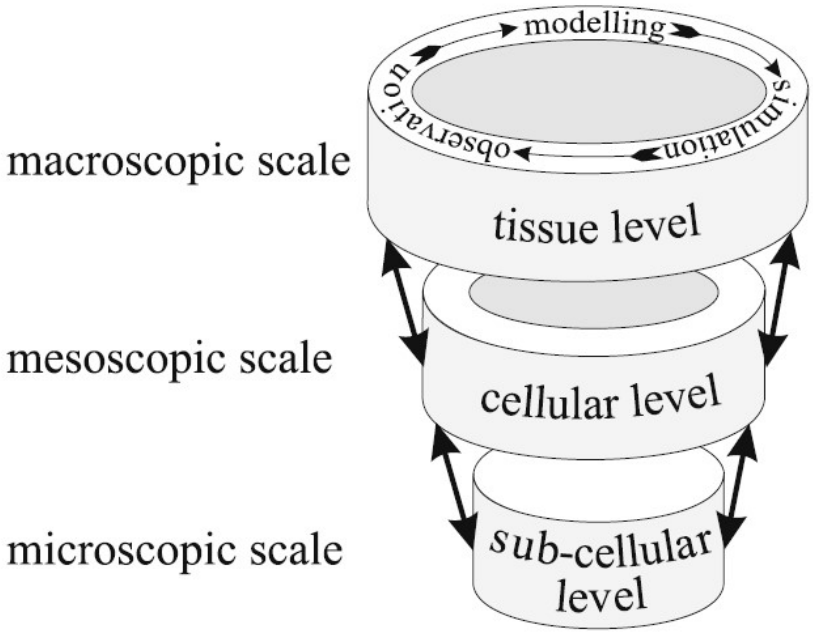

Figure 1.4: *Schematic representation of the scales that phenomena of cancer occurs* [15].

activation or inactivation of receptors, transduction of chemical signals between cells that regulate cellular activities, such as duplication, motion, adhesion, or detachment [15].

The mesoscopic scale refers to the cellular level and, therefore, to the main activities of the cell populations, e.g., statistical description of the progression and activation state, interactions among tumor cells and the other types of cells present in the body such as endothelial cells, macrophages, lymphocytes, proliferative and destructive interactions, aggregation and disaggregation properties, and intravasation and extravasation processes [15].

The macroscopic scale refers to the tissue level and, therefore, to those phenomena typical of continuum systems, e.g., cell migration, convection and diffusion of nutrients and chemical factors, mechanical responses, interactions with external tissues, diffusion of metastases, and phase transitions. Of course, what happens at a particular scale is strongly linked to what happens at other scales. Therefore it is impossible to completely describe a phenomenon without taking into account others occurring at a smaller or a larger scale. This means that mathematical models and methods characteristic of different scales could be combined to achieve a better description of the phenomena [15].

Chapter 2

Mathematical Models for Tumor Development

Accurate and reliable model representations of cancer dynamics are milestones in cancer research. Mathematical modeling approaches are abundantly used in cancer research as these quantitative approaches can contribute to validating various hypotheses related to cancer dynamics and thus to elucidate complexly involved interlaced mechanisms [14].

2.1 The Types of Mathematical Tumor Models

Through the years, numerous mathematical models have been developed to study the progression of cancer [16]. Cancer dynamics involves many complex mechanisms, and several interrelated biological factors influence it. Analysis of such complex and interlaced phenomenon with multiple interlaced parameter influences can be significantly simplified using appropriate mathematical models. For instance, mathematical models enable one to predict the system's behavior in a future time scale and to analyze the effect of each variable or parameter on the overall cancer dynamics. These parameters can be related to the patient's physiology, disease type, and treatment modality. Such predictions and analyses are often difficult to make, maybe risky, or costly to implement using an in vivo/vitro experimental setup or a clinical trial. So, they can be implemented numerically to give rise to in silico models of these phenomena [14].

Most mathematical models fall into two broad categories based on how the tumor tissue is represented: **continuum models** and **discrete cell-based models**. Although the continuum and discrete approaches have each provided significant insight into cancer-related processes occurring at particular length and time scales, the complexity of cancer and the interactions between the cell- and tissue-level scales may be elucidated further through a multiscale (**hybrid models**) approach that uses both continuum and discrete representations of tumor cells and components of the tumor microenvironment. Biological phenomena from the molecular and cellular scales are coupled to the tumor scale. Such an approach can, for example, capture transitions from collective to individual behavior and combine the best features of continuum and discrete models [16].

Continuum models provide an excellent modeling strategy in larger-scale systems such as the macroscopic scale of tumor growth. The approach draws upon principles from continuum mechanics to describe variables as continuous fields related by means of partial differential equations, and it allows for the development of fast numerical solvers. These models treat a tumor as a tissue collection for which densities or volume fractions of cells are described. The model parameters may represent volume fractions of various cell species and concentrations of cell substrates such as glucose, oxygen, and growth factors. On the one hand, the parameters at this macro-scale are somewhat easier to obtain, analyze, and control compared with those required for discrete models, which typically involve cellular and subcellular measurements. On the other hand, although continuum models are appropriate at the tissue scale, where gross tumor behavior can be quantified, they cannot represent individual cells and discrete events (e.g., epithelial-to-mesenchymal phenotypic transitions that lead to individual cell migration). Continuum models are essential when studying the effect of genetic, cellular, and microenvironment characteristics on overall tumor behavior [16].

A basic continuum model is the **Avascular Tumor Growth**, which represents tumor cells proliferating in such a way that they form a small sphere-like structure without direct access to the vasculature. During this avascular growth, the tumor cells receive oxygen, nutrients, and growth factors via diffusion from the surrounding host tissue [16]. To transition from the avascular to the vascular phase of growth, a tumor must induce new blood vessels to sprout from the existing vascular network and grow towards the tumor, eventually penetrating it. These continuum models are called **Vascularized Tumor Growth**. The process starts when a small avascular tumor exceeds a critical size greater than can be sustained by the normal tissue vasculature. Accordingly, tumor cells become hypoxic and secrete diffusible chemical signals, collectively called angiogenic factors, such as the vascular endothelial cell growth factor (VEGF). These molecules diffuse into the host microenvironment and bind to specific cell membrane receptors on the (vascular) endothelial cells that line existing blood vessels. This process activates the endothelial cells, which respond by degrading the basement membrane surrounding the existing vessel to form new vessel sprouts. The endothelial cells then proliferate as they form new vessels in the direction of the tumor [17].

Numerous mathematical continuum models have been developed; Ward and King [18], and Breward et al. [19] modeled avascular cancer growth through a two-phase description comprising tumor and dead tissue (extracellular space) and incorporated a model of cell-cell adhesion. Breward et al. [20] extended avascular modeling to include vascular tumor growth, thus incorporating a third phase to describe blood vessels' spatial and temporal distribution. Byrne et al. [21] studied the region of solid tumor growth as a two-phase liquid. Hubbard and Byrne [22] presented multiphase modeling of vascular tumor growth in two spatial dimensions. Recently, Lampropoulos et al. [23] described a multiphase model for vascular heterogeneous tumor growth extending the work of Breward et al. [20] and Hubbard and Byrne [22]. It is a two-dimensional continuum model tumor treating the tissue as a composition of six distinct and interacting phases.

Discrete cell-based models are models in which the behavior of one or more individual cells as they interact with one another and the microenvironment is addressed. Today, discrete cell modeling has advanced to study a broad swath of cancer biology, spanning carcinogenesis, tumor growth, invasion, and angiogenesis. Discrete, or individual-based, models are generally divided into two categories: lattice-based (including **cellular automata**) and lattice-free (**agent-based**). Both approaches to track and update individual cells according to a set of biophysical

rules. Typically these models involve a composite discrete–continuum approach in the sense that the microenvironment variables (glucose, oxygen, extracellular matrix, growth factors, etc.) are described using continuum fields while the cells are discrete [16].

In lattice-based modeling, the cells are confined to a regular two-dimensional or three-dimensional lattice. Each computational mesh point is updated in time according to deterministic or stochastic rules derived from physical conservation laws and biological constraints. Some models use a high-resolution mesh to discretize the cells and the surrounding microenvironment at subcellular resolution, allowing a description of the cells' finite sizes, morphologies, and biomechanical interactions. **Cellular automata (CA) models**, which describe each cell with a single computational mesh point, can be viewed as a special case of the lattice-based approach [16].

Lattice-free models, frequently referred to as **agent-based models**, do not restrict the cells' positions and orientations in space. This allows more complex and accurate coupling between the cells and their microenvironment and imposes fewer artificial constraints on the behavior of multicellular systems. The cells are treated as distinct objects or agents and are allowed to move, divide, and die individually according to biophysically based rules [16].

In the literature, there are lots of references to cellular automata modeling. Anderson et al. [24, 25] developed a composite discrete–continuum model of solid tumor growth with microenvironmental interactions. The microenvironment variables, i.e., the extracellular matrix (ECM) density and matrix metalloproteinases (MMPs), are represented as continuous concentrations, and the tumor cells are described as cellular automata. Moreover, Mallet and De Pillis [26] presented a cellular automata model of the tumor to describe the interactions between a growing tumor next to a nutrient source and the immune system of the host organism. More recently, Kavousanakis et al. [27] studied the efficient coarse simulation of a growing avascular tumor. The composite model used in this study consists of a discrete description of tumor cells, which obey a set of rules specifying their motility and proliferation capabilities, and a continuum description of nutrients and oxygen, which follow reaction-diffusion partial differential equations.

Recently, **Hybrid Models** have been proposed to combine the advantages of the continuum and the discrete approaches to simulate multiscale multibody problems; these provide more realistic descriptions of microscopic mechanisms while efficiently evolving the entire system to obtain macroscopic observations. Solid-tumor growth is one example of such multiscale problems, where the cellular and subcellular scale pathways have been intensively studied and are relatively well understood, while the tissue-scale tumor morphology is of interest in clinical applications [16].

An example of a hybrid tumor growth model can be found in Bearer et al. [28] and Frieboes et al. [29], where vascularized tumor growth is presented. Tumor cells are known to secrete vascular endothelial growth factors (VEGFs) under hypoxic conditions, thus inducing vascular growth. Lastly, Kim et al. [30] developed a hybrid tumor model that describes the growth of multicellular tumor spheroids (MCTSs).

2.1.1 Comparison Between Continuum and Discrete Models

- Continuum Models can be too coarse-scaled to capture the spatial complexity of tissue microarchitecture when the cells are polarized or during individual cell motility. Furthermore, continuum models tend to combine multiple physical properties into one or two phenomenological parameters. While this eases mathematical analysis of the physical systems, it cannot be easy to directly match such lumped parameters to physical measurements [16].
- Some key patient-specific measurements occur at the molecular and cellular scales, i.e., at finer scales than continuum models. In contrast, in some cases, discrete cell models can be directly matched to such measurements. Discrete models have some drawbacks when compared with continuum approaches. Because they rely upon the behavior of individual cells to determine emergent system properties, they can be difficult to analyze. In addition, the computational cost of the methods increases rapidly with the number of cells modeled, the lattice resolution (for lattice-based methods), and the complexity of each cell object (for agent models). This can make such models difficult or impossible to apply to large systems, even with parallel programming [16].

2.2 Model Development: Mathematical Formulation for Continuum Tumor Model

The model described below is based on Hubbard, and Byrne [22]. It is a two-dimensional continuum mathematical model of vascular tumor growth, an extension of the work of Breward, Byrne, and Lewis [19, 20]. It is a multiphase model in which the tissue is decomposed into four distinct and interacting phases. The conservation of mass and momentum principles are applied to the: i) normal/healthy cells, ii) cancer/tumor cells, iii) blood vessels, and iv) extracellular material. Each phase mentioned above is assumed to behave like a viscous fluid. The inclusion of a diffusible nutrient supplied by the blood vessels allows the vasculature to have a nonlocal influence on the other phases so that it can influence tissue at a distance from the vessel. Including healthy and cancer cells in the underlying mathematical model also allows interactions between the growing tumor and the healthy tissue.

It is crucial to present the mathematical formulation for this particular continuum tumor model analytically. We extend it below to apply it in our computational study of combination therapies in growing tumors.

The volume fractions, velocities, and pressures are denoted respectively by θ_i, $\vec{u_i}$ and p_i ($i = 1, ..., 4$) and equations are derived for their evolution by applying to each phase the principles of mass and momentum balance with appropriate constitutive assumptions. It is also considered a single, diffusible species (c), such as oxygen or glucose, which is supplied by the blood vessels and acts as a source of nutrients for normal and cancerous cells. The domain is denoted by Ω, which the equations hold, and by Γ, its boundary.

2.3 The Mass Balance Equations

Under the assumption that density in living tissue is uniform and constant, the mass balances for the four phases are simplified as follows:

$$\frac{\partial \theta_i}{\partial t} + \vec{\nabla} \cdot (\theta_i \vec{u_i}) = q_i, \qquad i = 1, ..., 4. \tag{2.1}$$

In Equation (2.1) the term $\vec{\nabla} \cdot (\theta_i \vec{u_i})$ formulates mass transfer through convection, θ_i is the volume fraction of phase i and $\vec{u_i}$ its velocity. The source term q_i represents the mass transfer between the different phases (i=1,...,4) that is associated with processes including cell mitosis (proliferation), death, angiogenesis, and vessel occlusion.

It is further assumed [20], that the tissue has no voids and is covered only by the four phases so that :

$$\sum_{i=1}^{4} \theta_i = 1. \tag{2.2}$$

Also, total mass must be conserved so that any volume lost from one phase via a source term will be balanced by an equal volume increase in another phase (and vice versa). Under this expectation:

$$\sum_{i=1}^{4} q_i = 0. \tag{2.3}$$

The source terms associated with each phase are described in the following subsections.

2.3.1 Source Terms for Healthy and Cancer Cell Phases (θ_1, θ_2)

We take for granted that the volume fractions of the healthy and tumor cells (θ_1, θ_2, respectively) increase through cell proliferation and decrease due to cell death, with extracellular material (θ_4) supplying the material needed to drive cell growth and mitosis, and both rates being regulated by the local nutrient concentration. The proliferation rates are assumed to be monotonically increasing and saturating functions of c, increasing from zero when $c = 0$ to a finite maximum $k_{1,i}$ in the limit as $c \to \infty$, (i=1 for healthy cells, i=2 for cancer cells). The cell death rate for each phase is assumed to be proportional to the volume fraction of that phase and to decrease monotonically with c from a maximum value of $k_{2,i}c_{c_1}/c_{c_2}$ when $c = 0$ (i.e., maximal necrosis under hypoxia) to a minimum or basal rate of $k_{2,i}$ as $c \to \infty$. Combining the above assumptions, we obtain mass balance source terms for the healthy and cancer cells of the form:

$$q_1 = \underbrace{k_{1,1}\theta_1\theta_4\left(\frac{c}{c_p + c}\right)}_{\text{cell birth}} - \underbrace{k_{2,1}\theta_1\left(\frac{c_{c_1} + c}{c_{c_2} + c}\right)}_{\text{cell death}}. \tag{2.4}$$

$$q_2 = \underbrace{k_{1,2}\theta_2\theta_4\left(\frac{c}{c_p + c}\right)}_{\text{cell birth}} - \underbrace{k_{2,2}\theta_2\left(\frac{c_{c_1} + c}{c_{c_2} + c}\right)}_{\text{cell death}}. \tag{2.5}$$

In Equation (2.4) $k_{1,1}$ is the healthy cells mitosis rate constant, $k_{2,1}$ is the healthy cells death rate constant. The first term on the right-hand side of Equation (2.4) models mitosis (cell birth), with c_p denoting the nutrient concentration at which the mitosis rate becomes half-maximal and the second term on the right-hand side of the same Equation, represents the death rate of healthy cells; c_{c_1}, c_{c_2} denote threshold nutrient concentration values regulating the cellular death rate. Finally, in order to ensure that the death rate increases as the nutrient concentration decreases, we select: $c_{c_1} > c_{c_2}$.

Equation (2.5) describes the relative processes for the cancer cell phase. The term $k_{1,2}$ is the cancer cells mitosis rate constant, and $k_{2,2}$ is the cancer cells death rate constant. The other terms remain the same as described in the previous Equation (2.4).

Since Tumor cells typically increase more rapidly and are less likely to die under nutrient-poor conditions than Normal cells, it is supposed that $k_{1,2} \geq k_{1,1}$ and $k_{2,2} \leq k_{2,1}$, so for cancer cells are observed higher mitosis and lower death rates. Finally, for simplicity, it is assumed that the threshold nutrient concentrations, c_p, c_{c_1} and c_{c_2}, are identical for normal and cancer cells.

2.3.2 The Blood Vessel Phase (θ_3)

The volume fraction of blood vessels increases through angiogenesis and decreases due to occlusion. Accordingly, it is supposed that vessels are removed from the vasculature if the pressure exerted on them by the surrounding cells, $(\theta_1 p_1 + \theta_2 p_2)$, exceeds the critical value p_{crit} (in practice, the vessels first become occluded, then their blood flow declines, reducing the wall shear stress that they experience and ultimately leading to their regression). The rate of new vessel formation is assumed to be proportional to the volume fraction of blood vessels (θ_3) and the total volume fraction of the cells ($\theta_1 + \theta_2$), the cells acting as a source of angiogenic factor. It is assumed that vessel growth is inhibited when there is too little extracellular material to form new vessels. The growth rate increases monotonically towards a bounded maximum as θ_4, the extracellular material, increases.

It is supposed that the rate of angiogenesis depends on the local nutrient/oxygen concentration by assuming further that vessel growth is suppressed when nutrient levels are either low or high and maximal for intermediate values of c (this means that the cells only express the angiogenic factors, such as VEGF, that stimulate vessel growth when nutrient levels are between these threshold values). Healthy cells and tumor cells are assumed to act identically as sources of angiogenic factor. Combining the above assumptions the following expression occurs for q_3, the mass balance source term, using Equation (2.1):

$$q_3 = \underbrace{-k_3\theta_3\mathcal{H}\left(\theta_1 p_1 + \theta_2 p_2 - p_{crit}, \epsilon_3\right)}_{\text{occlusion}} + \underbrace{k_4\left(\theta_1+\theta_2\right)\theta_3\left(\frac{\theta_4}{\varepsilon+\theta_4}\right)\left(\frac{c}{\left(c_\alpha+c\right)^2}\right)}_{\text{angiogenesis}}. \tag{2.6}$$

$$\mathcal{H}\left(p,\epsilon\right) = \frac{1}{2}\left(1 + tanh\frac{p}{\epsilon}\right), \qquad \epsilon \ll 1, \tag{2.7}$$

In Equation (2.6), k_3 is the occlusion rate constant, and k_4 is the angiogenesis rate constant. The first term on the right-hand side of Equation (2.6) models vessel occlusion, with p_{crit} denoting the critical pressure for vessel occlusion and ϵ_3 denoting the smoothness of occlusion pressure dependence. The second term on the right-hand side of the same Equation represents the vessel angiogenesis with ϵ denoting the blood vessel volume fraction at which the angiogenesis rate becomes half-maximal, c_α is the nutrient concentration at which the rate of angiogenesis is maximal, and Equation (2.7) is a smooth approximation to the Heaviside step function.

2.3.3 The Extracellular Material Phase (θ_4)

The extracellular material is a simplistic representation of the phase that includes the additional material required to create volume in the other phases, i.e., during mitosis and angiogenesis, and the material that remains when volume from another phase is lost, i.e., during apoptosis, necrosis, and vessel occlusion. The system is assumed to be closed, with no external replenishment of resources except that related to balancing fluxes across the boundary of the computational domain. Therefore, the extracellular material equation to be consistent with the mass source term Equation (2.3) is formulated as:

$$\begin{aligned} q_4 = -q_1 - q_2 - q_3 \quad = & \underbrace{-k_{1,1}\theta_1\theta_4\left(\frac{c}{c_p+c}\right)}_{\text{healthy cell birth}} \underbrace{+k_{2,1}\theta_1\left(\frac{c_{c_1}+c}{c_{c_2}+c}\right)}_{\text{healthy cell death}} \\ & \underbrace{-k_{1,2}\theta_2\theta_4\left(\frac{c}{c_p+c}\right)}_{\text{tumor cell birth}} \underbrace{+k_{2,2}\theta_2\left(\frac{c_{c_1}+c}{c_{c_2}+c}\right)}_{\text{tumor cell death}} \\ & \underbrace{+k_3\theta_3\mathcal{H}\left(\theta_1 p_1 + \theta_2 p_2 - p_{crit}, \epsilon_3\right)}_{\text{occlusion}} \\ & \underbrace{- k_4\left(\theta_1+\theta_2\right)\theta_3\left(\frac{\theta_4}{\epsilon+\theta_4}\right)\left(\frac{c}{\left(c_\alpha+c\right)^2}\right)}_{\text{angiogenesis}}. \end{aligned} \tag{2.8}$$

Since the extracellular material (ECM) is essentially a passive medium that provides material for or accepts material from processes relating to the other phases, its volume fraction is calculated

using the no-voids condition Equation (2.2) instead of its mass balance equation. In other words, the equation used to update the ECM phase volume fraction is:

$$\theta_4 = 1 - \theta_1 - \theta_2 - \theta_3. \tag{2.9}$$

This Equation (2.9) ensures that the conservation of mass is preserved when the system is discretized.

2.3.4 Initial and Boundary Conditions

In order to close the mass balance equations, initial and boundary conditions are imposed. Initial conditions must be provided on the computational domain, Ω. Equation (2.1) is applied, θ_i is prescribed for each phase and all $t \geq 0$ on the corresponding inflow section of the boundary ${\Gamma_i}^{Inflow}$. The inflow sections are defined to be those parts of Γ on which $\vec{u_i} \cdot \vec{n} < 0$, where $\vec{n}$ is the outward-pointing unit normal to the boundary. No condition is required on the remainder of the boundary since the mass balance equations are hyperbolic.

2.4 The Momentum Balance Equations

Supposing that the Reynolds number of the flow is low enough to neglect inertial terms (creeping flow), the conservation of momentum can be written in the following form:

$$\vec{\nabla} \cdot (\theta_i \boldsymbol{\sigma}_i) + \vec{F_i} = 0, \qquad i = 1, ..., 4. \tag{2.10}$$

where $\boldsymbol{\sigma}_i$ denotes the stress tensor in each individual phase and $\vec{F_i}$, denotes the corresponding momentum source terms, which include the effects of pressure and inter-phase drag. These equations are not, on their own, enough to determine the velocities $\vec{u_i}$, which govern the flow in the mass balance equations. A continuity equation must supplement them for the phase mixture, which immediately follows from summing Equation (2.1) to give:

$$\sum_{i=1}^{4} \vec{\nabla} \cdot (\theta_i \vec{u_i}) = 0, \tag{2.11}$$

and appropriately defined constitutive relations for phase pressures.

2.4.1 Momentum Balance Equations for the Four Phases $(\theta_1, \theta_2, \theta_3, \theta_4)$

The mechanical behavior of the tissue is modeled by assuming that each phase behaves like a viscous and compressible fluid and the stress tensor associated with it has the form:

$$\boldsymbol{\sigma}_i = -p_i \boldsymbol{I} + \mu_i \left(\vec{\nabla} \vec{u_i} + \left(\vec{\nabla} \vec{u_i} \right)^T \right) + \lambda_i \left(\vec{\nabla} \cdot \vec{u_i} \right) \boldsymbol{I}, \qquad i = 1, ..., 4 \tag{2.12}$$

in which p_i are the phase pressures, and μ_i, λ_i are the dynamic shear and bulk viscosities, respectively. This work assumes that the phases are in local thermodynamic equilibrium, so $\lambda_i = -\frac{2}{3}\mu_i$ throughout. The effects of pressure are also included in the momentum sources in Equation (2.10), along with terms representing inter-phase drag. This leads to the following:

$$\vec{F_i} = p_i \boldsymbol{I} \vec{\nabla} \theta_i + \sum_{j=1, j \neq i}^{4} d_{ij} \theta_i \theta_j \left(\vec{u_j} - \vec{u_i} \right), \qquad i = 1, ..., 4 \tag{2.13}$$

in which d_{ij} is the drag coefficient associated with the relative movement between phases i and j surfaces.

For calculating both pressures and velocity fields for each phase, constitutive relationships between phase pressures are prescribed through the continuity equation for the phase mixture Equation (2.11). First, it is assumed that the pressure in the blood vessel phase is constant, so that $p_3 = {p_3}^*$, where ${p_3}^*$ is the externally-imposed pressure in the vasculature. Second, the healthy and tumor cells are assumed to act like isotropic fluids, with additional cell-cell interactions, so that:

$$p_1 = p_2 = p_4 + \Sigma \left(\theta \right), \tag{2.14}$$

where $\theta = \theta_1 + \theta_2$ is the total cell volume fraction. For simplicity, the healthy cells and the tumor cells are assumed to interact with each other in precisely the same manner. The cells have a natural density θ^*, below which they are so sparsely distributed that they experience no stress and do not interact. For $\theta = \theta_1 + \theta_2 > \theta^*$, the cells move to reduce their stress. Accordingly, the functional form used to define $\Sigma \left(\theta \right)$ is [22]:

$$\Sigma \left(\theta \right) = \begin{cases} \frac{\Lambda(\theta - \theta^*)}{(1-\theta)^2} & \text{if } \theta \geq \theta^* \\ 0 & \text{if } \theta < \theta^* \end{cases} \tag{2.15}$$

where Λ is a tension constant measuring the tendency of cells to restore their natural density, θ^* is the cellular volume fraction value in healthy tissue, $\Sigma \left(\theta \right)$ is a function calculating the increase in pressure exerted by cells whenever their local density exceeds their natural value.

2.4.2 Boundary Conditions

The system which couples the momentum balance equations (2.10) with the compressibility constraint Equation (2.11) and the pressure relations Equation (2.14) requires additional conditions on the boundary of the domain Γ before the profiles of $\vec{u_i}$ and p_i can be found.

For sections of the boundary, $\vec{u_i} = 0$ is imposed for $i = 1, ..., 4$. If the whole of Γ is a solid obstacle, p_i must also be specified at one point in the domain to obtain a unique solution. For the remaining sections of the boundary, the normal stress $\boldsymbol{\sigma}_i \cdot \vec{n}$ is specified, where $\vec{n}$ is the outward-pointing unit normal to Γ. It is impossible to determine the normal stress around the whole boundary for all phases: $\vec{u_i}$ must be specified along some boundary section for at least one phase to obtain a unique solution.

2.5 Nutrient (Oxygen)

The contribution of the diffusible nutrient to the overall volume is assumed to be negligible, and its transport is taken to be diffusion dominated. Furthermore, it is considered that the timescales of transport and reaction processes for nutrient are considerably shorter (order of minutes) compared to the timescales of processes associated with fluid phase changes of volume fractions (order of days or weeks). Under this assumption, the nutrient is governed by the quasi-steady state, and the general form of its reaction-diffusion equation is the following:

$$D_c \vec{\nabla}^2 c_j + q_c = 0, \qquad j = 1, ..., N_d, \tag{2.16}$$

in which c_j $(j = 1, ..., N_d)$ denote the concentration of the diffusible nutrient. The diffusion coefficient for the nutrient D_c is assumed constant, and the q_c represents the source term associated with the nutrient.

2.5.1 Mass Balance Equation for Nutrient (c)

The diffusible nutrient used here is oxygen, denoted by c. The nutrient supplied by the vasculature and consumed by both normal and cancer cells, providing them with the energy that they need not only to remain alive but also to proliferate. For simplicity, the rate at which the two cell types consume nutrient to carry out normal baseline activities is assumed to be proportional to the nutrient concentration and their respective volume fractions. In addition, the nutrient is consumed by the normal and cancer cells at rates that are proportional to their proliferation rates (see Equations (2.4) (2.5)). Combining these processes leads to a source term q_c in the nutrient diffusion Equation (2.16), which takes the form:

$$q_c = \underbrace{k_5\theta_3\left(c_v - c\right)}_{\text{replenishment}} \underbrace{-k_{6,1}\theta_1 c - k_{6,2}\theta_2 c}_{\text{baseline consumption}} \underbrace{-k_{7,1}\theta_1\theta_4\left(\frac{c}{c_p + c}\right) - k_{7,2}\theta_2\theta_4\left(\frac{c}{c_p + c}\right)}_{\text{consumption due to cell birth}}. \tag{2.17}$$

where k_5 is the nutrient replenishment rate constant for the replenishment performed by the local vasculature while c_v represents the constant concentration of the nutrient within the blood vessels, $k_{6,i}$, $i = 1, 2$, denote the consumption rate constants for cell sustenance of healthy and cancer cells, respectively, and $k_{7,i}$, $i = 1, 2$ are the rate constants for the consumption of nutrient for mitosis for healthy and cancer cells, respectively. The parameter c_p is identical to that used in the cell phase source terms of Equations (2.4), (2.5). We assumed that $k_{7,1}/k_{7,2} = k_{1,1}/k_{1,2}$ for consistency with the cell birth terms in Equations (2.4), (2.5).

2.5.2 Boundary Conditions

Equation (2.16) for the distribution of the diffusible nutrient, c_j, can be closed by prescribing either Dirichlet or Neumann boundary conditions. For the former, c_j is specified on the domain

boundary Γ, while for the latter, $\vec{\nabla} c_j \cdot \vec{n}$ is specified, where $\vec{n}$ is the outward-pointing unit normal to Γ. In our case, we imposed the Neumann boundary condition.

2.6 Nondimensionalisation

It is convenient to recast the model in dimensionless form to solve it. In addition, when we insert the model in Comsol Multiphysics ®, we put it in its dimensionless form. Since the phase volume fractions, by definition, θ_1, θ_2, θ_3 and θ_4 are dimensionless, only the independent variables, $\vec{x}$ and t, the phase velocities $\vec{u_i}$, the pressures p_i, and the nutrient concentration c are nondimensionalized. This is done in the following way:

$$t = \frac{t^{'}}{k_{1,1}}, \quad \vec{x} = L_0 \vec{x}^{'}, \quad \vec{u_i} = L_0 k_{1,1} \vec{u_i}^{'}, \quad p_i = \Lambda p_i^{'}, \quad c = c_v c^{'}, \tag{2.18}$$

where primes ($'$) denote dimensionless variables and asterisks (*) denote dimensionless parameters. The birth rate parameter for healthy cells, $k_{1,1}$, is used to scale time, L_0 is a typical length scale (taken later to be the initial radius of the tumor seeded in the healthy tissue), Λ is the cell-cell interaction tension constant (see Equation (2.15)), and c_v is the nutrient concentration in the blood vessels (see Equation (2.17)).

2.6.1 Mass Balance Equations

Substituting from Equations (2.18) in Equations (2.1) leads to the following evolution equations for θ_1, θ_2 and θ_3, the phase volume fractions of the healthy cells, cancer cells, and blood vessels, respectively:

$$\frac{\partial \theta_1}{\partial t^{'}} + \vec{\nabla}^{'} \cdot \left(\theta_1 \vec{u_1}^{'} \right) = \underbrace{\theta_1 \theta_4 \left(\frac{c^{'}}{c_p^* + c^{'}} \right)}_{\text{cell birth}} - \underbrace{k_{2,1}^* \theta_1 \left(\frac{c_{c_1}^* + c^{'}}{c_{c_2}^* + c^{'}} \right)}_{\text{cell death}}. \tag{2.19}$$

$$\frac{\partial \theta_2}{\partial t^{'}} + \vec{\nabla}^{'} \cdot \left(\theta_2 \vec{u_2}^{'} \right) = \underbrace{k_{1,2}^* \theta_2 \theta_4 \left(\frac{c^{'}}{c_p^* + c^{'}} \right)}_{\text{cell birth}} - \underbrace{k_{2,2}^* \theta_2 \left(\frac{c_{c_1}^* + c^{'}}{c_{c_2}^* + c^{'}} \right)}_{\text{cell death}}. \tag{2.20}$$

$$\begin{aligned} \frac{\partial \theta_3}{\partial t^{'}} + \vec{\nabla}^{'} \cdot \left(\theta_3 \vec{u_3}^{'} \right) = & \underbrace{-k_3^* \theta_3 \mathcal{H} \left(\theta_1 p_1^{'} + \theta_2 p_2^{'} - p_{crit}^*, \epsilon_3^* \right)}_{\text{occlusion}} \\ & \underbrace{+ k_4^* \left(\theta_1 + \theta_2 \right) \theta_3 \left(\frac{\theta_4}{\varepsilon + \theta_4} \right) \left(\frac{c^{'}}{\left(c_\alpha^* + c^{'} \right)^2} \right)}_{\text{angiogenesis}}. \end{aligned} \tag{2.21}$$

in which

$$k_{2,1}^* = \frac{k_{2,1}}{k_{1,1}}, \quad k_{1,2}^* = \frac{k_{1,2}}{k_{1,1}}, \quad k_{2,2}^* = \frac{k_{2,2}}{k_{1,1}}, \quad k_3^* = \frac{k_3}{k_{1,1}}, \quad k_4^* = \frac{k_4}{c_v k_{1,1}},$$

$$c_p^* = \frac{c_p}{c_v}, \quad c_\alpha^* = \frac{c_\alpha}{c_v}, \quad c_{c_1}^* = \frac{c_{c_1}}{c_v}, \quad c_{c_2}^* = \frac{c_{c_2}}{c_v}, \tag{2.22}$$

$$p_{crit}^* = \frac{p_{crit}}{\Lambda} \quad , \epsilon_3^* = \frac{\epsilon_3}{\Lambda}.$$

The phase volume fraction of extracellular material is calculated from the no-voids condition (see Equation (2.2)), which remains unchanged by the nondimensionalisation,i.e., $\theta_4 = 1-\theta_1-\theta_2-\theta_3$. When imposing boundary conditions, θ_i is prescribed for each phase on Γ_i^{Inflow}, the sections of Γ for which $\vec{u_i}^{'} \cdot \vec{n}^{'} < 0$ where $\vec{n}^{'}$ is the outward-pointing unit normal to the boundary.

2.6.2 Momentum Balance Equations

Equations (2.10)-(2.14) transform to give the following equations for the dimensionless phase velocities $\vec{u_i}^{'}$ and phase pressures $p_i^{'}$:

$$\sum_{j=1, j\neq i}^{4} d_{ij}^* \theta_i \theta_j \left(\vec{u_j}^{'} - \vec{u_i}^{'}\right) - \theta_i \vec{\nabla}^{'} \cdot \left(\Lambda^* p_i^{'} \boldsymbol{I}\right)$$

$$+\vec{\nabla}^{'} \cdot \left[\theta_i \left[\mu_i^* \left(\vec{\nabla}^{'} \vec{u_i}^{'} + \left(\vec{\nabla}^{'} \vec{u_i}^{'}\right)^T\right) + \lambda_i^* \left(\vec{\nabla}^{'} \cdot \vec{u_i}^{'}\right) \boldsymbol{I}\right]\right] = 0, \quad i, j = 1, 2, 3, 4. \tag{2.23}$$

$$\sum_{i=1}^{4} \vec{\nabla}^{'} \cdot \left(\theta_i \vec{u_i}^{'}\right) = 0. \tag{2.24}$$

$$p_1^{'} = p_2^{'} = p_4^{'} + \Sigma^{'}(\theta). \tag{2.25}$$

$$p_3^{'} = \frac{p_3^*}{\Lambda}. \tag{2.26}$$

in which $d_{ij} = d_{ji}$,

$$d_{ij}^{*}=\frac{d_{ij}}{d_{12}},\quad \Lambda^{*}=\frac{\Lambda}{d_{12}k_{1,1}L_0^2},\quad \mu_i^{*}=\frac{\mu_i}{d_{12}L_0^2},\quad \lambda_i^{*}=\frac{\lambda_i}{d_{12}L_0^2}, \tag{2.27}$$

where $i,j=1,...,4$ and $j\neq i$, and

$$\Sigma^{'}(\theta)=\begin{cases}\frac{(\theta-\theta^{*})}{(1-\theta)^2} & \text{if } \theta\geq\theta^{*}\\ 0 & \text{if } \theta<\theta^{*}\end{cases} \tag{2.28}$$

with $\theta=\theta_1+\theta_2$. On Γ we impose the Dirichlet boundary condition: $\vec{u_i}^{'}=0$, $i=1,...,4$.

2.6.3 Reaction-Diffusion Equation for Nutrient

Finally, the nutrient concentration equation (2.16), with source term (2.17), becomes:

$$\begin{aligned}D_c^{*}\vec{\nabla}^{'2}c^{'}=&\underbrace{\theta_3\left(1-c^{'}\right)}_{\text{replenishment}}\underbrace{-k_{6,1}^{*}\theta_1c^{'}-k_{6,2}^{*}\theta_2c^{'}}_{\text{baseline consumption}}\\ &\underbrace{-k_{7,1}^{*}\theta_1\theta_4\left(\frac{c^{'}}{c_p^{*}+c^{'}}\right)-k_{7,2}^{*}\theta_2\theta_4\left(\frac{c^{'}}{c_p^{*}+c^{'}}\right)}_{\text{consumption due to cell birth}}.\end{aligned} \tag{2.29}$$

in which

$$D_c^{*}=\frac{D_c}{k_5L_0^2},\quad k_{6,1}^{*}=\frac{k_{6,1}}{k_5},\quad k_{6,2}^{*}=\frac{k_{6,2}}{k_5},\quad k_{7,1}^{*}=\frac{k_{7,1}}{c_vk_5},\quad k_{7,2}^{*}=\frac{k_{7,2}}{c_vk_5} \tag{2.30}$$

Here Equation (2.17) has been divided by k_5, the timescale on which nutrient exchanges between the tissue and the blood vessels. On the boundary, we impose the Neumann condition, $\vec{\nabla}^{'}c^{'}\cdot\vec{n}^{'}=0$.

2.7 Inserting the Mathematical Model into Comsol Multiphysics

All computations in the present thesis are performed in the environment of Comsol Multiphysics®, version 5.3a, which is based on the Finite Elements Method (FEM). Engineers and scientists use this software to simulate designs, devices, and processes in all engineering, manufacturing, and scientific research fields. COMSOL Multiphysics ®, COMSOL for abbreviation, is a simulation platform that provides fully coupled multiphysics and single-physics modeling capabilities [31].

The tissue is modeled as a circular domain with (dimensionless) radius, $R_{tissue} = 16$. The computational mesh is an unstructured mesh generated with the Delaunay Triangulation method and contains approximately 20.000 elements, resulting in approximately 362.000 degrees of freedom.

All simulations are initialized by seeding a number of cancer cells on a healthy tissue, which prior to the tumor's appearance, is considered to be at an equilibrium state [23, 22] and satisfies the following assumptions:

- each phase is spatially uniform with zero velocity (i.e., $\vec{u_i} \equiv 0$, $i = 1, 3, 4$),
- initially there are no tumor cells present (i.e., $\theta_2 \equiv 0$),
- the volume fraction of healthy cells is such that $\theta_1 = \theta^* = 0.6$, the natural cell density, below which the cells do not interact or experience any stress,
- $p_3 = p_3^* = 0$ and $p_4 = 0$, so $p_1 = p_2 = 0$ because $\theta_1 = \theta^*$.

Equations (2.2), (2.19), (2.21) and (2.29) then reduce to the following system of nonlinear equations given by:

$$\theta^*\theta_4 \left(\frac{c^{'}}{c_p^* + c^{'}} \right) - k_{2,1}^* \theta^* \left(\frac{c_{c_1}^* + c^{'}}{c_{c_2}^* + c^{'}} \right) = 0. \tag{2.31}$$

$$-k_3^* \theta_3 \mathcal{H}\left(-p_{crit}^*, \epsilon_3^*\right) + k_4^* \theta^* \theta_3 \left(\frac{\theta_4}{\varepsilon + \theta_4} \right) \left(\frac{c^{'}}{(c_\alpha^* + c^{'})} \right) = 0. \tag{2.32}$$

$$\theta^* + \theta_3 + \theta_4 = 1 \tag{2.33}$$

$$\theta_3 \left(1 - c^{'}\right) - k_{6,1}^* \theta^* c^{'} - k_{7,1}^* \theta^* \theta_4 \left(\frac{c^{'}}{c_p^* + c^{'}} \right) = 0 \tag{2.34}$$

These equations are then solved for the unknown model variables θ_3, θ_4 and $c^{'}$, and one model parameter, chosen arbitrarily, here to be the angiogenesis rate constant k_4^* in order to obtain a unique solution. So, now there are four equations and four unknown variables for the system. The chosen solution must also satisfy θ_3, θ_4, $c^{'} \in [0, 1]$ and $k_4^* \geq 0$ to be valid physically. The solution for the remaining parameter values shown in Table 2.1 is given by:

$$\begin{aligned} &\theta_1 = 0.6, \;\; \theta_2 = 0.0, \theta_3 = 0.01749783, \;\; \theta_4 = 0.3825022, \\ &c^{'} = 0.2532031, \;\; p_1 = p_2 = p_3 = p_4 = 0.0, \;\; k_4^* = 0.002944900 \end{aligned} \tag{2.35}$$

The initial conditions of the problem were obtained by seeding a healthy tissue in a steady state with a small number of tumor cells. Consequently, the initial conditions for the current problem will be the same as the values presented above Equation (2.35) with the only difference in the volume fraction of cancer cells θ_2. At $t = 0$, a small tumor was seeded at the center of the healthy tissue so that:

Table 2.1: *Dimensionless parameter values for the simulations* [22].

Parameter	**Value**	**Description**
$k^*_{1,2}$	2.0	Tumor cell birth rate
$k^*_{2,1}$	0.15	Healthy cell death rate
$k^*_{2,2}$	0.075	Tumor cell death rate
k^*_3	0.1	Vessel occlusion rate
k^*_4	0.0029449	Angiogenesis rate
$k^*_{6,1}$	0.01	Nutrient consumption rate (healthy cell baseline)
$k^*_{6,2}$	0.01	Nutrient consumption rate (tumor cell baseline)
$k^*_{7,1}$	0.1	Nutrient consumption rate (healthy cell birth)
$k^*_{7,2}$	$k^*_{7,1} \times k^*_{1,2}$	Nutrient consumption rate (tumor cell birth)
c^*_p	0.25	Cell birth rate dependence on nutrient
$c^*_{c_1}$, $c^*_{c_2}$	0.2, 0.1	Cell death rate dependence on nutrient
c^*_α	0.05	Threshold nutrient concentration for angiogenesis rate
p^*_{crit}	0.3	Critical pressure for vessel occlusion
ϵ^*_3	0.2	Smoothness of occlusion pressure dependence
ε	0.01	Angiogenesis rate dependence on ECM
Λ^*	0.1	Cell tension constant
μ^*_i	10.0	Phase dynamic shear viscosities $(i = 1, ..., 4)$
λ^*_i	$-\frac{2}{3}\ \mu^*_i$	Phase bulk shear viscosities $(i = 1, ..., 4)$
d^*_{ij}	1.0	Interphase drag coefficients $(i, j = 1, ..., 4,\ j \neq i)$
D^*_c	1.0	Nutrient diffusion coefficient

$$\theta_2\left(x, y, t = 0\right) = \begin{cases} 0.05\cos^2\left(\frac{\pi r}{2}\right) & \text{for } r \leq 1 \\ 0 & \text{otherwise.} \end{cases} \tag{2.36}$$

where $r = \sqrt{x^2 + y^2}$. To compensate for the addition of tumor cells, the initial distribution of healthy cells was modified to be:

$$\theta_1\left(x, y, 0\right) = 0.6 - \theta_2(x, y, 0))\,, \tag{2.37}$$

while all other variables were initialized throughout the domain using the values given in Equation (2.35).

The boundary conditions were chosen as follows.

- For Equations (2.23)-(2.26) impose the following boundary condition on Γ. This allows the flow of cell and blood vessel phases through the boundary.

$$\boldsymbol{\sigma_i}' \cdot \vec{n} = 0 \quad \text{and} \quad \vec{u_4}' = 0 \tag{2.38}$$

- For Equation (2.29) impose the following boundary condition on Γ.

$$\vec{\nabla}' c' \cdot \vec{n} = 0 \tag{2.39}$$

- For Equations (2.22) impose the following boundary condition on Γ_i^{Inflow}, the region of Γ for which $\vec{u_i}' \cdot \vec{n} < 0$ ($\vec{n}$ being the outward-pointing unit normal to the boundary).

$$\theta_i = \theta_i^{\infty}, \;\; i = 1, 2, 3, 4. \tag{2.40}$$

The above conditions are inevitably artificial, in the sense that interactions with tissue outside the computational domain are neglected. The values of the remaining parameters are given in Table 2.1, where assumed that the tumour cells proliferate and die at, respectively, double and half the rate of their normal cells.

Chapter 3

Cancer Treatments

Nowadays, there are many techniques for cancer treatment, among which surgery, radiotherapy, and chemotherapy are the dominant ones [32]. In addition, there are more novel approaches that include antiangiogenic treatments, immunotherapy, and hormone therapy applied to a wide spectrum of this disease. Thus, there also exists uniformity that allows us to view the problem of cancer treatment from a more all-embracing perspective [3].

The main objectives of cancer treatments are two-fold: curative and palliative. Clearly, if feasible, complete tumor eradication is sought, and this is a realistic and viable option for certain types of cancer. In other situations, a total cure is unrealistic, and then the objective becomes to manage the disease, delay its further progression or maintain it at a tolerable level and alleviate the symptoms. For types of cancer that are still largely not curable, the objective simply becomes to improve the quality of life and survival probabilities by avoiding life-threatening toxicity. These are the objectives of palliative care. But at large, the main aim of cancer treatments is to eradicate the disease [3].

3.1 Radiotherapy

It is estimated that about one-half of all cancer patients receive radiotherapy during their course of treatment, either as a primary procedure or in conjunction with surgery and chemotherapy, i.e., as adjuvant therapy [33]. Radiation is energy that is carried by waves or a stream of particles. Radiation works by damaging the genes (DNA) in cells. Genes control how cells grow and divide. When radiation damages the genes of cancer cells, they cannot grow and divide anymore. Over time, the cells die. This means radiation can be used to kill cancer cells and shrink tumors [4].

3.1.1 Radiation Therapy Effect on Cell Cycle

The cell cycle phase is important because radiation usually kills the cells that are actively dividing. It does not work very quickly on cells in the resting stage (G0), dividing less often. The amount and type of radiation that reaches the cell and the speed of cell growth affect whether and how quickly the cell will die or be damaged. The term "radiosensitivity" describes how likely

radiation will damage the cell. Cancer cells tend to divide rapidly and grow out of control. Radiation therapy kills cancer cells that are dividing but also affects the dividing cells of normal tissues. Radiation therapy is always a balance between destroying the cancer cells and minimizing damage to the normal cells [4].

It has long been known that cells in different cell cycle phases display different radiosensitivity. Cells in the late S phase are usually the most radioresistant, and cells in the M phase are the most radiosensitive [34]. A classic paradigm is that radiation causes so-called mitotic death. Mitotic death is the most common way of radiation-induced cell death for all solid tumors and most of the hematopoietic tumors [35, 34]. This means that radiation does not kill the tumor cells right away, but that cell death occurs at some point after the first mitosis following irradiation. The irradiated cells may undergo one, two, or a few divisions before they die hours or days later [36, 4, 34]. Mitotic death is caused by chromosome damage resulting from unrepaired or misrepaired radiation-induced DNA breaks. In the presence of such chromosome damage, problems arise in mitosis when the cell needs to separate the DNA to produce two identical daughter cells [37]. Also, chromosome damage may cause the genetic material to be unevenly distributed between the two nuclei of the daughter cells [34].

It is also well known that radiation halts cell cycle progression by inducing arrest at the cell cycle checkpoints. Three major radiation-induced cell cycle checkpoints exist in G1, S, and G2 phases (see Figure 1.1). Because most irradiated tumor cells do not die before attempting to divide, the checkpoints are important to allow essential repair of the radiation damage. The G1 checkpoint depends on the tumor suppressor p53 and is often deficient or lacking in tumor cells. Tumor cells may therefore rely more on the S and G2 checkpoints for the repair of radiation damage compared to normal cells [34].

It is well known that radiation causes cells to arrest the progression through the cell cycle transiently [37]. This arrest takes place at the so-called cell cycle checkpoints in **G1**, **S**, and **G2** phases (see Figure 3.1) [34].

The **G1** checkpoint prevents damaged cells from entering S-phase and largely depends on the tumor suppressor p53 [38]. Defective G1 checkpoint control thus represents a major difference between cancer and normal cells [34].

The **S-phase** checkpoint does not stop the cells at a specific point in the cell cycle but is manifested as reduced DNA replication during the whole S-phase. Irradiated cells are thus moving more slowly through S-phase. The S-phase checkpoint depends on the cell cycle kinase Wee1, and radiation-induced activation of the ATR-Chk1 pathway [39, 40, 34].

The G2 checkpoint halts the cells in the late G2 phase and is the last checkpoint before cells enter mitosis. The G2 checkpoint is activated in both tumors and in cycling normal cells. Similar to the S-phase checkpoint, activation of the G2 checkpoint requires the ATR-Chk1, and Wee1 pathways [41, 42, 43]. The immediate G2 checkpoint measured within the first couple of hours after irradiation is also dependent on ATM kinase, as the checkpoint is partly abrogated in cells lacking functional ATM [34].

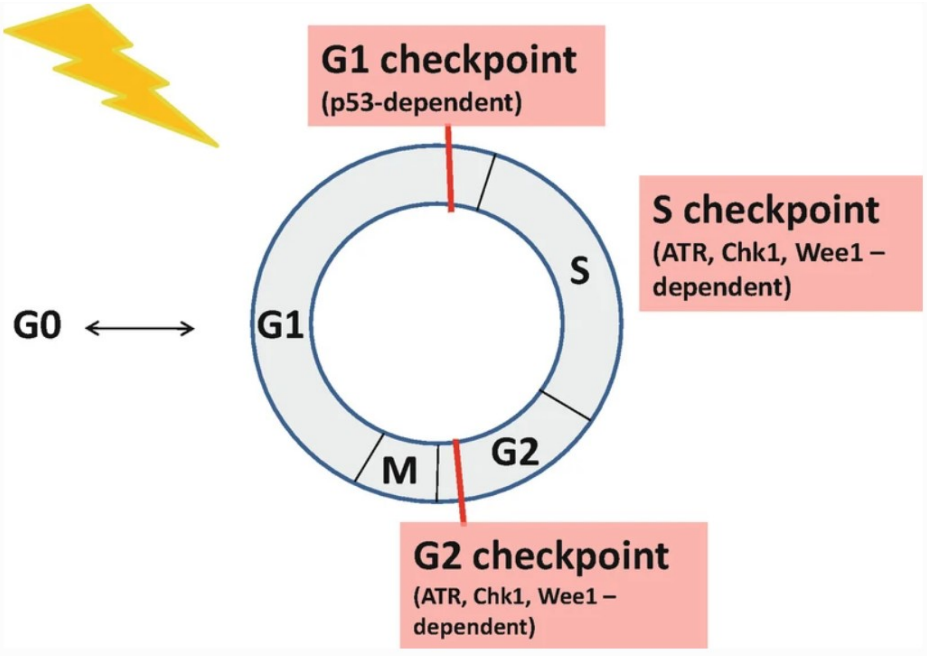

Figure 3.1: *Radiation-induced cell cycle checkpoints in G1, S, and G2 phases* [34].

3.1.2 Types of Radiation Used to Treat Cancer

Radiation used for cancer treatment is called ionizing radiation because it forms ions (electrically charged particles) in the cells of the tissues it passes through. It creates ions by removing electrons from atoms and molecules. This can kill cells or change genes, so the cells stop growing. Ionizing radiation can be sorted into two major types:

1) Photon radiation (x-rays and gamma rays)

2) Particle radiation (such as electrons, protons, neutrons, carbon ions, alpha particles, and beta particles)

Some types of ionizing radiation have more energy than others. The more energy, the more deeply the radiation can penetrate the tissues. The way each type of radiation behaves is vital in planning radiation treatments. A radiation oncologist selects the type of radiation most suitable for each patient's cancer type, and location [4].

The most common type of radiation used for cancer treatment by far is photon radiation which is a high-energy photon beam. It is the same type of radiation used in x-ray machines and comes from a radioactive source such as cobalt, cesium, or an apparatus called a linear accelerator. Photon beams of energy affect the cells along their path as they go through the body to get to cancer, pass through cancer, and exit the body [4].

3.1.3 The Main Types of Radiation Therapy

Radiation therapy can be administered in a number of ways. Sometimes radiation is given more than one way at the same time, or different types of radiation may be given one after the

other. There are two main types of radiation therapy, **External Beam Radiation** and **Internal Beam Radiation**. Sometimes **Radiopharmaceuticals** are used as an alternative type of radiation therapy.

1) **External Beam Radiation** is the most widely used type of radiation therapy, and it most often uses photon beams. The radiation comes from a machine outside the body and is focused on cancer. This type of radiation is often given by machines called linear accelerators (see Figure 3.2). External beam radiation can be used to treat large areas of the body. It also can treat more than one area, such as the main tumor and nearby lymph nodes [44].

2) **Internal Radiation Therapy** is also known as **Brachytherapy**, which means short-distance therapy. This method puts radiation sources into or near the area that needs treatment. The radiation only travels a short distance, so there's less risk of damaging nearby normal tissues. Brachytherapy can be used to deliver a high dose of radiation to a small area in a fairly short period of time. It is useful for tumors that need a high dose of radiation or are near normal tissues that are easily hurt by radiation [45]. The main types of internal radiation are:

   - Interstitial radiation: the radiation source is placed directly into or next to the tumor using small pellets, seeds, wires, tubes, or containers.
   - Intracavitary radiation: a container of radioactive material is placed in a cavity of the body such as the chest, rectum, etc.

   Ultrasound, x-rays, or CT scans are used to help the doctor put the radioactive source in the right place. The placement can be permanent or temporary (see Figure 3.3). **Permanent Brachytherapy** uses small containers, often called pellets or seeds, which are about the size of a grain of rice. Once in place, the pellets give off radiation for several weeks or months. Because they are very small and cause a little discomfort, they are left in place after their radioactive material is used. In **Temporary Brachytherapy**, any type that places such as hollow needles, tubes (catheters), or fluid-filled balloons into the area to be treated, then they are removed after treatment. Radioactive material can be put in these containers for a short time and then removed [4].

3) **Radiopharmaceuticals** are drugs that contain radioactive materials called radioisotopes. They may be put into a vein, taken by mouth, or placed in a body cavity. Depending on the drug and how it is administered, these materials travel to various parts of the body to treat cancer or relieve its symptoms. They put out radiation, mostly in the form of alpha and beta particles, that target the affected areas. They're most often used in small amounts for imaging tests, but larger doses can be used to deliver radiation [4].

3.1.4 Dosing and Treatment with External Beam Radiation

As External Beam Radiation is the most popular and widely used treatment in Radiotherapy, it is worth mentioning the dose and treatment associated with this method. The treatment gives cancer the strongest radiation dose while sparing normal tissue as much as possible. The dose and

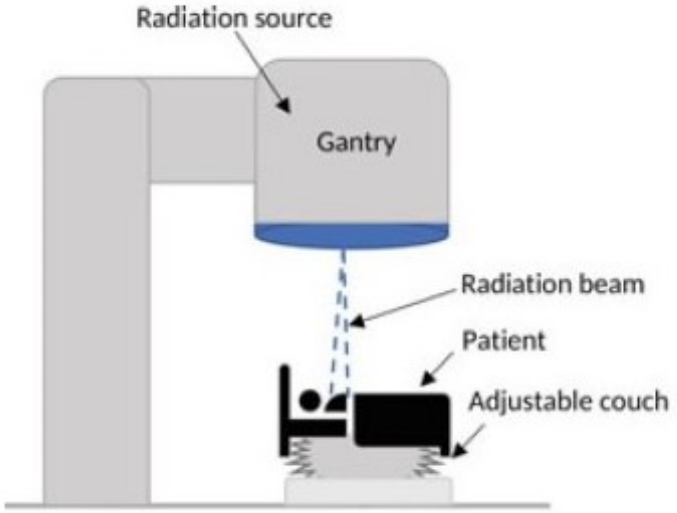

Figure 3.2: *In the case of external beam therapy, the radiation source is housed in a gantry, and an adjustable patient couch is used to position the patient appropriately* [14].

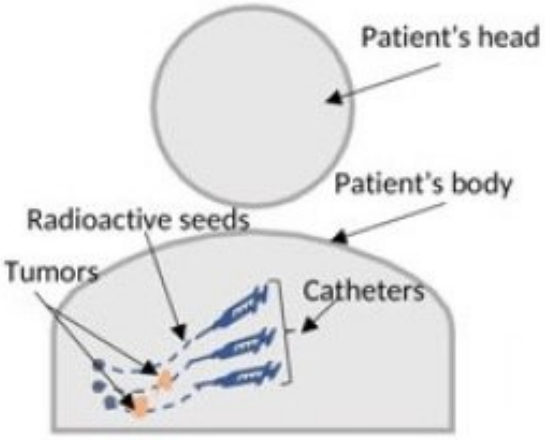

Figure 3.3: *In the case of Internal Beam Therapy or Brachytherapy, internal radiation is facilitated by using radioactive seeds and radiation catheters* [14].

the duration of treatment differ from one patient to another and depend on the size of the tumor, how sensitive the tumor is to radiation, and how well the normal tissue in the area can withstand the radiation [4].

The total amount of radiation is measured in units called Gray (Gy) or centigrade (cGy), which is one-hundredth of a Gray. Gray is the international unit of radiation dose: one joule per kilogram of matter ($1\,Gy = 1\,Gray = \frac{1Joule}{Kg}$) [46]. For External Radiation, the total dose is often divided into smaller doses called Fractions, typically given over a number of weeks. This allows the best dose to be given with the least damage to normal tissues. Every Fraction lasts about 30-45 minutes. Treatments are usually given 5 days a week, with a break at the weekend, for about 5 to 8 weeks [47]. The conventional treatment is 30 fractions of 2 Gy given one fraction per day, 5 days a week [33]. Moreover, doses for External Beam Radiation, as adjuvant therapy, typically range from 45 to 60 Gy (i.e., 1,5 Gy/fraction - 2Gy/fraction for 6 weeks) for the treatment of various cancer types such as breast, head, and neck, etc. [47].

Some cancers may be treated more often than once a day.

- Hyperfractionated radiation divides the daily dose into 2 treatment sessions without changing the length of the treatment. In this case, the patient is treated twice a day for several weeks.
- Accelerated radiation gives the total dose of radiation over a shorter period of time. In other words, giving more frequent doses (more than once a day) to get the same total dose of radiation may shorten the treatment course by a week or two.
- Hypofractionated radiation breaks radiation into fewer doses so that each dose is larger. Sometimes, this could mean it is given less often than once a day [4].

3.2 Chemotherapy

Chemotherapy is a standard treatment method used for managing many types of cancers. Chemotherapy is applied on its own or with a combination of other treatments, such as radiotherapy [48]. Chemotherapy involves using different drugs or drug combinations that can reduce the abnormal proliferation of cancer cells and lead to cell death. Cancer cell-lysis is achieved either by inducing cell-cycle arrest, manipulating the DNA structure necessary for replication, or altering metabolic pathways [14, 49].

Compared to other cancer therapy methods, such as surgery or radiation therapy, which can be localized to the area of interest, in the case of chemotherapy, treatment is facilitated by cytotoxic agents, which are transported via the circulatory system. Hence, the side effects are not localized. This considerably increases the concern regarding the type and amount of drugs used in this context. The potential side effects that come along with the excessive use of chemotherapeutic drugs call for more vigilant investigations on the drug dosing strategies to ensure optimal use of drugs which will minimize side effects and maximize desired effects due to treatment. Even though the cytotoxic agent can annihilate many cancer cells, some drug-resistant cells remain unaffected (see Figure 3.4). Moreover, the drug's use can also affect some normal cells (side-effect). Other

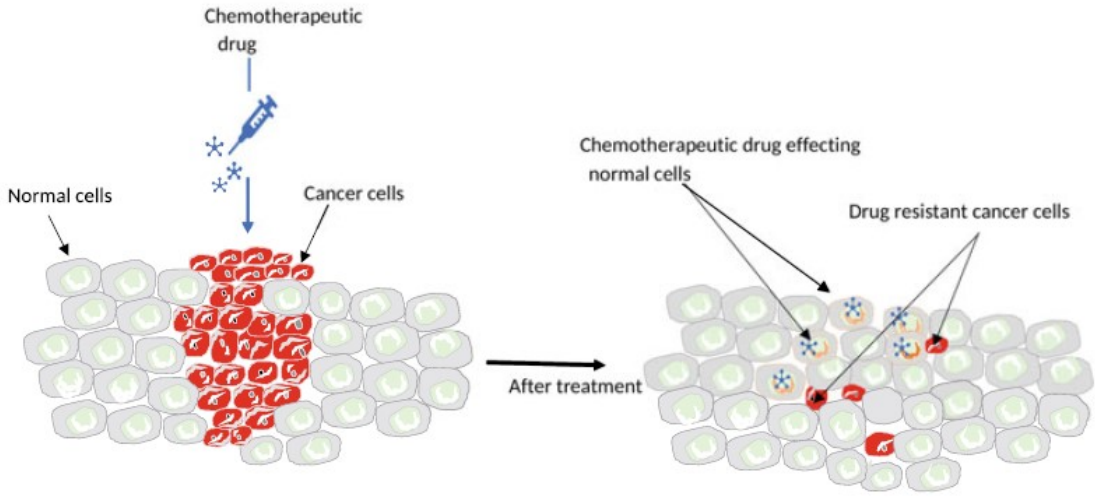

Figure 3.4: *Illustrative diagram showing the effect of a chemotherapeutic drug on cancer cells and normal cells* [14].

factors that affect the growth of the tumor and the efficacy of drugs used are the immune response and vascular delivery (which supplies oxygen, nutrients, and drug) to the tumor [14].

3.2.1 Cytotoxic Drugs: Taxanes

Cytotoxic drugs have a generic name, and they may also have one or more brand names. The generic name is the chemical name of the drug, for example, docetaxel. The brand or trade name is the name given to the drug by the company that makes it, such as Taxotere. Drugs can be produced by more than one company and may have more than one brand name. For some drugs, the brand or trade name is the most commonly used name. For other drugs, the generic name is the most often used [48, 50].

Few new classes of antineoplastic agents have stimulated as much excitement and activity as the Taxanes [51]. Of these, **Paclitaxel** which was initially extracted from the bark of the Pacific yew tree, Taxus Brevifolia, is the archetypal taxane and was the first to be isolated and characterized as having anticancer activity in rodents during the early 1970s [52, 53]. It was later shown to promote microtubule assembly/stabilization and prevent microtubule depolymerization and the assortment of replicated chromosomes into the newly developing progeny [52, 54]. Accordingly, paclitaxel was successfully shown to preemptively block tumor cells from undergoing anaphase and to arrest them into the more radiosensitive phases of the cell cycle, predominantly G2 and M [54, 52]. These critical discoveries provided the catalyst for the further development of paclitaxel in preclinical and clinical settings [55, 52]. Once paclitaxel was shown to have clear clinical benefit in a spectrum of tumor types in phase I and II clinical trials, other analogs, and formulations were developed to improve upon its large-scale production and therapeutic efficacy, essential for widespread clinical use [52].

To improve upon the supply chain of the mitotic spindle toxin, Paclitaxel and **Docetaxel** (a Paclitaxel analog) were obtained by the semisynthesis of a complex and noncytotoxic renewable precursor molecule isolated from the needles of the English yew, Taxus baccata [52, 56]. Removing the needles from the yew tree, as opposed to the bark, for chemosynthesis is sustainable and enables the production of the chemotherapies on a scale large enough for clinical use with less environmental detriment. Most notably, docetaxel proved to be twice as potent as paclitaxel and, similar to paclitaxel, was found to have antitumor activity against a variety of transplantable tumors in mice [52, 56, 57].

Docetaxel (Taxotere) is a novel semisynthetic agent of the taxoid class that enhances tubulin polymerization and inhibits microtubule depolymerization. Microtubules are essential cellular components required to maintain cell shape, motility, transport between organelles, and cell division [51]. This leads to cell cycle arrest in the G2/M phase, known to be 2.5 times more sensitive to radiation than the G1/S phase [58]. A docetaxel-induced mitotic arrest occurs due to activation of the mitotic checkpoint (also known as the spindle assembly checkpoint), the major cell cycle control mechanism acting during mitosis to prevent chromosome missegregation. The mitotic checkpoint delays the separation of the chromosomes, which enter mitosis as replicated pairs of sister chromatids until each pair has made stable attachments to both poles of the mitotic spindle. This arrangement ensures that each daughter cell will receive one copy of every chromatid. Chromatids connect to spindle microtubules through their kinetochores, protein complexes that assemble on centromeric regions of DNA. Unattached kinetochores, which have not made stable attachments to microtubules, activate a signal transduction cascade that delays mitotic progression by inhibiting the anaphase-promoting complex/cyclosome [59, 60]. Docetaxel treatment arrests cells in mitosis due to the presence of a small number of unattached kinetochores. This is the way that Docetaxel kills cancer cells.[60]

3.3 Combined Therapies

In many cases, in order to eradicate cancer completely and to avoid the chance of cancer relapse, it is essential to use multiple treatment modes together or intermittently, which is referred to as a combination therapy [61, 14]. Combination therapy involves using various agents from different treatment modalities, as mentioned above, to facilitate a more effective cancer cure than that can be accomplished by using monotherapy [14].

3.3.1 Chemoradiotherapy Treatment

Chemoradiotherapy is the combination of chemo- and radiotherapy. Chemotherapy uses anticancer (cytotoxic) drugs to destroy cancer cells, such as Docetaxel. The drugs circulate throughout the body in the bloodstream. Radiotherapy uses radiation; usually x-rays, to destroy cancer cells [62]. Furthermore, cell cycle phase effects on radiosensitivity can be significant when radiotherapy is combined with chemotherapy or new targeted drugs. Drugs administrated several hours or days before irradiation may alter the cell cycle phase distribution and cause radioresistance or radiosensitivity. For instance, drugs causing the tumor cells to accumulate in mitosis before irradiation will likely cause radiosensitivity [63]. Drugs with this competence are Taxanes. On the other hand,

there may be no radiosensitizing effect if such drugs are added after irradiation. This is why, most of the time, it is more efficient to use a combination of Chemotherapy and Radiotherapy [34].

Taxanes are rapidly gaining prominence in the management of solid tumors [64]. Numerous studies have demonstrated the radiosensitizing properties of Taxanes in various cell lines [65]. Docetaxel (Taxotere) has been studied in combination with radiation with promising results. In phase II trials, docetaxel combined with radiation therapy resulted in response rates of up to 80 %, with the most commonly used schedule being docetaxel at 20 to $30 mg/m^2$, where m^2 denotes the patient's surface area, per week with concomitant radiation administered at fractions of 1.8 to 2.0 Gy, 5 days a week over 5 to 6 weeks [66].

Choy et al. [65] conducted a phase I study of weekly docetaxel with concurrent thoracic radiation therapy in patients with unresectable stage III NSCLC. Docetaxel was administered as a 1-hour infusion every week for 6 weeks at an initial dose of 20 mg/m^2, escalated in increments of 10 mg/m^2 as tolerated to each successive cohort of three patients. Thoracic radiation therapy was administered 5 days a week for 6 weeks to the primary tumor and regional lymph nodes (40 Gy), followed by a boost to the tumor and involved nodes (20 Gy). A total of 15 patients (11 males and 4 females)with a median age of 61 years were enrolled in the study. Patients had stage IIIA (nine) or IIIB (six) disease. The principal dose-limiting toxicity was esophagitis, and the maximum-tolerated dose of docetaxel with concurrent radiation therapy was 30 mg/m^2. Seven patients achieved a partial response for an overall response rate of 47% [66].

Koukourakis et al. [58] investigated the radiosensitizing effects of docetaxel and concomitant radiotherapy in 30 patients (all male) with advanced NSCLC, 18 of whom had stage IIIB disease and 12 who had stage IV disease. The median age was 65 years. Patients were treated with a 20-minute infusion of docetaxel, 20 to 40 $mg/m^2/wk$. Radiation therapy was administered at $5d/wk$ for 5 weeks to a total dose of 60 to 64 Gy using a concomitant boost technique. Esophagitis, asthenia, and anorexia were the dose-limiting toxicities noted at the docetaxel dose of $40 mg/m^2$. Complete responses were seen in 8 (27%) patients and partial responses in 15 (50%) for an overall response rate of 77%. The recommended phase II dose was $30 mg/m^2$ of docetaxel.

A phase II trial of docetaxel and radiation therapy in 35 patients with stage IIIA or IIIB NSCLC was conducted by Koukourakis et al. [67]. The dose of docetaxel, $30 mg/m^2/wk$, was established from their previous phase I trial [58]. In contrast to the phase I study, conventionally fractionated radiotherapy was used to achieve better tolerance, fewer side effects, and similar efficacy. Patients received docetaxel, $30 mg/m^2$, as a 1-hour infusion weekly for 6 weeks with concurrent radiation therapy ($2\,Gy/d$ for 5 days a week for a total dose of 64 Gy over 6.5 weeks). The median age of participants was 64 years, and 33 of the 35 patients were male. The main side effects were asthenia and radiation-induced esophagitis, which required 2-week treatment delays in 6 patients and minor delays of less than 1 week in 11 patients. Complete responses were seen in 12 of the 35 patients (34%) and partial responses in 16 (46%), for an overall response rate of 80%. The overall and local progression-free survival at 1 year was 60% and 48%, respectively.

Last but not least, combined chemoradiotherapy with taxane is widely used in many treatment protocols for various cancer types. Protocol using Carboplatin, Paclitaxel, and Radiation Therapy for Neoadjuvant Treatment of Esophageal and Gastroesophageal Carcinomas [68] is one example that taxanes are used officially in therapeutic protocols. Another example is a Cancer Protocol

using Carboplatin and Paclitaxel with Radiation Therapy for the Treatment of Locally Advanced Non-Small Cell Lung Cancer [1].

Chapter 4

Radiotherapy Simulations

Radiotherapy simulations were performed in this first section of our computational study of combination therapies in growing tumors. More specifically, the mathematical model described above in Sections 2.2-2.7 was used in our analysis of radiotherapy. Some extensions were developed to the aforementioned mathematical formulation to incorporate the term radiation in this continuum tumor model. Then the extended model formulation was added to Comsol Multiphysics, ® software concluding in our numerical results.

4.1 Problem Statement

We have developed the model based on Hubbard and Byrne [22]. We extended the model that we have already described in Chapter 2 with an additional term that models radiotherapy using insight from Boemo and Byrne [69], which assumed that the death rate of uninfected tumor cells caused by radiation is an exponentially decaying function of time with half-life r_t^{-1} which is written as follows:

$$R = k_{rad}\theta_2 \mathcal{H}\left(t - t_{rad}\right) e^{-r_t(t-t_{rad})}. \tag{4.1}$$

In Equation (4.1) k_{rad} is the strength of radiotherapy dose, θ_2 is the volume fraction of the tumour cells, $\mathcal{H}$ denotes the Heaviside step function where $\mathcal{H}(x) = 1$ if $x > 0$ and $\mathcal{H}(x) = 0$ otherwise. Moreover, t_{rad} is the time that each dose of radiotherapy starts, and r_t is the half-life of tumor cell death due to radiotherapy.

4.2 The Linear-Quadratic Formula of Radiotherapy

In the above attempt to find the terms k_{rad} and r_t from Equation (4.1), the Linear-Quadratic (LQ) Model of Radiotherapy helps us. The LQ model quantifies the Survival Fractions (SF) of cell colonies given a specific radiation dose, and it provides a simple and practical relationship between them and takes the form of an exponential function with a linear, and a quadratic term [70, 71].

For modeling the SF of each cell, at the specific dose level, d, is first calculated by Fowler [72] using the LQ cell survival model:

$$SF = e^{n\left(-\alpha d - \beta d^2\right)}. \tag{4.2}$$

where n is the number of fractions, d is the size of each dose fraction, so $n \times d$ is the total dose measured in Grays. Lastly, α and β are the linear and quadratic coefficients, respectively with $\alpha(Gy)$ and $\beta(Gy^2)$ [72, 73]. These two parameters are associated with cell-specific radiosensitivity, and for many tumors, the $\frac{\alpha}{\beta}$ ratio is estimated or known from empirical observations [73].

In a simulation, each cell is assigned specific values for α and β according to the intrinsic radiosensitivity of the cell type modeled [74] According to Williams et al., [75] for rapidly proliferating normal tissues and for tumors too, it is reasonable for the ratio $\frac{\alpha}{\beta}$ to be chosen equal to 10 [75].

$$\frac{\alpha}{\beta} = 10. \tag{4.3}$$

The LQ model has become the dominant mathematical model in modeling the survival fraction of cells in preclinical studies, partly motivated by its close links to clinical observations. Studies of fractionation effects in tissues and tumors demonstrated that not only did the LQ model effectively reproduce in vitro survival but also the effect of clinical fractionation, providing a consistent way to interpret these effects [76, 77].

4.3 Parameters Fitting

The attempt to find the terms k_{rad} and r_t from Equation (4.1) is continued, but first, it is reasonable for the two parameters α and β to be found, which are associated with the LQ model Equation (4.2). Higashi et al., [78] applied an irradiation dose of 30 Grays for a single fraction. After radiotherapy in the irradiated group, viable cell number decreased exponentially and showed a 6.25-fold decline from Day 0 to Day 12. So on 12^{th} Day, the cells were 6.25 times less compared with the initial cell population. In other words, the SF of the cells was:

$$SF = 0.16 = 16\%. \tag{4.4}$$

Applying (4.4) in the LQ model Equation (4.2) and combining the Equation (4.3) a system of equations was solved in order to the parameters to be found α and β.

$$\begin{cases} SF = 0.16 \\ \frac{\alpha}{\beta} = 10 \end{cases} \longrightarrow \begin{cases} 0.16 = exp\left[n\left(-\alpha \times d - \beta \times d^2\right)\right] \\ \frac{\alpha}{\beta} = 10 \end{cases}. \tag{4.5}$$

Since the clinical study reports a single fraction, we set $n = 1$ and $d = 30$ Grays for the irradiation dose, which are applied from Higashi et al. [78].

$$\begin{cases} 0.16 = exp\left[1\left(-\alpha \times 30 - \beta \times 30^2\right)\right] \\ \frac{\alpha}{\beta} = 10 \end{cases} \longrightarrow \tag{4.6}$$

$$\begin{cases} 0.16 = exp\left[-\alpha\left(1 + \frac{30\beta}{\alpha}\right)30\right] \\ \frac{\alpha}{\beta} = 10 \end{cases} \longrightarrow \begin{cases} \alpha = 0.015 \\ \beta = 0.0015 \end{cases} .$$

If we assume that cancer cells are uniformly distributed, then cancer cell death rate due to radiotherapy using Equation 4.1 can be formulated as:

$$\frac{d\theta_2}{dt} = -k_{rad}\theta_2 e^{-r_t(t-t_{rad})}. \tag{4.7}$$

Integrating Equation (4.7) :

$$\frac{1}{\theta_2}\, d\theta_2 = -k_{rad}\, \exp\left(-r_t\left(t - t_{rad}\right)\right) dt \longrightarrow$$

$$\left[\ln \theta_2\right]_{\theta_{2(0)}}^{\theta_2} = -k_{rad} \int_{t_{rad}}^{t} \exp\left(-r_t\left(t - t_{rad}\right)\right) dt \longrightarrow \tag{4.8}$$

$$\frac{\theta_2}{\theta_2(0)} = \exp\left[-\frac{k_{rad}}{r_t}\left[1 - \exp\left(-r_t\left(t - t_{rad}\right)\right)\right]\right].$$

The final form of Equation (4.8) was applied in MATLAB in order to fit parameters, k_{rad} and r_t against the LQ model (Equation 4.2). From Higashi [78] the concentration of tumor cells decreases 84% in 12 days, thus $\frac{\theta_2}{\theta_2(0)} = 0.16$. Hence, our parameter fitting aims at fitting parameters, k_{rad} and r_t so that $t = 12$ the concentration of θ_2 cells is $\frac{\theta_2}{\theta_2(0)} = 0.16$. Our goal was achieved, as can be confirmed in Figure 4.1

The fitting process produced the following values for r_t and k_{rad} are 0.5 and 0.91, respectively. Parameter $r_t = 0.5$, which denotes half-life cell death due to radiotherapy, remains fixed in our simulations because it depends particularly on the interaction among tumor cells. The value k_{rad}, which denotes the strength of radiotherapy, depends on the dose of irradiation applied every time, so it can be modified when applying a different schedule for radiotherapy (described below). As a result, from the above Parameter Fitting performed in MATLAB, the value for r_t that arose was used in our radiotherapy schedule, too, in which the dose of radiotherapy varies from the dose that Higashi et al. [78] applied in his research but r_t remains the same because there is no dependence on the strength of the radiation dose.

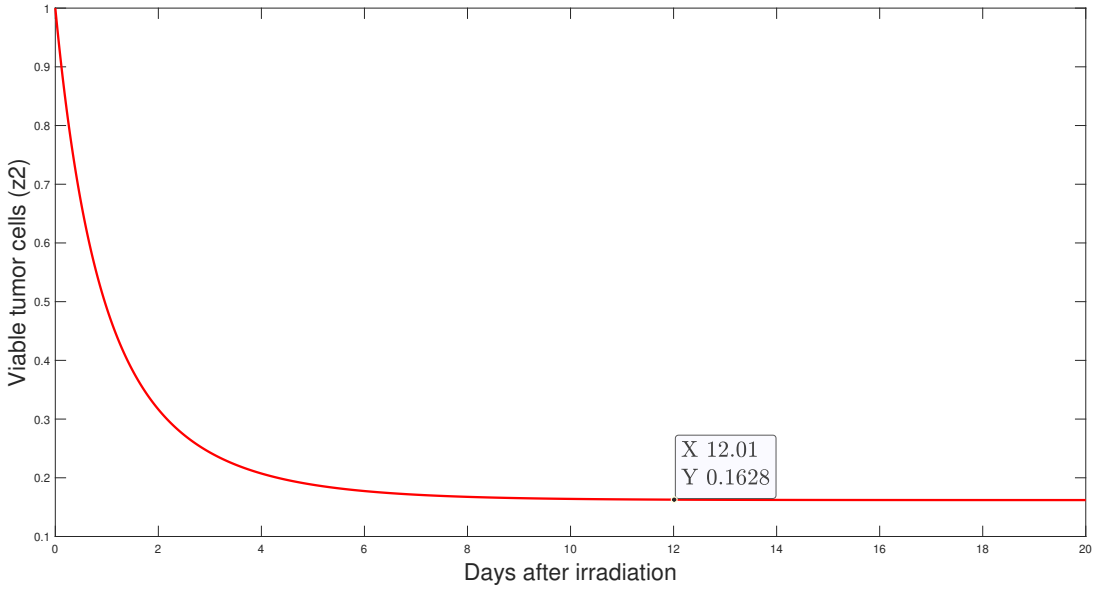

Figure 4.1: *Schematic representation of the viable tumor cells after irradiation.*

In this first section of our study, the radiation therapy simulations based on the schedule consisted of 1.5 Gy in 30 fractions (total dose, 45 Gy) administered 5 days a week, with a break at the weekends, for 6 weeks [79, 80]. Applying this schedule in the LQ model Equation (4.2) to find the total Survival Fraction (SF) after irradiation, we compute $SF = 0.45$ =45%. Taking for granted the radiotherapy schedule described above, the $SF = 0.45$ occurred for this trial, and the parameter $r_t = 0.5$ were applied in COMSOL. The parameter k_{rad} is not known because it depends on the radiation dose, so many values were tested to find the appropriate one.

4.4 Inserting the Mathematical Model into Comsol Multiphysics

Before presenting the way that the mathematical model with radiotherapy is implemented into Comsol Multiphysics ®, we describe the computational tools used in this thesis. A commercial finite elements code, Comsol Multiphysics, Version 5.3a, was used to implement the model. The tissue is modeled as a circular domain with (dimensionless) radius, $R_{tissue} = 16$.

To implement the mathematical model in COMSOL, various models were used that are already in the software as well as the form of Coefficient Form PDE, which provides a general interface for specifying and solving many well-known PDEs in the coefficient form. More precisely, the interface "Transport of Diluted Species" (tds) of Comsol Multiphysics ® was used for the mass balance equations of healthy and cancer cell phases and the blood vessel phase. The module of the "Transport of Diluted Species" was used to calculate the concentration field of a dilute solute in a solvent. Transport and reactions of the species dissolved in a gas, liquid, or solid can be handled with this interface. The driving forces for transport can be diffusion by Fick's law, convection when coupled to a flow field, and migration when coupled to an electric field. The interface supports the

simulation of transport by convection and diffusion in 1D, 2D, and 3D, as well as for axisymmetric components in 1D and 2D. The dependent variable is the molar concentration, c. In our case, "convection" is chosen as a Trasport Mechanism to be described better [81]. The equation form used in our case is the following:

$$\frac{\partial c_i}{\partial t} + \nabla \cdot (-D_i \nabla c_i + \vec{u_i} c_i) = R_i, \qquad i = 1, 2, 3. \tag{4.9}$$

The term $\nabla \cdot (-D_i \nabla c_i)$ denotes the diffusion mechanism, which has no effect on the movement of the fluid and the term D_i is practically zero. The conservative form of the equation is chosen as suitable to render the dynamic behavior of a compressible fluid such as the fluid studied. Linear shape functions were used to discretize the mass balance equations. A source term (Reaction) R_i was added to the basic model to describe the source terms q_i, with $i = 1, 2, 3$.

The boundary conditions, which have been implemented in our mathematical model formulation, have already been mentioned in Section 2.7 but shortly mentioned here too. Boundary conditions were set, along the length of the boundary as an "Open Boundary". The equation of this boundary condition, given the negligible factor, D_i is:

$$c_i = c_{i,borderline}, \text{ for } \vec{u_i} \cdot \vec{n} < 0, \text{ with } i = 1, 2, 3. \tag{4.10}$$

where $\vec{n}$ is the outward-pointing unit normal to the boundary. Equation (4.10) ensures the supply of each component to the boundary sections whenever there is a mass inflow. The "Coefficient Form PDE" interfaces with shape functions were used to calculate velocities through the momentum conservation equations. The boundary conditions chosen for the calculation equations of $\vec{u_i}$ with $i = 1, 2, 3$ are the "Zero Flux" conditions, that is, of the form:

$$-\vec{n} \cdot (-c \nabla \vec{u_i} - \alpha \vec{u_i} + \gamma) = 0, \text{ with } i = 1, 2, 3. \tag{4.11}$$

while, for the last momentum conservation equation corresponding to the extracellular material phase, the Dirichlet-type boundary conditions were chosen along the boundary:

$$\vec{u_4} = 0. \tag{4.12}$$

As in the case of the velocity calculation, the pressure calculation of p_4 was carried out by inserting the continuity equations for the four-phase mixture into the "Coefficient Form PDE" model. In this case, linear shape functions are chosen.

The pressures of the two cell phases (healthy and cancer cells) as well as the volume fraction of the extracellular material phase are calculated algebraically.

Finally, the "Transport of Diluted Species" interface of Comsol Multiphysics was used again to calculate the nutrient concentration c. The stationary form of the equation is chosen in this case, while additional transport mechanisms are not taken into account. As in the case of mass balances of the volume phases, a source term (Reaction) is added to describe the source term q_c. Along the

Table 4.1: *Dimensionless parameter values for the radiotherapy simulations.*

Parameter	Value	Description
k^*_{rad}	0.22	Strength of radiotherapy
r^*_t	0.5	Half-life of tumour cell death due to radiotherapy
t^*_{rad}	60	Time that radiation starts its activity
T^*_p	1	Time period between two doses of radiotherapy

length of the boundary, a "Zero Flux" boundary condition of the component mass is chosen. The form of the described equation and the boundary condition for the nutrient is as follows:

$$\nabla \cdot (-D_c \nabla c) = R_c \tag{4.13}$$

and

$$-\vec{n} \cdot (-D_c \nabla c) = 0, \tag{4.14}$$

respectively.

As mentioned above, radiotherapy simulations were performed in COMSOL, and many simulations were made in order to select an appropriate value for the strength of radiotherapy so that the SF be 0.45 or 45%. Eventually, the suitable value was $k_{rad} = 0.22$. The resulting diagram for this computation analysis is illustrated and described in Section 4.5.

To incorporate the radiotherapy effect in the mathematical model presented in Sections 2.2-2.7, we modify the mass balance equations as follows:

$$\begin{aligned} \frac{\partial \theta_2}{\partial t'} + \vec{\nabla}' \cdot \left(\theta_2 \vec{u_2}'\right) = & \underbrace{k^*_{1,2}\theta_2\theta_4 \left(\frac{c'}{c^*_p + c'}\right)}_{\text{cell birth}} - \underbrace{k^*_{2,2}\theta_2 \left(\frac{c^*_{c_1} + c'}{c^*_{c_2} + c'}\right)}_{\text{cell death}} \\ & \underbrace{- k^*_{rad} \exp\left[-r^*_t \left(t' - t^*_{rad}\right)\right] \theta_2 \cdot \text{ONOFF}}_{\text{radiotherapy}} \end{aligned} \tag{4.15}$$

Equation (4.15) is in its dimensionless form because this is the form of equation incorporated in COMSOL. The dimensionless variable is t' and the dimensionless parameters are k^*_{rad}, r^*_t and t^*_{rad}. The value and the description for each parameter are given in Table 4.1.

The $ONOFF$ term is a controller that indicates the beginning of radiotherapy, so it is activated when $t^*_{rad} = 60$ in our case.

$$\text{ONOFF} = \begin{cases} \text{ON} \ \ 1 \\ \text{OFF} \ \ 0 \end{cases} \tag{4.16}$$

Closing this Section, the Events (ev) interface was added to our mathematical model because it was used to create solver events. In our case, the fractions of radiotherapy are simulated as events because each fraction occurs at a different time. In other words, each event (fraction) starts at a later time compared with the previous events and at an earlier time compared with the future events. For example, for Event 1, the event starts at $t_i = t^*_{rad}$, for Event 2, the event starts at $t_i = t^*_{rad} + T^*_p$, for Event 3, the event starts at $t_i = t^*_{rad} + 2 \cdot T^*_p$, etc. The parameter T^*_p, as reported in Table 4.1, is the time period between two consecutive doses of radiotherapy.

4.5 Numerical Results

Before we proceed with the presentation of the radiotherapy results, we briefly report information regarding the computational mesh and the solvers used to solve the problem.

The tissue is modeled as a circular domain with (dimensionless) radius, $R_{tissue} = 16$. The computational mesh is generated with the Extra fine mesh option of the Fluid dynamics mesh category. The computational mesh is also an unstructured mesh generated with the Delaunay Triangulation method for the grid's tessellation. The model contains a total of approximately 20.000 elements, which results in approximately 400.000 degrees of freedom. The maximum element surface is equal to 0.416 square units, and the minimum element surface is equal to 0.0048 square units for the present section. In Figures 4.2a and 4.2b, the computational grid for the examined tissue is depicted.

The direct MUMPS direct solver was chosen to solve the system. The MUMPS solver works on linear systems of the form $Ax = b$ and uses several preordering algorithms to permute the columns and thereby minimize the fill-in [82]. Furthermore, the BDF solver was chosen for the time integration. The Segregated solution approach was chosen. This way of solving does not deal with all the variables at once; instead, it separates them into two or more groups (segregated steps). Each group is solved sequentially at each time step, reducing the required memory. In this model, the system of equations was divided into three groups. In the first step, the mass balance equations of the four phases were introduced; in the second step, the momentum balance equations were applied; and in the third step, the mass balance equation of the nutrient component was applied. The segregated solution allows the definition of a lower limit for the tumor cell volume fraction to prevent the system from going to zero or having negative values for the volume fraction. For this purpose, the lower limit was set equal to $1 \cdot 10^{-15}$ [83].

In the present section, the results from COMSOL are presented. More precisely, the "Surface Integration" was utilized through the Surface Integration option of the "Derived Values" to calculate the total number of cancer cells on the domain's surface. The integral $\iint_S \theta_2 \, dxdy$ calculates the total surface area occupied by cancer cells; thus, it is related to the total number of living cancer cells. As illustrated in Figure 4.3, the number of living cancer cells (SF) decreases when irradiation is applied.

To recap those mentioned above, the strength of the irradiation dose applied in our model is $k_{rad} = 0.22$. Radiotherapy starts on the 60^{th} day (t=60) and ends after 6 weeks (t=101) with 5 days a week of irradiation to be applied to the patient with a break (2 days) at the weekends.

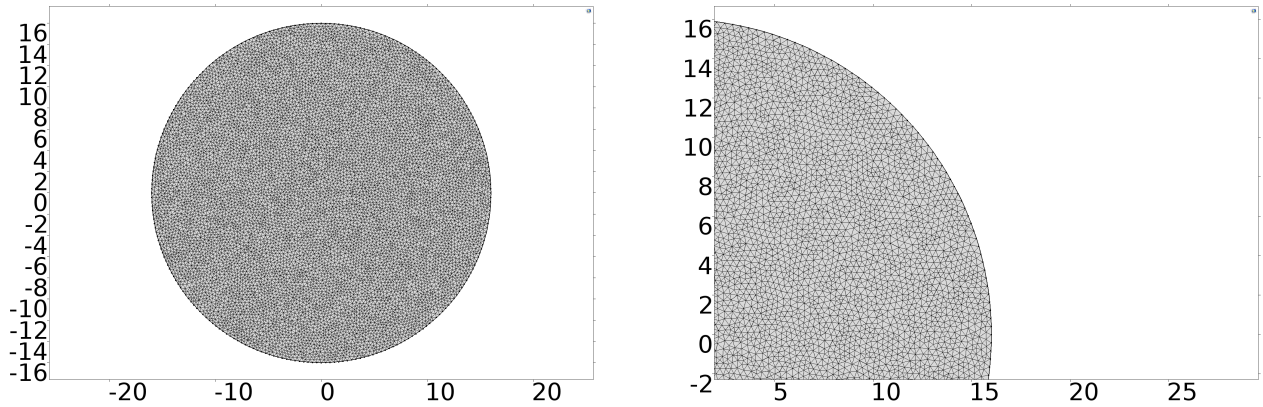

(a) *Mesh for the examined tissue* (b) *More detailed mesh for the same tissue*

Figure 4.2: *Computational Grid*

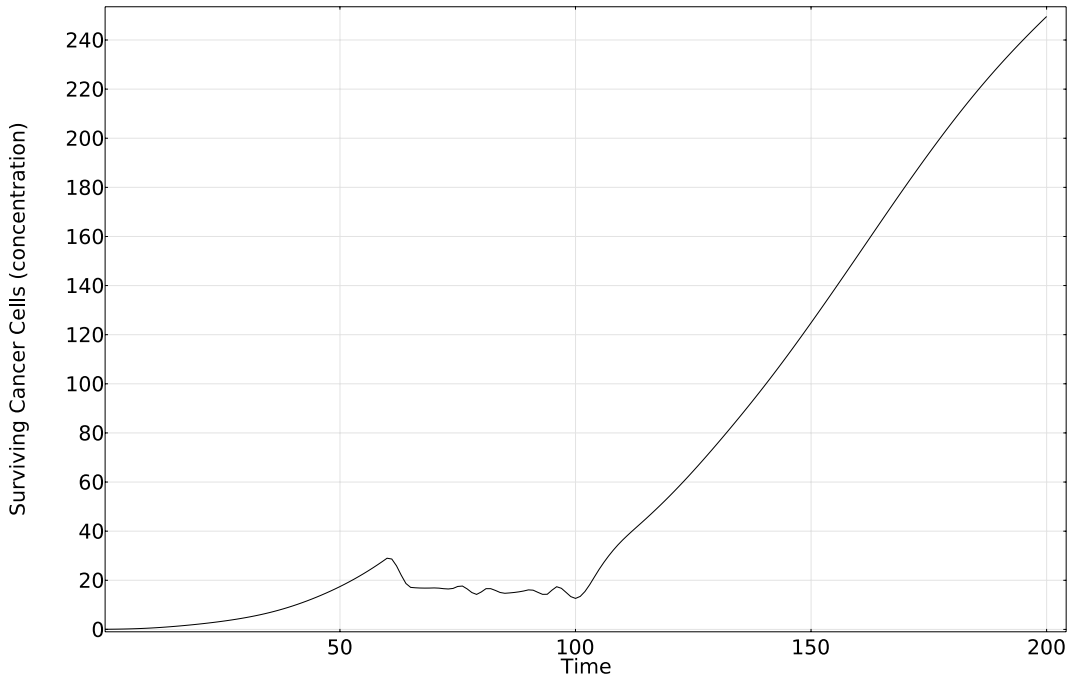

Figure 4.3: *The Value of* $\iint_S \theta_2 \, dxdy$ *in relation to Time(days) when radiotherapy is applied in the tissue.*

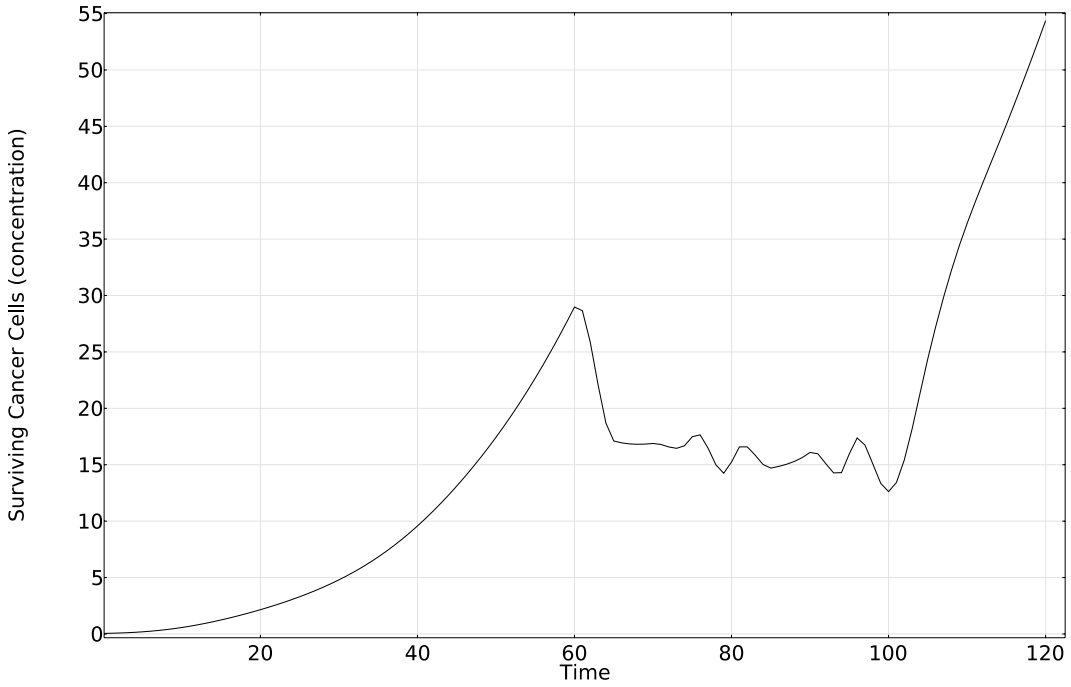

Figure 4.4: *The Value of* $\iint_S \theta_2 \, dxdy$ *in relation to Time(days) when radiotherapy is applied in the tissue in a more detailed depiction.*

As shown in Figure 4.3, throughout irradiation is applied the concentration of surviving cancer cells remains at low levels. The survival fraction in our case is $SF = 45\%$, as derived from the application of the dose of 1.5 Gray/fraction in the LQ model for a total of 30 fractions. Indeed, the decrease in the concentration of cancer cells comparing the number of cancer cells when radiotherapy starts and the remaining surviving cancer cells when radiotherapy ends is a 45% decrease. Specifically, at $t = 60$ the concentration is ~ 29 and at $t = 101$ is ~ 13.

Applying radiotherapy in the growing tumor model, oscillations were observed during the fractions. This can be explained because when irradiation is applied, the concentration of cancer cells decreases rapidly. When the delivery of irradiation to the patient stops, i.e., at the weekends, the surviving cancer cells proliferate again. This fluctuation in the population of tumor cells creates these oscillations.

Last but not least, a more detailed illustration of applied radiotherapy is depicted in Figure 4.4. It is clear that the tumor cells decrease directly when irradiation is applied and remain at low levels throughout radiotherapy. When irradiation is not applied anymore, the surviving cancer cells increase rapidly. This means that the effect of radiation doesn't remain in the tissue since radiotherapy is completed. The result is reasonable, i.e., the curve decreases and increases rapidly when radiation starts and ends, respectively, because this is the formalism of radiation. In other words, when irradiation is applied, the cancer cells that have to die are dying directly with no delay. In closing, the form of this continuum model enables us to regulate the Survival Fraction of tumor cells. For example, in our case, the SF equals $SF = 45\%$ and k_{rad} equals $k_{rad} = 0.22$. Now, in another case, the SF may be 50% or 30%, so the only thing that we have to do in this present model is to decrease or increase, respectively, the value of the parameter k_{rad}.

Chapter 5

Combined Chemoradiotherapy Simulations

Combined chemoradiotherapy simulations were performed in this second section of our computational study of combination therapies in growing tumors. More specifically, the mathematical model described above in Sections 2.2-2.7 is based on the work of Breward et al. [20] and Hubbard and Byrne [22], combined with the radiotherapy term described in Section 4.4 was used in our computational analysis. Moreover, we incorporate chemotherapy based on the model of Lampropoulos et al. [23]. Finally, this model formulation was added to the environment of Comsol Multiphysics ® software concluding our numerical results.

5.1 The Established Cancer Protocol

Our chemoradiotherapy simulations are based on a cancer protocol to examine the consequences to cancer cells. More precisely, this cancer protocol is for treating locally advanced Non-Small Cell Lung Cancer (NSCLC) using cytotoxic therapy combined with radiation therapy [1]. The cytotoxic drug is Taxane (Docetaxel), concurrent with radiation therapy. The application of this way of treatment was selected because, as mentioned in Section 3.3 Docetaxel (Taxotere) has been studied concurrently with radiation with favorable results, and this combination of therapy (Taxane+Radiotherapy) is gaining prominence in preclinical and clinical studies.

The treatment process that is followed is :

- 60 Gy external beam thoracic radiotherapy in 30 fractions over 6 weeks, which means 2 Gy/fraction.
- 45 mg/m^2 Docetaxel starting the first day of radiation therapy and repeating weekly $\times$ 6 weeks, concurrent with radiation therapy.

5.2 Importing the Modeling of Cytotoxic Therapy in our Mathematical Model

In this section, we extend the two-dimensional, continuous, multiphase, mathematical model for vascular tumor growth described in Chapter 2 to incorporate cytotoxic therapy.

In order to model the cytotoxic therapy and study the efficiency of chemotherapeutic treatment, the current model has been extended to incorporate the effect of a cytotoxic drug (e.g., taxanes, with Docetaxel a prime example of this drug category) in the dynamics of a growing tumor. The drug is treated as a diffusible species, which is administered to the body intravenously [23, 84], thus delivered to the tissue via the circulatory system and subsequently exponentially depleting in the bloodstream due to hepatic metabolism [23, 85]. The drug gets consumed by healthy and cancer cells alike, at a rate described by the Michaelis–Menten kinetics, and selectively targets fast proliferating cells. Finally, it is assumed that the drug's decay rate in the tissue is proportional to its concentration and modeled by first-order kinetics. Combining the above, the following mass balance equation for the drug is obtained:

$$\begin{aligned} -D_w \nabla^2 w = k_{rep,d}\, \theta_3\, max(w_c - w, 0) - k_{d,d} \cdot w \\ -\frac{w}{w_m + w} \sum_{i=1,2} k_{cn,i} \theta_i \mathcal{H}\left(l_i - l_{cr}, h_d\right), \end{aligned} \tag{5.1}$$

where w is the concentration of the cytotoxic drug, D_w is the diffusion coefficient of the drug, $k_{rep,d}$ denotes the drug replenishment (due to the surrounding vasculature) rate constant, $k_{d,d}$ is the drug decay rate constant in the tissue, w_m denotes the value at which drug consumption rate by cells is half-maximal, $k_{cn,i}$ are the constants of drug consumption by healthy ($i = 1$) and cancer cells ($i = 2$), respectively and l_{cr} is the limit value that sets the level distinguishing the proliferating and quiescent state of a cancerous cell.

The concentration of the drug in the bloodstream,w_c, decays exponentially in time:

$$w_c = w_v e^{-k_{el}(t - t_{inj})}, \tag{5.2}$$

with w_v denoting the concentration of the drug in the bloodstream at the moment of the injection, t_{inj}, and k_{el} is the rate constant for the drug expulsion from the bloodstream.

In order to confine the drug to target only the fast-proliferating cells, the smooth transition Heaviside step function $\mathcal{H}$ is utilized with h_d, the smoothness parameter for cytotoxic therapy:

$$\mathcal{H}\left(p, \epsilon\right) = \frac{1}{2}\left(1 + tanh\frac{p}{\epsilon}\right), \qquad \epsilon \ll 1, \tag{5.3}$$

with ϵ denoting the blood vessel volume fraction at which the angiogenesis rate is half-maximal.

By adopting this approach, one can distinguish whether mitosis is taking place for healthy ($i = 1$) or cancer cells ($i = 2$). In particular, the following expression quantifies whether healthy and cancer cells have enough sources to divide or remain in a quiescent state:

$$l_i = k_{m,i}\theta_4 \frac{c}{c_p + c}, \quad \text{for } i = 1, 2, \tag{5.4}$$

where c is the nutrient concentration, $k_{m,i}$ is cell mitosis rate constant and c_p is the threshold nutrient concentration for mitosis.

Finally, Neumann-type boundary conditions are imposed for the drug (similarly to the diffusible nutrient case):

$$\nabla w \cdot \vec{n} = 0 \tag{5.5}$$

where $\vec{n}$ is the outward-pointing unit normal to the domain boundary.

To incorporate the effect of the cytotoxic drug on healthy and cancer cells, the source terms in Equations 2.4 and 2.5 are modified respectively, taking the following form:

$$\begin{aligned} q_1 = \underbrace{k_{1,1}\theta_1\theta_4\left(\frac{c}{c_p + c}\right)}_{\text{cell birth}} - \underbrace{k_{2,1}\theta_1\left(\frac{c_{c_1} + c}{c_{c_2} + c}\right)}_{\text{cell death}} \\ - \underbrace{k_{ap,1}\theta_1 \frac{w}{w_m + w}\mathcal{H}\left(l_1 - l_{cr}, h_d\right)}_{\text{effect of the cytotoxic drug}}, \end{aligned} \tag{5.6}$$

$$\begin{aligned} q_2 = \underbrace{k_{1,2}\theta_2\theta_4\left(\frac{c}{c_p + c}\right)}_{\text{cell birth}} - \underbrace{k_{2,2}\theta_2\left(\frac{c_{c_1} + c}{c_{c_2} + c}\right)}_{\text{cell death}} \\ - \underbrace{k_{ap,2}\theta_2 \frac{w}{w_m + w}\mathcal{H}\left(l_2 - l_{cr}, h_d\right)}_{\text{effect of the cytotoxic drug}}, \end{aligned} \tag{5.7}$$

where $k_{ap,1}$ and $k_{ap,2}$ are the drug-induced apoptosis rate constants for healthy and cancer cells, respectively.

5.3 Nondimensionalisation

For the dimensionless form of the drug's mass balance, the concentration in the plasma immediately after injection, w_v, is considered as a characteristic drug concentration and is nondimensionalized using:

$$w^{'} = \frac{w}{w_v}. \tag{5.8}$$

The resulting dimensionless mass balance for the drug is:

$$\begin{aligned} -D_w^* \nabla^2 w^{'} &= k_{rep,d}^* \, \theta_3 \, max(w_c^* - w^{'}, 0) - k_{d,d}^* \cdot w^{'} \\ &- \frac{w^{'}}{w_m^* + w^{'}} \sum_{i=1,2} k_{cn,i}^* \theta_i \mathcal{H} \left(l_i^* - l_{cr}^*, h_d^* \right), \end{aligned} \tag{5.9}$$

where

$$\begin{aligned} D_w^* = \frac{D_w}{k_{rep} R_0^2}, \;\; k_{rep,d}^* = \frac{k_{rep,d}}{k_{rep}}, \;\; k_{d,d}^* = \frac{k_{d,d}}{k_{rep}}, \\ w_m^* = \frac{w_m}{w_v}, \;\; h_d^* = \frac{h_d}{k_{m,1}}, \;\; l_{cr}^* = \frac{l_{cr}}{k_{m,1}}, \end{aligned} \tag{5.10}$$

where R_0 is a typical length scale; in our case, R_0 is the radius of the initial cancerous seed,

and

$$l_i^* = \frac{l_i}{k_{m,1}} = k_{m,i}^* \theta_4 \frac{c^{'}}{c_p^* + c^{'}}, \;\; k_{cn,i}^* = \frac{k_{cn,i}}{k_{rep} w_v} \;\; \text{for i=1,2.} \tag{5.11}$$

The dimensionless concentration of the drug in the bloodstream, w_c, decays exponentially in time (i.e., clearance rate of the drug) is:

$$w_c^* = e^{-k_{el}^* \left(t^{'} - t_{inj}^* \right)}, \tag{5.12}$$

where

$$k_{el}^* = \frac{k_{el}}{k_{m,1}}, \;\; t_{inj}^* = t_{inj} \cdot k_{m,1} \;\; , t^{'} = k_{m,1} \cdot t \;\; \text{and} \;\; w_c^* = \frac{w_c}{w_v} \tag{5.13}$$

The modified dimensionless source terms for the case of cytotoxic therapy on healthy and cancer cells are:

$$q_1^{'} = \underbrace{\theta_1\theta_4\left(\frac{c^{'}}{c_p^* + c^{'}}\right)}_{\text{cell birth}} - \underbrace{k_{2,1}^*\theta_1\left(\frac{c_{c_1}^* + c^{'}}{c_{c_2}^* + c^{'}}\right)}_{\text{cell death}} - \underbrace{k_{ap,1}^*\theta_1\frac{w^{'}}{w_m^* + w^{'}}\mathcal{H}\left(l_1^* - l_{cr}^*, h_d^*\right)}_{\text{effect of the cytotoxic drug}}, \tag{5.14}$$

$$q_2^{'} = \underbrace{k_{1,2}^*\theta_2\theta_4\left(\frac{c^{'}}{c_p^* + c^{'}}\right)}_{\text{cell birth}} - \underbrace{k_{2,2}^*\theta_2\left(\frac{c_{c_1}^* + c^{'}}{c_{c_2}^* + c^{'}}\right)}_{\text{cell death}} - \underbrace{k_{ap,2}^*\theta_2\frac{w^{'}}{w_m^* + w^{'}}\mathcal{H}\left(l_2^* - l_{cr}^*, h_d^*\right)}_{\text{effect of the cytotoxic drug}}, \tag{5.15}$$

where

$$k_{ap,i}^* = \frac{k_{ap,i}}{k_{m,1}} \text{ for 1=1,2.} \tag{5.16}$$

5.4 Implementation of Cytotoxic Therapy Model into Comsol Multiphysics

Before adding the Cytotoxic Therapy to the mathematical formulation in the environment of Comsol Multiphysics ®, it is essential to describe how radiotherapy's parameters r_t and k_{rad} were adapted to the current irradiation dose. By applying the LQ model's Equations 4.2 and 4.6 and applying the dose of radiation 30 Gy, the survival fraction of viable cancer cells after radiotherapy was $SF = 0.33$ or 33%. As is already mentioned, the value of r_t remains constant at $r_t = 0.5$ because there is no effect from radiation dose; however, the value of the strength of radiation changes because it depends on the current radiation dose. Many simulations were performed employing different values of k_{rad} in the environment of Comsol before resulting in the appropriate one that gives SF=0.33 or 33%. The best values for parameters to describe the current irradiation dose of the treatment process are $r_t = 0.5$ and $k_{rad} = 0.23$.

All computations were performed in the environment of COMSOL Version 5.3a using the same tools described in Section 4.4. After inserting the cytotoxic therapy in the mathematical model into Comsol Multiphysics ®, there are some additional terms in some of the equations. The source

terms of healthy and cancer cells are modified accordingly.

The mass balance equation for healthy cells takes the following form:

$$\frac{\partial \theta_1}{\partial t^{'}} + \vec{\nabla}^{'} \cdot \left(\theta_1 \vec{u_1}^{'}\right) = \underbrace{\theta_1 \theta_4 \left(\frac{c^{'}}{c_p^* + c^{'}}\right)}_{\text{cell birth}} - \underbrace{k_{2,1}^* \theta_1 \left(\frac{c_{c_1}^* + c^{'}}{c_{c_2}^* + c^{'}}\right)}_{\text{cell death}} - \underbrace{k_{ap,1}^* \theta_1 \frac{w^{'}}{w_m^* + w^{'}} \mathcal{H}\left(l_1^* - l_{cr}^*, h_d^*\right)}_{\text{effect of the cytotoxic drug}}, \tag{5.17}$$

where

$$l_1^* = k_{m,1}^* \theta_4 \frac{c^{'}}{c_p^* + c^{'}}. \tag{5.18}$$

The mass balance equation for cancer cells takes the following form:

$$\frac{\partial \theta_2}{\partial t^{'}} + \vec{\nabla}^{'} \cdot \left(\theta_2 \vec{u_2}^{'}\right) = \underbrace{k_{1,2}^* \theta_2 \theta_4 \left(\frac{c^{'}}{c_p^* + c^{'}}\right)}_{\text{cell birth}} - \underbrace{k_{2,2}^* \theta_2 \left(\frac{c_{c_1}^* + c^{'}}{c_{c_2}^* + c^{'}}\right)}_{\text{cell death}} - \underbrace{k_{rad}^* \exp\left[-r_t^* \left(t^{'} - t_{rad}^*\right)\right] \theta_2}_{\text{radiotherapy}} - \underbrace{k_{ap,2}^* \theta_2 \frac{w^{'}}{w_m^* + w^{'}} \mathcal{H}\left(l_2^* - l_{cr}^*, h_d^*\right)}_{\text{effect of the cytotoxic drug}}, \tag{5.19}$$

where

$$l_2^* = k_{m,2}^* \theta_4 \frac{c^{'}}{c_p^* + c^{'}}. \tag{5.20}$$

Moreover, the cytotoxic drug (Taxane) is added, and the form of the dimensionless mass balance for the drug is the following:

$$-D_w^* \nabla^2 w^{'} = k_{rep,d}^* \, \theta_3 \left(w_c^* - w^{'}\right) - k_{d,d}^* \cdot w^{'} - \frac{w^{'}}{w_m^* + w^{'}} \left[k_{cn,1}^* \theta_1 \mathcal{H}\left(l_1^* - l_{cr}^*, h_d^*\right) + k_{cn,2}^* \theta_2 \mathcal{H}\left(l_2^* - l_{cr}^*, h_d^*\right)\right]. \tag{5.21}$$

Table 5.1: *Dimensionless parameter values used in the simulations with cytotoxic drug* [23].

Parameter	Value	Description
D_w^*	0.1	Drug diffusion coefficient
$k_{ap,1}^*$	60	Healthy cell drug induced apoptosis rate constant
$k_{ap,2}^*$	60	Cancer cell drug induced apoptosis rate constant
$k_{cn,1}^*$	0.209	Drug consumption by healthy cells rate constant
$k_{cn,2}^*$	0.209	Drug consumption by cancer cells rate constant
$k_{rep,d}^*$	1	Drug replenishment constant
k_{el}^*	3.36	Drug expulsion rate constant
$k_{d,d}^*$	$4.27 \cdot 10^{-3}$	Drug decay rate constant
w_m^*	2	Drug concentration at which drug induced apoptosis rate is half-maximal
w_v^*	1	Concentration of drug in the bloodstream at the moment of injection
T_{p-cyt}^*	7	Period between two consecutive doses of chemotherapy
$t_{chemo-cyt}^*$	60	Time that chemotherapy starts its cytotoxic activity
l_{cr}^*	0.28	Critical proliferation values
h_d^*	$0.01 \cdot h$	Smoothness parameter for cytotoxic therapy mass balances

To simulate the cytotoxic drug injections, the Events (ev) interface was applied to the environment of COMSOL. In our case, the injections of cytotoxic therapies are simulated as events because each injection happened at different time instances. In other words, each event (injection) starts at a later time compared with the previous events and at an earlier time compared with the future events. For example, for Event 1, the event starts at $t_i = t_{chemo-cyt}^*$, and for Event 2, the event starts at $t_i = t_{chemo-cyt}^* + T_{p-cyt}^*$, for Event 3, the event starts at $t_i = t_{chemo-cyt}^* + 2 \cdot T_{p-cyt}^*$, etc. The parameters $t_{chemo-cyt}^*$ and T_{p-cyt}^* are described in Table 5.1

The parameters used in the simulations with the cytotoxic drug are summarized in Table 5.1. The values of these dimensionless parameters used for the cytotoxic chemotherapy application model are described below:

- Determination of D_w^*: The Einstein-Stokes equation is used to determine the diffusion coefficient of the drug:

$$D = \frac{k_B T}{6\pi\eta r}, \tag{5.22}$$

where k_B is the Boltzmann constant, T the temperature, η denotes the dynamic viscosity, and r corresponds to the hydrodynamic radius of the molecule. Since the case of docetaxel is examined, its hydrodynamic radius is approximately 1.59 nm [23, 86]. For simplification, the nutrient species is considered to be oxygen, with a hydrodynamic radius 152 pm = 0.152 nm [23, 87]. Then, by applying Einstein - Stokes equation for both docetaxel and oxygen (dimensionless) diffusion coefficients:

$$\frac{D_w^*}{D_c^*} = \frac{\frac{k_B T}{6\pi\eta r_w}}{\frac{k_B T}{6\pi\eta r_c}} = \frac{r_w}{r_c} = \frac{0.152\ nm}{1.59\ nm} \Longrightarrow$$

$$\frac{D_w^*}{D_c^*} = 0.1 \Longrightarrow \frac{D_w^*}{1} = 0.1 \Longrightarrow D_w^* = 0.1, \tag{5.23}$$

where $D_c^* = 1.0$, is the nutrient diffusion coefficient see Table 2.1.

- Determination of $k_{ap,1}^*$ and $k_{ap,2}^*$: By assuming that the mitosis rate of healthy cells typically ranges in timescales of days, is defined that:

$$\frac{1}{k_{m,1}} = 1\ day \Longrightarrow k_{m,1} = \frac{1}{day} = \frac{1}{86400}\ \frac{1}{s}. \tag{5.24}$$

It is also assumed that healthy and cancer cells are affected through the same mitosis-inhibiting mechanism by the drug. This reflects to the following relations for (dimensionless) drug induced apoptosis rate and drug consumption rate constants:

$$k_{ap,1}^* = k_{ap,2}^*, \tag{5.25}$$

$$k_{cn,1}^* = k_{cn,2}^*. \tag{5.26}$$

In addition, it is assumed that drug consumption rate constants are linked with apoptosis rate constants by multiplying them with a characteristic drug concentration, which is assumed to be the drug concentration in the bloodstream during injection, w_v. The w_v parameter is calculated below.

$$k_{cn,1} = w_v \cdot k_{ap,1}, \tag{5.27}$$

$$k_{cn,2} = w_v \cdot k_{ap,2}. \tag{5.28}$$

The drug induced apoptosis rate constant is calculated [23, 88]

$$k_{ap,1} = 1.8 \cdot 10^{-4}\ \frac{1}{s}. \tag{5.29}$$

To calculate the parameters $k^*_{ap,1}$ and $k^*_{ap,2}$ is enough one of them to be calculated according to Equation 5.25. With the help of Equations 5.16, 5.24 and 5.29:

$$k^*_{ap,1} = \frac{k_{ap,1}}{k_{m,1}} = \frac{1.8 \cdot 10^{-4} \ \frac{1}{s}}{\frac{1}{86400} \ \frac{1}{s}} = 15.552 \Longrightarrow$$
$$k^*_{ap,1} = k^*_{ap,2} = 15.552. \tag{5.30}$$

In COMSOL simulations, we applied a larger value in these parameters for the needs of the simulations with the cytotoxic drug, i.e. $k^*_{ap,1} = k^*_{ap,2} = 60$.

- Determination of w^*_v: A typical drug schedule of docetaxel is 45 mg/m^2 weekly [1]. Based on that, the dimensionless period between two doses is equal to (see Table 5.1):

$$T^*_{p-cyt} = 7. \tag{5.31}$$

A course of docetaxel-based chemotherapy is simulated and divided into six sessions. The first session takes place at (dimensionless) time (see Table 5.1):

$$T^*_{chemo-cyt} = 60, \tag{5.32}$$

and as explained above, each two consecutive doses are $T^*_{p-cyt} = 7$ apart. To calculate the drug concentration in the bloodstream,w_v it is assumed that the patient is 1.70 m tall, weighing 70 kg and his total blood volume is 4.6 L. The empirical Du Bois equation [89] is applied to calculate the total body surface area:

$$BSA = 0.007184 \, W^{0.425} H^{0.725}, \tag{5.33}$$

where W is the patient's weight in kg and H is the patient's height in cm. By considering the typical drug schedule of $45 mg/m^2$ weekly, the concentration in the blood of the patient at the moment of injection is calculated below:

$$BSA = 0.007184 \, 70^{0.425} 170^{0.725} = 1.8097 \, m^2, \tag{5.34}$$

$$45 \, \frac{mg}{m^2} \times BSA = 45 \, \frac{mg}{m^2} \times 1.8097 \, m^2 = 81.4365 \, mg = 0.0814365 \, g, \tag{5.35}$$

The molar mass of Docetaxel is:

$$Mr_{Docetaxel} = 807.879 \, \frac{g}{mol}, \tag{5.36}$$

The Equations 5.35 and 5.36 are divided and the result is the following:

$$\frac{0.0814365 \, g}{807.879 \, \frac{g}{mol}} = 1.008 \cdot 10^{-4} \, mol. \tag{5.37}$$

The Equation 5.37 is divided by the patient's total blood volume which is 4.6 L in order for w_v to be calculated:

$$w_v = \frac{1.008 \cdot 10^{-4} \, mol}{4.6 \, L} \Longrightarrow w_v = 2.1913 \cdot 10^{-5} \, \frac{mol}{L}. \tag{5.38}$$

The dimensionless w_v^* equals 1 (see Table 5.1).

- Determination of $k^*_{rep,d}$: For the drug replenishment term through the vasculature, it is assumed that the kinetic constant rate, $k^*_{rep,d}$ is equal to the corresponding one for the nutrients, c, thus its dimensionless value is:

$$k_{rep,d} = k_{rep} \rightarrow k_{rep,d} = 1. \tag{5.39}$$

In particular, by assuming the replenishment of oxygen through the circulatory system in the timescale of minutes, k_{rep} has the following form:

$$k_{rep} = \frac{1}{5} \; min^{-1} = \frac{1}{300} \; s^{-1}. \tag{5.40}$$

From Equations 5.10, 5.39 and 5.40 the parameter $k^*_{rep,d}$ is calculated (see Table 5.1):

$$k^*_{rep,d} = \frac{k_{rep,d}}{k_{rep}} = \frac{k_{rep}}{k_{rep}} = \frac{\frac{1}{5} \; min^{-1}}{\frac{1}{5} \; min^{-1}} = 1 \longrightarrow k^*_{rep,d} = 1. \tag{5.41}$$

- Determination of the parameters $k^*_{cn,1}$ and $k^*_{cn,2}$: From Equations 5.27, 5.29 and 5.38 $k_{cn,1}$ is defined:

$$k_{cn,1} = w_v \cdot k_{ap,1} = 2.1913 \cdot 10^{-5} \frac{mol}{L} \cdot 1.8 \cdot 10^{-4} \frac{1}{s} \longrightarrow$$
$$k_{cn,1} = 3.9443 \cdot 10^{-9} \frac{mol}{L \cdot s} \tag{5.42}$$

From Equations 5.11, 5.38, 5.40 and 5.42 $k^*_{cn,1}$ is defined:

$$k^*_{cn,i} = \frac{k_{cn,i}}{k_{rep} w_v} \text{ for i=1,2} \Longrightarrow$$

$$k^*_{cn,1} = \frac{k_{cn,1}}{k_{rep} w_v} = \frac{3.9443 \cdot 10^{-9} \frac{mol}{L \cdot s}}{\frac{1}{300} s^{-1} 2.1913 \cdot 10^{-5} \frac{mol}{L}} \Longrightarrow \tag{5.43}$$

$$k^*_{cn,1} = \frac{3.9443 \cdot 10^{-9} \frac{mol}{L \cdot s}}{7.3043 \cdot 10^{-8} \frac{mol}{L \cdot s}} \Longrightarrow k^*_{cn,1} = 0.0540.$$

From Equation 5.26:

$$k^*_{cn,1} = k^*_{cn,2} = 0.209, \tag{5.44}$$

because is applied a larger value in these parameters for the needs of the simulations in COMSOL (see Table 5.1).

- Determination of k^*_{el}: To estimate the rate constant for the drug expulsion from the bloodstream, k^*_{el} is adopted as a commonly applied equation in compartment models used in pharmacokinetics [23, 90, 91]:

$$k^*_{el} = \frac{CL/V_D}{k_{m,1}}, \tag{5.45}$$

where CL is the clearance rate and V_D the volume of distribution. In Equation (5.45), the denominator denotes the kinetic constant rate of mitosis of healthy cells, and it is applied in order to obtain the dimensionless value for k^*_{el}. Typical values [84] for:

$$CL = 15.7 \frac{L}{m^2 h}, \tag{5.46}$$

and

$$V_D = 112\frac{L}{m^2}, \tag{5.47}$$

From Equations 5.45, 5.46, 5.47 and 5.24 :

$$k_{el}^* = \frac{CL/V_D}{k_{m,1}} = \frac{\frac{15.7\ \frac{L}{m^2 h}}{112\ \frac{L}{m^2}}}{\frac{1}{24\ h}} = \frac{0.1402}{\frac{1}{24}}\ \frac{\frac{1}{h}}{\frac{1}{h}} \Longrightarrow k_{el}^* = 3.3621. \tag{5.48}$$

Thus, the dimensionless value for k_{el}^* equals 3.36 (see Table 5.1).

- Determination of $k_{d,d}^*$: For the drug's decay rate constant, the following relation is used [91]:

$$k_{d,d}^* = \frac{\ln 2/T_{half}}{k_{rep}}, \tag{5.49}$$

where T_{half} is the half-life of the cytotoxic drug. The expression is divided by k_{rep} in order to compute the dimensionless value of $k_{d,d}^*$. The half-life of docetaxel is as follows:

$$T_{half} = 13.5\ \ h = 810\ \ min, \tag{5.50}$$

[84]. From Equations (5.49), (5.50) and (5.40) :

$$k_{d,d}^* = \frac{\frac{\ln 2}{810\ min}}{\frac{1}{5\ min}} = \frac{8.5574 \cdot 10^{-4}}{0.2}\ \frac{\frac{1}{min}}{\frac{1}{min}} \Longrightarrow k_{d,d}^* = 4.27 \cdot 10^{-3}. \tag{5.51}$$

Thus, the dimensionless value of the decay rate constant is $k_{d,d}^* = 4.27 \cdot 10^{-3}$ (see Table 5.1).

- The dimensionless value of w_m^* is obtained directly from the paper from Lampropoulos et al. [23] (see Table 5.1).

- Determination of l_{cr}^*: For parameter l_{cr}^*, is considered that its value needs to satisfy:

$$l_1 < l_{cr}^* < l_2 \tag{5.52}$$

based on the assumption that healthy cells are practically unaffected by cytotoxic therapy. It is determined (through a series of simulations) that a value close to $l_{cr} = 0.28$ produces the most realistic results [23] (see Table 5.1).

- The dimensionless value of h_d^* is obtained directly from the paper from Lampropoulos et. al [23] (see Table 5.1). Practically, the value of the steepness parameter h_d^* is small, and that means that no smoothing is added to the model.

5.5 Numerical Results

Initially, the tissue for our computational analysis is modeled as a circular domain with (dimensionless) radius, $R_{tissue} = 20$. The computational mesh is generated with the Extra fine mesh option of the Fluid dynamics mesh category. The computational mesh is an unstructured mesh generated with the method of Delaunay Triangulation, generating approximately 20.000 elements and about 400.000 degrees of freedom. The maximum element surface is equal to 0.52 square units, and the minimum element surface is equal to 0.006 square units. The computational grid for the examined tissue is the same as depicted in Figure 4.2 (4.2a and 4.2b). The solvers were used, MUMPS and BDF, as referred to in Section 4.5 to solve the system and for time integration, respectively. The Segregated solution approach was chosen as mentioned in Section 4.5. The lower limit for this computational analysis was set equal to $1 \cdot 10^{-15}$.

The simulations which are examined in this second section of our computational study of combination therapies in growing tumors are the following:

1. *Computational analysis applied "No Therapy"*
2. *Computational analysis applied "Only Radiotherapy"*
3. *Computational analysis applied "Only Chemotherapy"*
4. *Computational analysis applied "Combined Chemoradiotherapy"*

In this section, our results are divided into three categories. In the first category, we have the "Surface Integration" of cancer cells where the integral $\iint_S \theta_2 \, dxdy$ is used to calculate the total surface area occupied by cancer cells, thus related to the total number of living cancer cells. In the second category, we have the "Surface Integration" of blood vessels where the integral $\iint_S \theta_3 \, dxdy$ is used to calculate the total surface area occupied by blood vessels. When the integral of vessels is calculated, a limitation is imposed $\iint_S \theta_3 \cdot (\theta_2 > 10^{-3}) \, dxdy$. With this restriction, only the vessels close to tumor cells are being studied. In the third category, snapshots of spatial volume fraction distribution of cancer cells and blood vessels phase are depicted. These two-dimensional diagrams are referred for treatment free, radiotherapy, chemotherapy, and chemoradiotherapy simulations.

Regarding the first category of our results, Figure 5.1 depicts the evolution of cancer cell surface for the cases; No Treatment, Radiotherapy, Chemotherapy, and Chemoradiotherapy. More specifically, the total number of living cancer cells decreases when some type of therapy is applied, while cancer cells increase rapidly when No therapy is applied. Moreover, as illustrated in the same Figure 5.1, by applying Combined Chemoradiotherapy, cancer cells decreased more when compared to the other cases. As a result, the survival fraction of tumor cells, in the case of Combined Chemoradiotherapy, is the smallest. Consequently, Combined Chemoradiotherapy is better than Only Radiotherapy or Only Chemotherapy when applied for cancer treatment.

Continuing to the second category of our results, Figure 5.2 presents the evolution of blood vessels surface for the cases; No treatment, Radiotherapy, Chemotherapy, and Chemoradiotherapy. As demonstrated in Figure 5.2, the total number of blood vessels decreases when a therapy is applied, while vessels increase rapidly when No Treatment is applied. As clearly illustrated

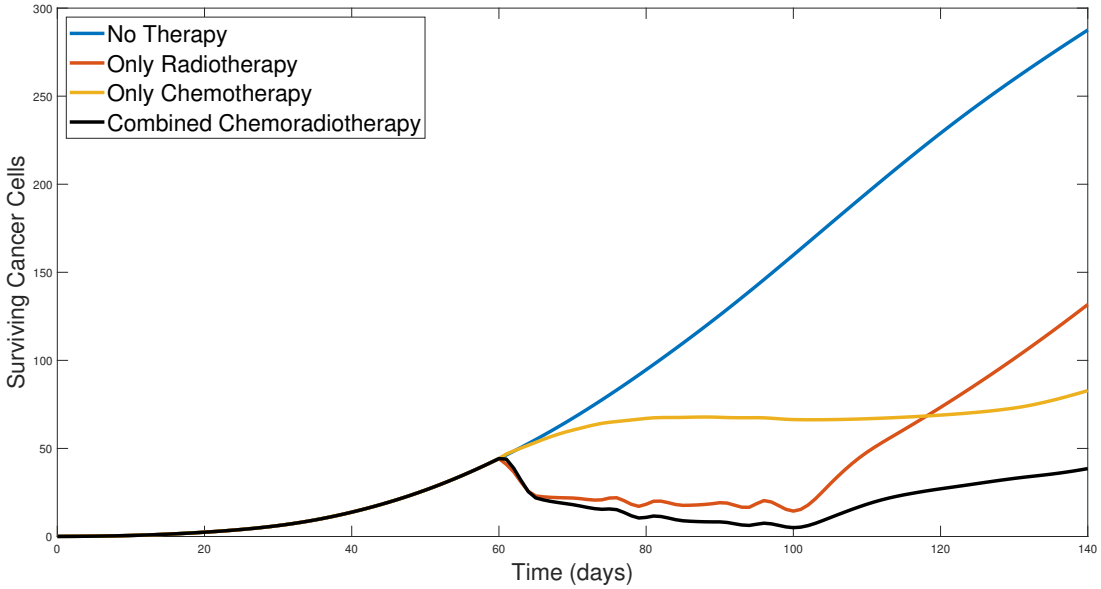

Figure 5.1: *Evolution of* $\iint_S \theta_2 \, dxdy$ *for treatment free, radiotherapy, chemotherapy, and chemoradiotherapy simulations.*

by applying Combined Chemoradiotherapy, the blood vessels decreased the most. Consequently, Combined Chemoradiotherapy is better than Only Radiotherapy or Only Chemotherapy when applied for cancer treatment, as suggested by our results.

It is worth noting why we studied the blood vessels in all of the cases mentioned above. When cancer cells have access to more vessels, the possibility for metastasis is higher compared to the case where the number of vessels is restricted, so the chance for cancer cells to metastasize is smaller. The blood vessels behave differently in each treatment, and this situation affects the dynamics of tumor metastasis. For instance, when Only Radiotherapy is applied, the number of vessels that occupy the tissue's domain is larger than if Only Chemotherapy is applied, in which the vessels decrease more. As depicted in Figure 5.2, if No Therapy is applied, the chance for tumor metastasis is the greatest. On the contrary, in Combined Chemoradiotherapy, the number of vessels is decreased significantly. As a result, in Combined Chemoradiotherapy, the chance of metastasis is the smallest compared with the other three cases.

In the third category of our results, two-dimensional distribution diagrams are illustrated. The results of Treatment Free and Radiotherapy simulations are presented in Figure 5.3. While the cancerous population is constantly increasing in the case that no treatment is applied to the growing tumor, the distribution of surviving cancer cells gets suppressed by radiotherapy. The duration of irradiation treatment is six weeks starting at the dimensionless time, Time=60, and completing at the dimensionless time, Time=102. At the dimensionless time, Time=200, it can be obtained that in the case of treatment free, the cancer cells reach the limits of the tissue domain very early compared to the irradiation therapy. The formulation of the necrotic core is observed at the irradiated cancer cells at Time=200.

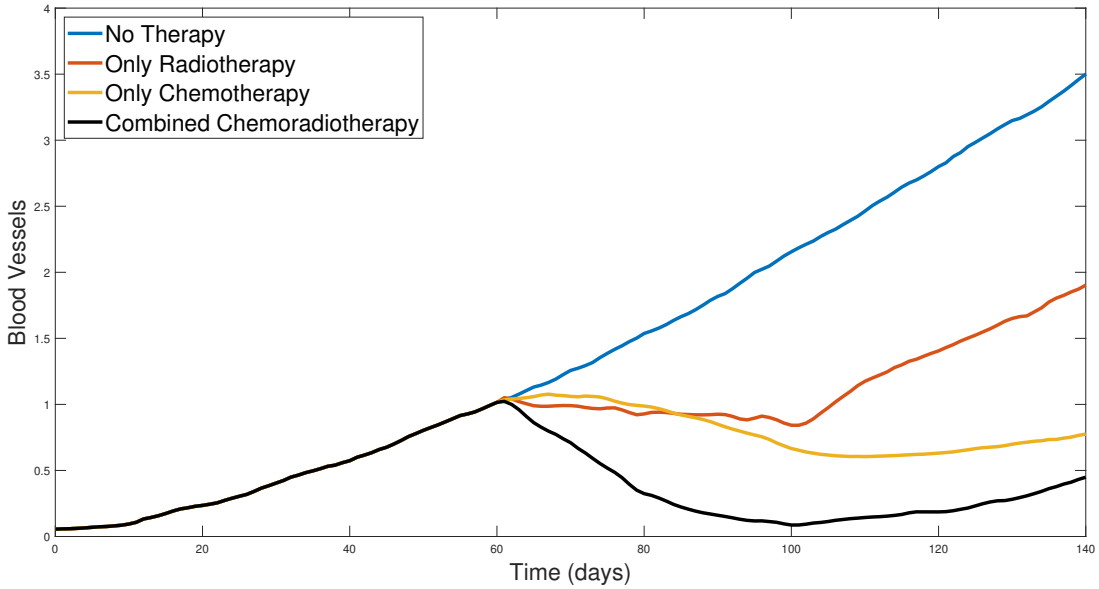

Figure 5.2: *Evolution of* $\iint_S \theta_3 \cdot (\theta_2 > 10^{-3})$ *dxdy for treatment free, radiotherapy, chemotherapy, and chemoradiotherapy simulations.*

Figure 5.4 depicts snapshots of the cancer volume fraction. One can observe that chemotherapy suppresses the growing tumor since, at dimensionless times, such as Time=120, chemotherapy isn't applied anymore. The most significant suppression of the growing tumor can be observed when chemoradiotherapy is applied. The duration of chemotherapy and chemoradiotherapy treatment is six weeks starting at the dimensionless time, Time=60, and completing at the dimensionless time, Time=102. Moreover, the formulation of the necrotic core is observed at later time intervals in comparison with the cases in Figure 5.3. When chemotherapy is used, the formulation of the necrotic core is observed at the dimensionless time, Time=240. In the case of combined chemoradiotherapy, the necrotic core appeared at Time=300. This confirms the long lasting effect of the cytotoxic drug in the bloodstream. Docetaxel remains in the patient's body for more time interval, so it continues to decrease tumor growth after the treatment is over. Especially in combined chemoradiotherapy, the formulation of necrotic core delays the most compared to the above mentioned cases.

Snapshots of the spatial distribution of blood vessels are illustrated in Figure 5.5. If no therapy is applied to the growing tumor, the population of blood vessels increases constantly. On the other hand, the vascular fraction distribution is smaller when radiotherapy is applied. This resulted that the inflammation in the tissue will be less than in the treatment-free case, in which a noticeable increase in vessel volume fraction is inevitable.

Finally, snapshots of the spatial distribution of vessels are depicted in Figure 5.6. These results suggest that when radiotherapy and chemotherapy are given together is more successful at reducing the blood vessels phase than treatment with only chemotherapy delivered. As the growth of vascular system is suppressed the most, in a chemoradiotherapy-treated tumor, the inflammation is the smallest. Reaching to conclusion, combined chemoradiotherapy is the most effective way of reducing both tumor size and blood vessel population, as concluded from the results.

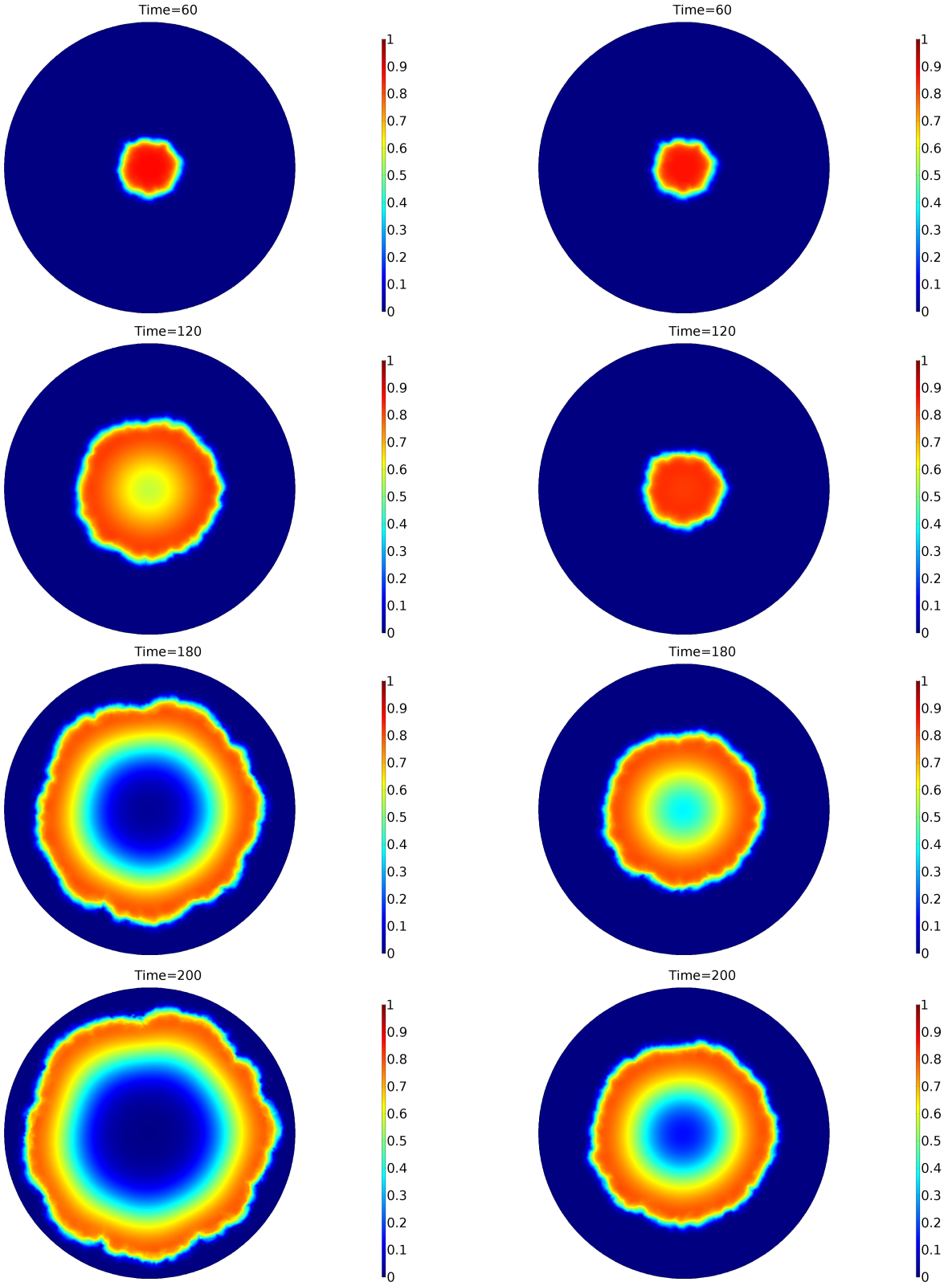

(a) *Treatment Free* (b) *Radiotherapy*

Figure 5.3: *Snapshots of spatial volume fraction distribution of cancer cells: (a) in a no-treated tumor (left column) and (b) in a radiotherapy-treated tumor (right column) at dimensionless times, Time=60, 120, 180 and 200 with applying radiotherapy at the dimensionless time, Time=60.*

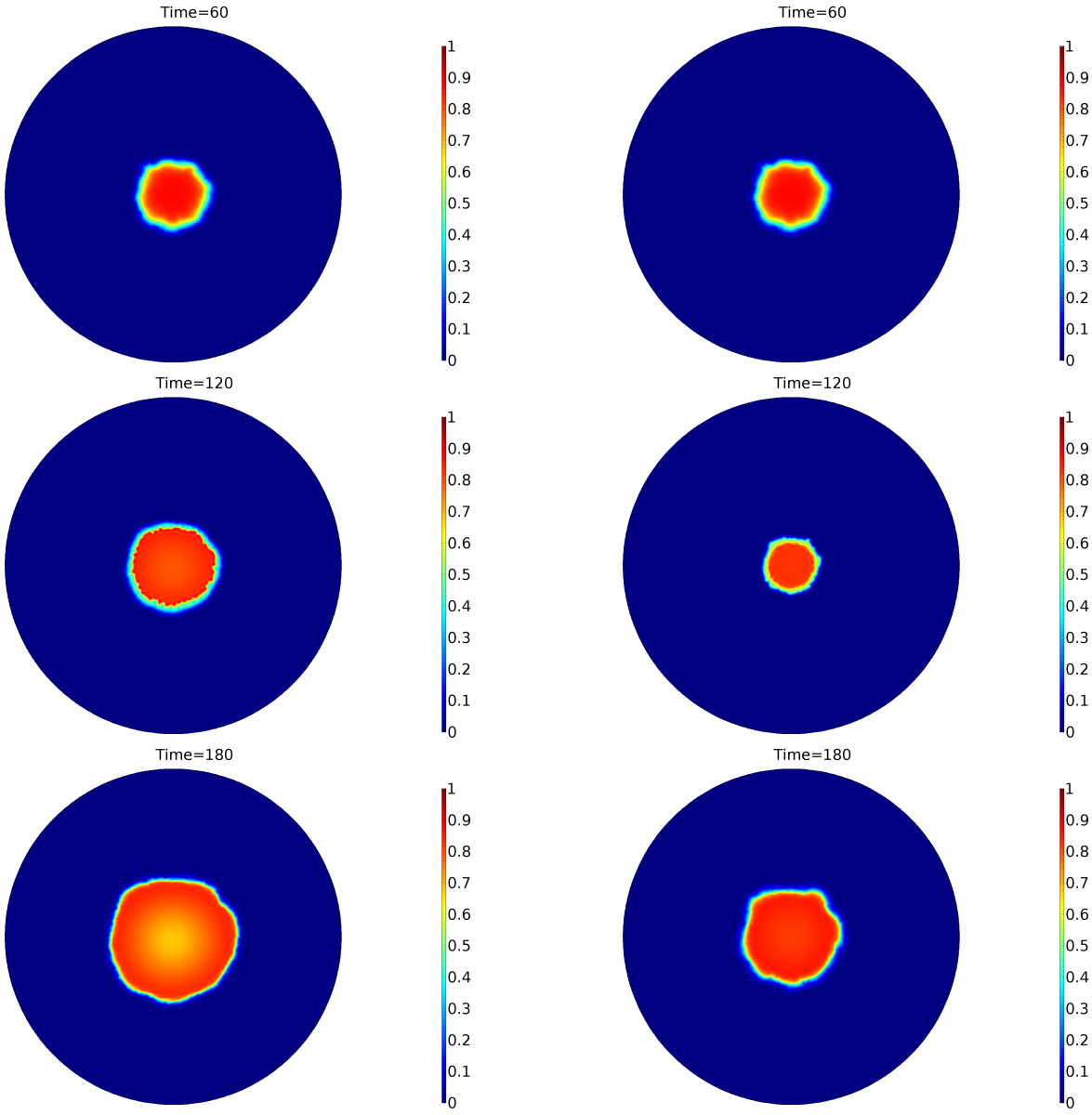
Time=60
1
0.9
0.8
0.7
0.6
0.5
0.4
0.3
0.2
0.1
0
Time=60
1
0.9
0.8
0.7
0.6
0.5
0.4
0.3
0.2
0.1
0
Time=120
1
0.9
0.8
0.7
0.6
0.5
0.4
0.3
0.2
0.1
0
Time=120
1
0.9
0.8
0.7
0.6
0.5
0.4
0.3
0.2
0.1
0
Time=180
1
0.9
0.8
0.7
0.6
0.5
0.4
0.3
0.2
0.1
0
Time=180
1
0.9
0.8
0.7
0.6
0.5
0.4
0.3
0.2
0.1
0

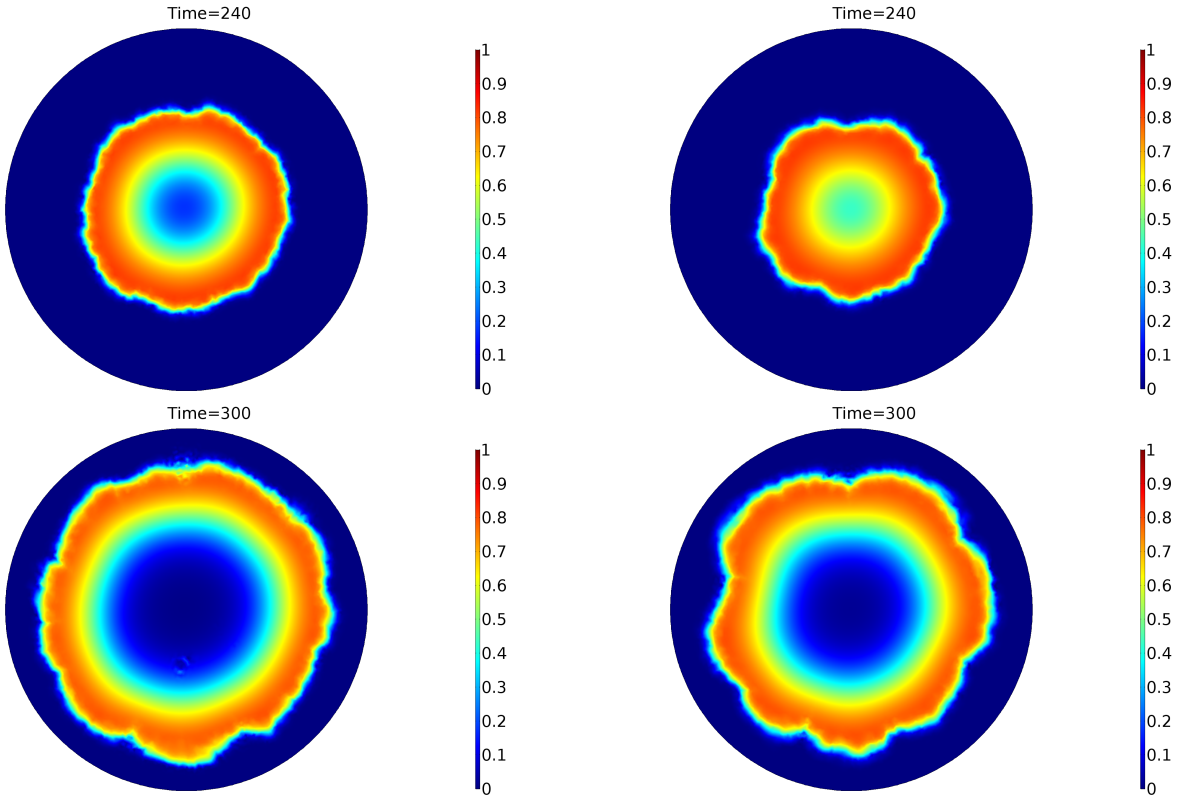

(a) *Chemotherapy* (b) *Chemoradiotherapy*

Figure 5.4: *Snapshots of cancer cells volume fraction distribution: (a) in a chemotherapy-treated tumor (left column) and (b) in a chemoradiotherapy-treated tumor (right column) at dimensionless times, Time=60, 120, 180, 240 and 300 with applying both chemotherapy and chemoradiotherapy at the dimensionless time, Time=60.*

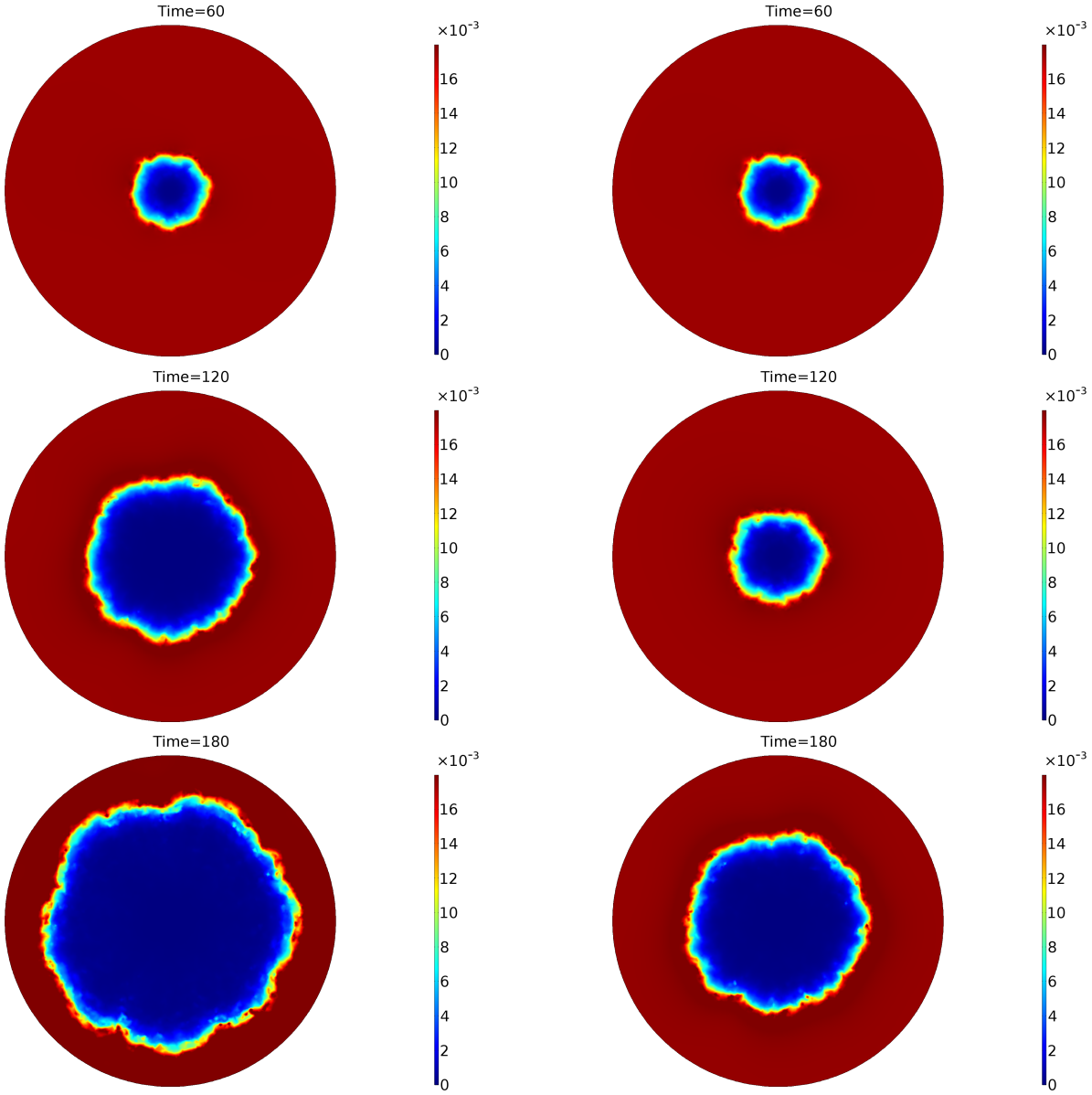

(a) *Treatment Free* (b) *Radiotherapy*

Figure 5.5: *Snapshots of the spatial distribution of blood vessels rates: (a) in a no-treated tumor (left column) and (b) in a radiotherapy-treated tumor (right column) at dimensionless times, Time=60, 120 and 180 with applying radiotherapy at the dimensionless time, Time=60.*

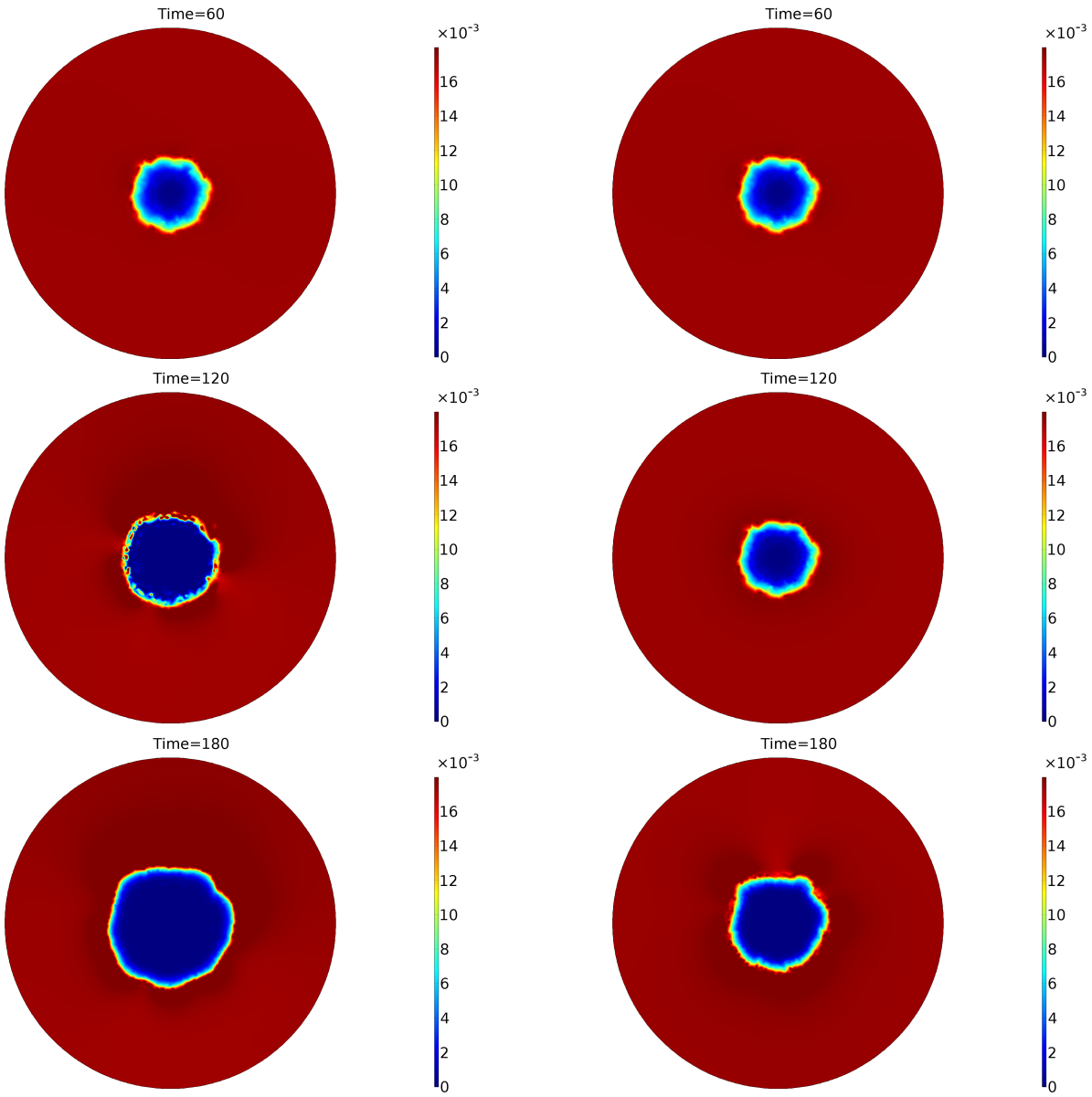

(a) *Chemotherapy* (b) *Chemoradiotherapy*

Figure 5.6: *Snapshots of spatial volume fraction distribution of blood vessels: (a) in a chemotherapy-treated tumor (left column) and (b) in a chemoradiotherapy-treated tumor (right column) at dimensionless times, Time=60, 120 and 180 with applying both chemotherapy and chemoradiotherapy at the dimensionless time, Time=60, and completing at the dimensionless time, Time=102.*

Chapter 6

Different Schedules of Concurrent Chemoradiotherapy Simulations

In this final section of our results, various cases of combined chemoradiotherapy have been studied. In these cases, radiotherapy and chemotherapy are applied at different time intervals.

6.1 Examined Cases

In Chapter 5, the case of Combined Chemoradiotherapy with concurrent application of the two therapies was applied. More specifically, radiotherapy was applied for six consecutive weeks, and once a week, chemotherapy was applied analogously for the same time duration according to the established cancer protocol [1]. In this Chapter, together with the aforementioned main case, 12 additional cases are being studied, which are linked to the main case, but radiotherapy and chemotherapy are applied at a different time than the main case.

More particularly, we have the following therapeutic cases:

1. $t_{radio} = 60$, $t_{chemo} = 60$. In this case, radiotherapy and chemotherapy start concurrently on the 60^{th} day.

2. $t_{radio} = 60$, $t_{chemo} = 67$. In this case, radiotherapy starts on the 60^{th} day and chemotherapy one week later.

3. $t_{radio} = 60$, $t_{chemo} = 74$. In this case, radiotherapy starts on the 60^{th} day and chemotherapy two weeks later.

4. $t_{radio} = 60$, $t_{chemo} = 81$. In this case, radiotherapy starts on the 60^{th} day and chemotherapy three weeks later.

5. $t_{radio} = 60$, $t_{chemo} = 88$. In this case, radiotherapy starts on the 60^{th} day and chemotherapy four weeks later.

6. $t_{radio} = 60$, $t_{chemo} = 95$. In this case, radiotherapy starts on the 60^{th} day and chemotherapy five weeks later.

7. $t_{radio} = 60$, $t_{chemo} = 102$. In this case, radiotherapy starts on the 60^{th} day and chemotherapy six weeks later.

8. $t_{chemo} = 60$, $t_{radio} = 67$. In this case, chemotherapy starts on the 60^{th} day and radiotherapy one week later.

9. $t_{chemo} = 60$, $t_{radio} = 74$. In this case, chemotherapy starts on the 60^{th} day and radiotherapy two weeks later.

10. $t_{chemo} = 60$, $t_{radio} = 81$. In this case, chemotherapy starts on the 60^{th} day and radiotherapy three weeks later.

11. $t_{chemo} = 60$, $t_{radio} = 88$. In this case, chemotherapy starts on the 60^{th} day and radiotherapy four weeks later.

12. $t_{chemo} = 60$, $t_{radio} = 95$. In this case, chemotherapy starts on the 60^{th} day and radiotherapy five weeks later.

13. $t_{chemo} = 60$, $t_{radio} = 102$. In this case, chemotherapy starts on the 60^{th} day and radiotherapy six weeks later.

6.2 Numerical Results

In the present chapter, our results are divided into two main categories. In the first category, our results are presented in the form of 2D and 3D diagrams made in MATLAB. All these diagrams describe the Percentage of Therapeutic Efficacy for each of the 13 cases mentioned above. In the 2D graphs, Therapeutic Efficacy is interpreted as Surface Coverage Reduction from cancer cells (%); in 3D diagrams, it is interpreted as Treatment Efficacy (%). In any case, the percentage of therapeutic efficacy is calculated with the following equation:

$$\text{therapeutic efficacy} = \frac{\left(\iint_S \theta_2 \, dxdy\right)_{untreated} - \left(\iint_S \theta_2 \, dxdy\right)_{case\ i}}{\left(\iint_S \theta_2 \, dxdy\right)_{untreated}} = f(t). \tag{6.1}$$

Where subscript i=1,2,3,...13 denotes the examined cases as mentioned above, $f(t) \quad where \quad t \in [t_f, \ t_f + \text{j months}]$, with t_f denoting the time that the last dose of radiotherapy or chemotherapy was applied to the human body and t_f + j months, the months following the last dose of radiotherapy or chemotherapy. In this work, we examine till six months after treatment, i.e., t_f + 1 month, t_f + 2 months, t_f + 3 months,...,t_f + 6 months.

In general, the therapeutic efficacy is calculated before cancer cells reach the boundary of the tissue's domain. If tumor cells surpass that limit, there is no reason for the therapeutic efficiency to be studied, as the results would be unreliable. In the *No Treatment* case, cancer cells reach the limits of the domain very early compared to the cases where a combination of treatments is applied. The trendline of growing cancer cells in the *No Treatment* case is derived by linear extrapolation.

In the second category, we have the "Surface Integration" of blood vessels where the integral $\iint_S \theta_3 \, dxdy$ is used to calculate the total surface area occupied by blood vessels as we have in the results of Chapter 5. When the integral of vessels is calculated, a limitation is imposed $\iint_S \theta_3 \cdot (\theta_2 > 10^{-3}) \, dxdy$. With this restriction, the vessels close to tumor cells are being studied. The number of blood vessels is calculated for each case separately, while a general graph combines all cases.

For the Parametric Analysis, in this section, MATLAB was used to produce the following corresponding diagrams. The first category of our results is presented in 2D graphs and describes Therapeutic Efficacy for the 13 treatment cases described above. Figure 6.1 shows a summarizing graph including all 13 Therapeutic Cases. In this figure, the x-axis represents the Months after the Last Treatment Administration, and the y-axis represents the Percentage of Surface Coverage Reduction. As one can observe, the dashed lines represent the cases that Chemotherapy precedes radiotherapy, while the solid lines represent the cases where Radiotherapy precedes chemotherapy.

In cases where chemotherapy precedes radiotherapy (dashed lines), each case starts with a high percentage of surface coverage reduction. Hence, an increased number of cancer cells continue to die in the first month after the last treatment administration. This happens due to the the high rate of killing cancer cells of chemotherapy. After all, the cytotoxic drug remains within the human body for some time, so its impact is long-lasting. Approximately, after the first month of the last treatment's administration, the percentage of surface coverage reduction decreases quickly because the impact of chemotherapy weakens. Hence, it remains only to radiotherapy in which cancer cells are killed directly. This happens because the effect of radiotherapy on cancer cells is immediate, so there is no need for some time to pass in order to kill cancer cells. In other words, radiotherapy's effect is way shorter than chemotherapy, which remains in the human body for quite some time.

The rate of surface coverage reduction from cancer cells is high when chemotherapy is applied first, before radiotherapy. This happens because, firstly, chemotherapy has killed a satisfying number of cancer cells, and secondly when radiotherapy is applied it kills cancer cells directly, so it decreases the number of cancer cells even more. The resulting peak of this combination is high, especially till the first month after the last treatment administration. Indeed, this peak is higher when chemotherapy and radiotherapy are close in time distance. For example, the highest percentage of surface coverage reduction is observed when chemotherapy and radiotherapy abstain for one week, i.e., $t_{chemo} = 60$, $t_{radio} = 67$. Lower percentages are observed when chemotherapy and radiotherapy abstain for more than one week. For example two weeks $t_{chemo} = 60$, $t_{radio} = 74$, three weeks $t_{chemo} = 60$, $t_{radio} = 81$, etc.

In cases where radiotherapy precedes chemotherapy (solid lines), every case starts with a lower percentage of surface coverage reduction compared to the rates when chemotherapy is applied first (dashed lines) as described above. In the cases where radiotherapy is applied second, the percentages of surface coverage reduction are still high because of the long-lasting effect of chemotherapy. After the first month of the last treatment administration, the percentage of surface coverage reduction starts to decrease more slowly than in the cases mentioned above (dotted lines). This is explained as chemotherapy in these cases (solid lines) is applied after radiotherapy, and the impact of the cytotoxic drug is still high and delays the decrease of the percentage of surface coverage reduction. Hence, we can easily conclude that cytotoxic drug stays in the human bloodstream longer after the end of combined chemoradiotherapy; that's why the rate of surface coverage re-

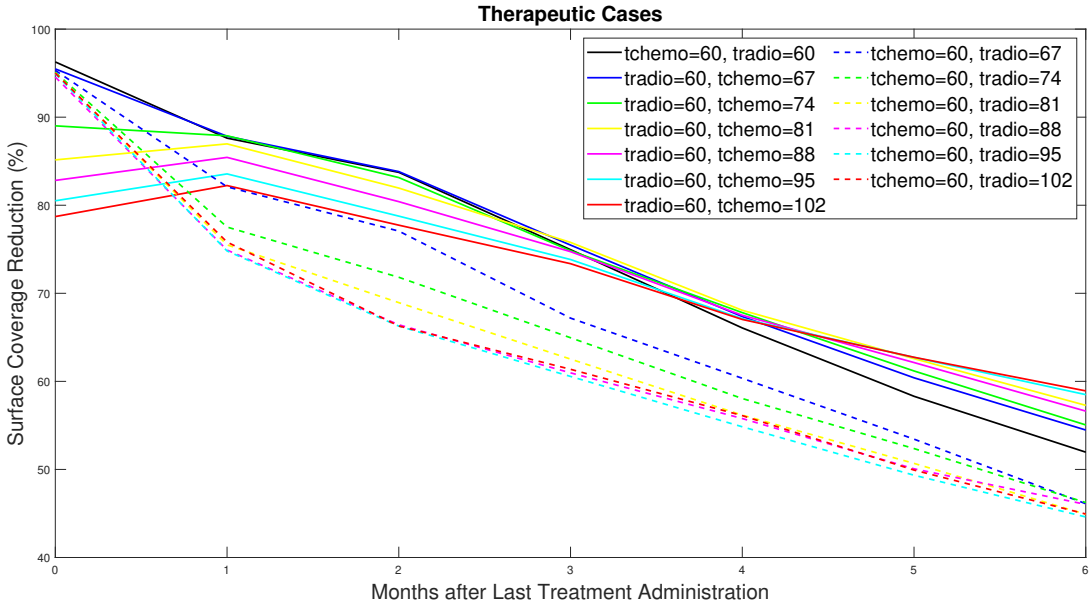

Figure 6.1: *Summarizing graph of the percentage of Surface Coverage Reduction compared with Months after the Last Treatment Administration for all Therapeutic Cases.*

duction does not decrease rapidly. The chemotherapy drug needs some time to react with the cancer cells; that's why we can observe on the graph that after one month of the last chemotherapy treatment administration, its impact is still high. Lastly, this rate is high when radiotherapy and chemotherapy were administered close in time. For example, higher percentages are presented in the cases that radiotherapy and chemotherapy start within a one or two weeks apart from each other, $t_{radio} = 60$, $t_{chemo} = 67$ and $t_{radio} = 60$, $t_{chemo} = 74$. Lower percentages are observed when radiotherapy and chemotherapy abstain for more than one or two weeks. For example three weeks $t_{radio} = 60$, $t_{chemo} = 81$, four weeks $t_{radio} = 60$, $t_{chemo} = 88$, etc.

Figure 6.2 presents all the therapeutic cases where chemotherapy was applied first (dashed lines). The case that chemotherapy and radiotherapy are applied concurrently, i.e., $t_{chemo} = 60$, $t_{radio} = 60$, (solid black line) is illustrated, too. In concurrent combined chemoradiotherapy, the percentage of surface coverage reduction starts from higher levels compared with the therapeutic cases (dashed lines) in which chemotherapy precedes radiotherapy. So in the concurrent case of chemoradiotherapy, the rates of surface coverage reduction with cancer cells are high to one up to three months after the last treatment was applied. Last but not least, the rate of surface reduction for the concurrent therapy for six months after the last treatment administration is higher than the corresponding rates in dashed lines. Indeed, this has a sensible explanation, as in the cases represented with dashed lines, in which chemotherapy was applied first. There the percentage is high, and as months pass by, the cytotoxic drug expels from the human body, so the long-lasting effect has completely disappeared till six months after the last treatment administration. As a result, the dashed lines are observed at lower rates of surface coverage reduction six months after the treatment, compared to concurrent chemoradiotherapy. The therapeutic case in which $t_{chemo} = 60$, $t_{radio} = 60$ is applied, has a good percentage of surface coverage reduction and is acceptable because it is, in essence, the way that combined chemoradiotherapy is applied in clinical protocols.

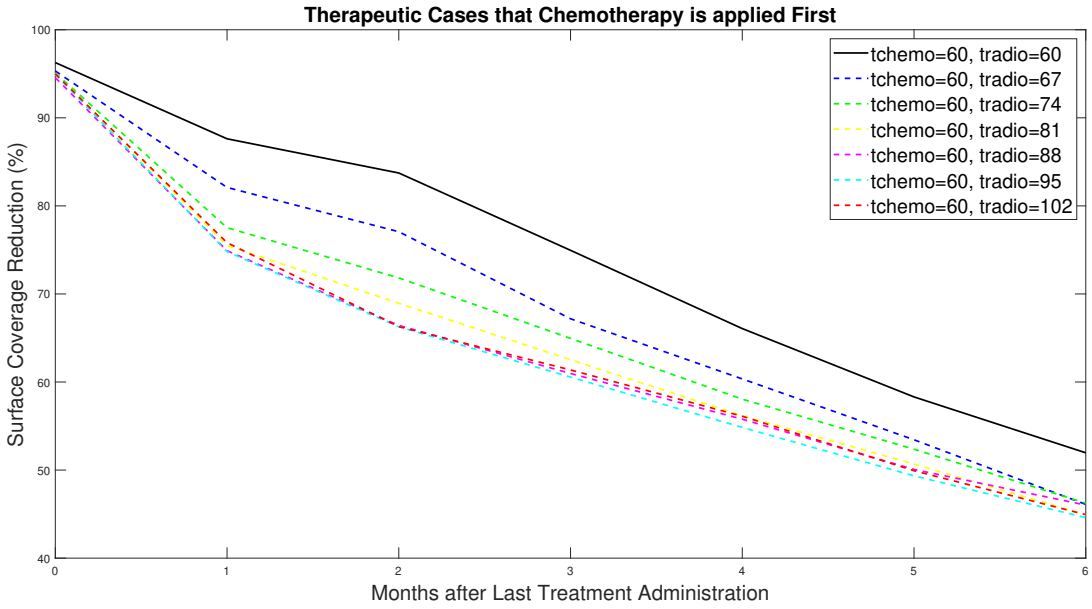

Figure 6.2: *Graph of the percentage of Surface Coverage Reduction compared with Months after the Last Treatment Administration for Therapeutic Cases that Chemotherapy is applied First.*

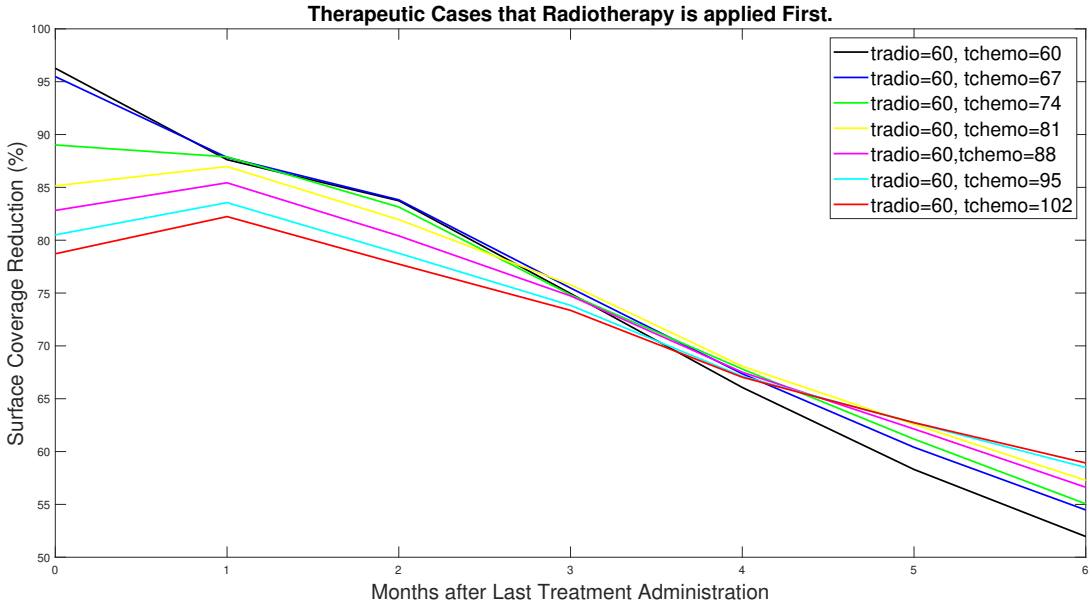

Figure 6.3: *Graph of the percentage of Surface Coverage Reduction compared with Months after the Last Treatment Administration for Therapeutic Cases that Radiotherapy is applied First.*

Figure 6.3 presents all therapeutic cases where radiotherapy was applied first (solid lines). The case where chemotherapy and radiotherapy are applied concurrently, i.e., $t_{chemo} = 60$, $t_{radio} = 60$, (solid black line) is illustrated, too. In concurrent combined chemoradiotherapy, the percentage of surface coverage reduction starts from higher levels compared to the therapeutic cases (solid lines) in which radiotherapy precedes chemotherapy. But in concurrent chemoradiotherapy, the rate of surface reduction decreases faster compared to the rest therapeutic cases in which radiotherapy precedes chemotherapy, concluding after six months of the last treatment administration to have the lowest percentage. Indeed, this can be explained by the fact that chemotherapy and radiotherapy are applied concurrently, in the case where $t_{chemo} = 60$, $t_{radio} = 60$. In the other cases, radiotherapy and chemotherapy are applied at different time instances, mostly because the chemotherapy effect is long-lasting and impacts cancer cells for subsequent intervals. This is the reason why the percentage decreases slower. Consequently, concurrent chemoradiotherapy has the most prominent peak, but its rate decreases slightly faster than the rest.

Except for 2D graphs, the first category of our results is presented in the form of 3D graphs similarly. In Figure 6.4 total 3D Surface Plotting Graph of the Examined Therapeutic Cases is illustrated. The z-axis represents the percentage of Therapeutic Efficacy (%), the y-axis the time after the last treatment administration measured in months, and the x-axis represents the time difference between therapy starts (Δt). Each case has a unique (Δt), which is determined from the difference: $\Delta t = t_{radio} - t_{chemo}$. From each case, the ($\Delta$t) is determined below:

1. $t_{radio} = 60$, $t_{chemo} = 60$. The time difference between the two therapies is $\Delta t = t_{radio} - t_{chemo} \rightarrow \Delta t = 0$.
2. $t_{radio} = 60$, $t_{chemo} = 67$. The time difference between the two therapies is $\Delta t = t_{radio} - t_{chemo} \rightarrow \Delta t = -7$.
3. $t_{radio} = 60$, $t_{chemo} = 74$. The time difference between the two therapies is $\Delta t = t_{radio} - t_{chemo} \rightarrow \Delta t = -14$.
4. $t_{radio} = 60$, $t_{chemo} = 81$. The time difference between the two therapies is $\Delta t = t_{radio} - t_{chemo} \rightarrow \Delta t = -21$.
5. $t_{radio} = 60$, $t_{chemo} = 88$. The time difference between the two therapies is $\Delta t = t_{radio} - t_{chemo} \rightarrow \Delta t = -28$.
6. $t_{radio} = 60$, $t_{chemo} = 95$. The time difference between the two therapies is $\Delta t = t_{radio} - t_{chemo} \rightarrow \Delta t = -35$.
7. $t_{radio} = 60$, $t_{chemo} = 102$. The time difference between the two therapies is $\Delta t = t_{radio} - t_{chemo} \rightarrow \Delta t = -42$.
8. $t_{chemo} = 60$, $t_{radio} = 67$. The time difference between the two therapies is $\Delta t = t_{radio} - t_{chemo} \rightarrow \Delta t = 7$.
9. $t_{chemo} = 60$, $t_{radio} = 74$. The time difference between the two therapies is $\Delta t = t_{radio} - t_{chemo} \rightarrow \Delta t = 14$.
10. $t_{chemo} = 60$, $t_{radio} = 81$. The time difference between the two therapies is $\Delta t = t_{radio} - t_{chemo} \rightarrow \Delta t = 21$.

11. $t_{chemo} = 60$, $t_{radio} = 88$. The time difference between the two therapies is $\Delta t = t_{radio} - t_{chemo} \rightarrow \Delta t = 28$.

12. $t_{chemo} = 60$, $t_{radio} = 95$. The time difference between the two therapies is $\Delta t = t_{radio} - t_{chemo} \rightarrow \Delta t = 35$.

13. $t_{chemo} = 60$, $t_{radio} = 102$.The time difference between the two therapies is $\Delta t = t_{radio} - t_{chemo} \rightarrow \Delta t = 42$.

This figure shows clearly which therapeutic cases have the best treatment efficiency and till what time (in months) this efficiency remains at high levels after the last therapy application.

For example, $\Delta t = 0$ has been detected with the highest percentage of treatment efficacy right after the last treatment administration (zero months), with efficacy 96.27%. Moreover, in this case, the therapeutic efficacy levels (up to 80%) remain high two months after the last therapy application.

All the aforementioned percentages, and the others described below, are presented in Figure 6.5, which is the same graph with Figure 6.4. Now, the related cases and their associated points have been labeled for more ease.

Following the graph in Figure 6.5, the lowest percentage of treatment efficacy is detected when $\Delta t = -42$ with a percentage of 78.71%, exactly after the last treatment administration (zero months). Indeed, in this case, the percentage of therapeutic efficiency is lower compared to the case mentioned above, the one with the highest therapeutic efficiency. Still, the decrease rate of this therapeutic efficiency is lower than the $\Delta t = 0$ case. In the case where $\Delta t = -42$, the decrease of efficiency after six months is only 20% compared to the case in which $\Delta t = 0$, where reduction of efficiency after the same time is 44%.

Another case that requires commenting is the case where $\Delta t = 42$. It begins with a high percentage of therapeutic efficiency exactly after the last treatment administration (zero months) 95%. Still, after six months, the reduction of the therapeutic efficiency is 50%.

Figure 6.6 presents the contour graph, which is a 2D projection of the 3D surface graph by plotting constant z-slices called contours in a 2-dimensional format. In this 2D contour plot, the x-axis is the time difference between therapy starts (Δt), the y-axis is the time after the last treatment administration (months), while the z-axis which represents the therapeutic efficacy (%) of the examined therapeutic cases is represented as contours. With this contour plot, it is more easily observable how the value of the axis z, in our case the therapeutic efficacy, changes as a function of the inputs of the x and y axis, respectively $z = f(x, y)$. This representation is another way to observe how the therapeutic efficacy of every case changes over time. In addition, it can be observed these cases that exhibit the higher percentages of treatment efficiency and which the lower. In other words, it is an alternative way to see how the percentages of all cases range.

Figure 6.7 illustrates the evolution of the value of $\iint_S \theta_3 \, dxdy$ for treatment free, and various schemes of concurrent chemoradiotherapy simulations are applied in the tissue. The graph shows that when *No Therapy* is applied (black dotted line), the vessels are constantly increasing. On the other hand, the blood vessels are decreasing when combined therapy (dashed and solid lines)

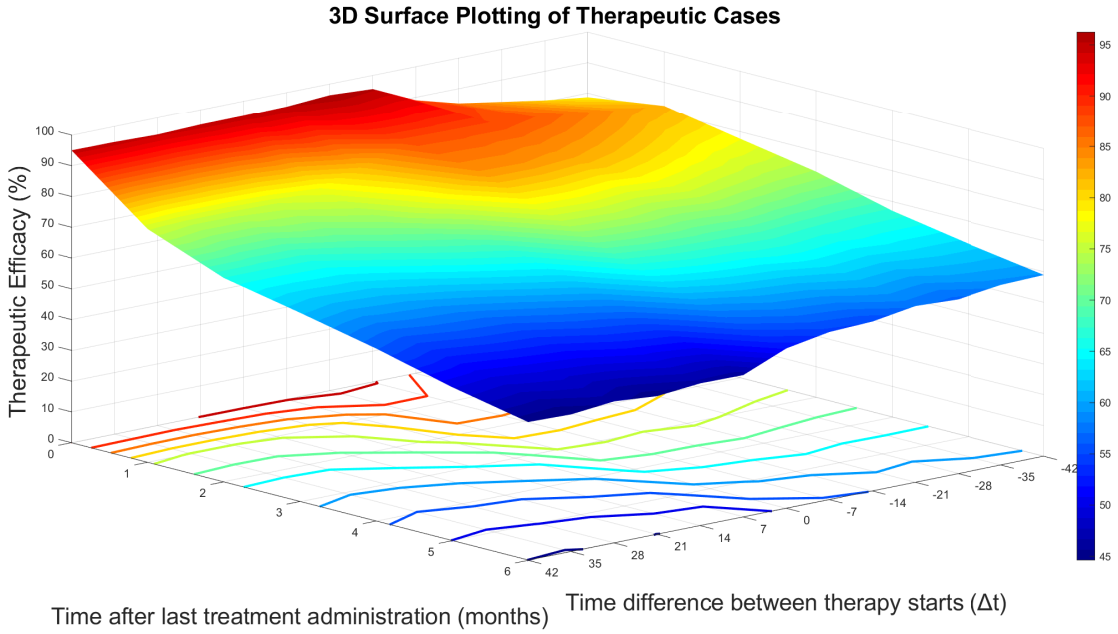

Figure 6.4: *Total 3D Surface Plotting Graph of the Examined Therapeutic Cases compared with Time after last treatment administration (months) and the Time difference between therapy starts (Δt).*

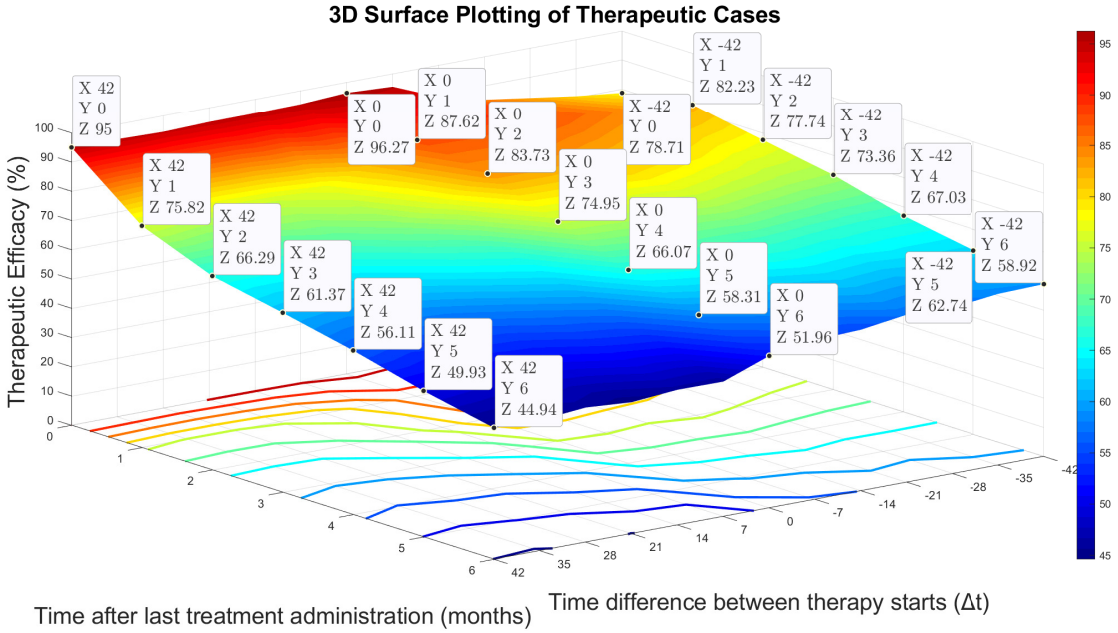

Figure 6.5: *Therapeutic Efficacy (%) of the Examined Therapeutic Cases compared with Time after last treatment administration (months) and the Time difference between therapy starts (Δt) with labeled in the three extreme cases.*

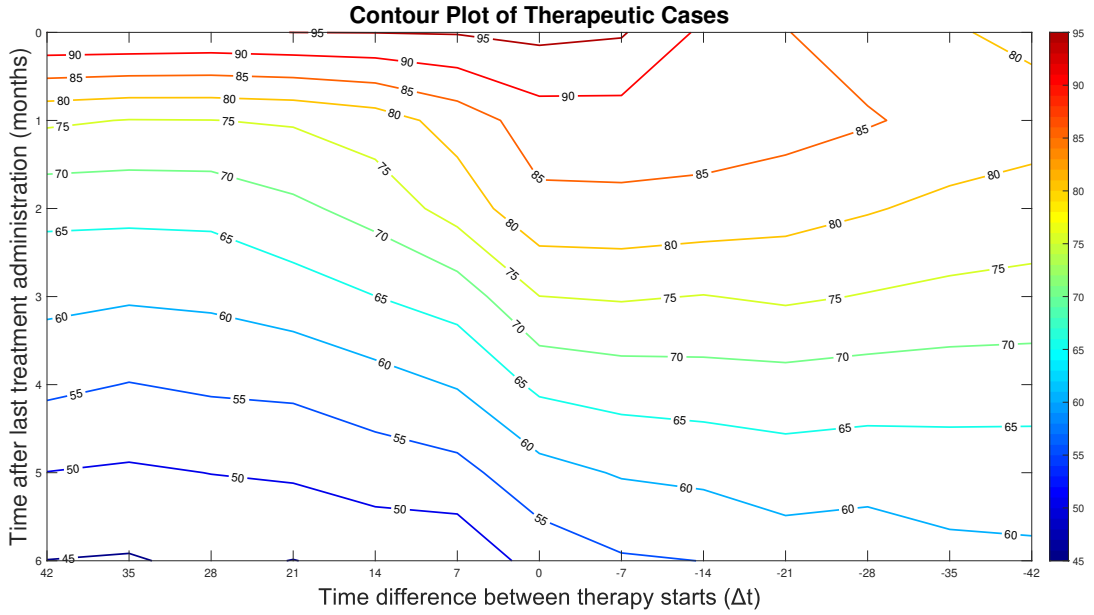

Figure 6.6: *Contour plot of therapeutic cases as an alternative to the 3D surface plot.*

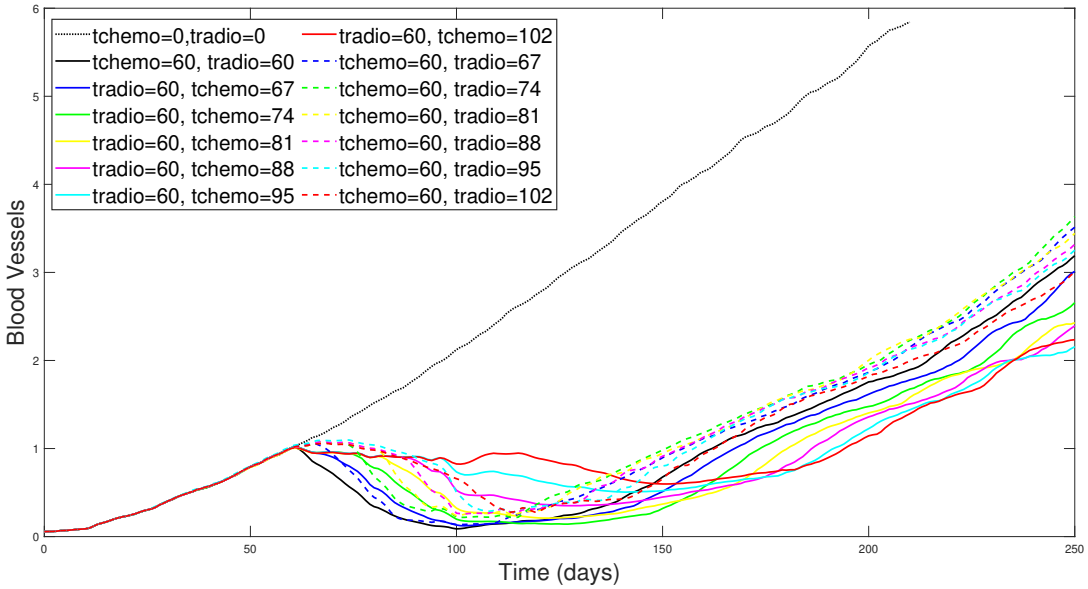

Figure 6.7: *Evolution of the value of* $\iint_S \theta_3 \cdot (\theta_2 > 10^{-3})\, dxdy$ *for treatment free, and different schedules of concurrent chemoradiotherapy simulations are applied in the tissue.*

is applied. In other words, the total surface area occupied by blood vessels is decreasing notably when the combined therapy is applied. The evolution of vessels surface is increasing again when the effect of chemoradiotherapy is decreasing. This increment in blood vessels depends on whether chemotherapy is applied before or after radiotherapy.

In cases where chemotherapy precedes radiotherapy (dashed lines), the number of blood vessels increases at a higher rate than in cases in which chemotherapy is applied after radiotherapy (solid lines). When radiotherapy precedes chemotherapy, the rate of increased blood vessels is lower (solid lines).

The reason behind this outcome is stemming from the long-lasting effect of chemotherapy, which remains inside the human body's bloodstream for a significant time period, until the cytotoxic drug expels completely. When the application of combined chemoradiotherapy comes to an end, cancer cells are still being killed with the cytotoxic drug's assistance, which remains present in the bloodstream. As a consequence, blood vessels that are connected with tumor cells are being killed also. On the other hand, the impact of radiotherapy is not long-lasting, so it kills not only cancer cells, but also blood vessels when applied to human tissue. To sum up, in the cases where the number of blood vessels increases at a lower rate (solid lines), the probability of tumor metastasis is lower compared to the cases where the number of blood vessels increases at a higher rate (dashed lines), hence the probability of tumor metastasis becomes bigger.

Chapter 7

Conclusions and Discussion

7.1 Conclusions

The present master of science thesis deals with the computational study of combination therapies in growing tumors: the combination of chemotherapy and radiotherapy. Research that tackles cancer is a scientific field with plenty of prospects because it investigates problem solving with global interest. Exploiting computational simulations, accompanied with mathematical models, is an efficient and helpful way to accelerate research in this global scourge. Through these methods, useful information can be understood for the progression of the disease and, most importantly, the treatment of this disease through various therapeutic techniques.

Thus, the present master of science thesis attempted the study of various cancer treatments, for example, radiotherapy, chemotherapy, as well as combined chemoradiotherapy. In this regard, combined chemoradiotherapy is applied concurrently, or at different time instances, under the scope to ascertain how effective each therapeutic way is by placing the spotlight on the pros and cons of each treatment.

The 2D continuum mathematical model we applied is an extension of previous modeling attempts [22]. The model was elaborated in the environment of COMSOL Multiphysics ® and was attempted to be combined with various cancer treatments with the goal to observe how cancer cells grow when different treatments are being applied. COMSOL Multiphysics ® is an extensively used software package. In COMSOL, someone can edit the results in the same environment that calculations are made, so the pre-process and post-process are embedded in the same software.

Firstly, radiotherapy was incorporated in the aforementioned mathematical model with the Linear-Quadratic formula for radiotherapy [72]. The LQ model is the oldest model of the application of radiotherapy and, in essence, quantifies the survival fraction of remaining cancer cells after the application of radiotherapy on cancer cells. All this rationality, as mentioned above, was integrated with success in COMSOL, which assured the quick solving of the systems of the mathematical model in a relatively short computational time. In other words, it was proved that the studied mathematical model with the radiotherapy term, which was incorporated in the model's equations, can be used to predict the percentage of surviving cancer cells and, therefore, the percentage of killed cancer cells after the application of specified strength of irradiation which can be applied on the tissue in fractions.

Secondly, in the already existing mathematical model with integrated radiotherapy, cytotoxic therapy was incorporated in order to come up with the mathematical model of combined chemoradiotherapy. The cytotoxic therapy was added to our model based on Lampropoulos et al. [23]. So by having a complete mathematical model, including radiotherapy and chemotherapy, computational simulations were made to determine if truly the combined treatment, in our case chemoradiotherapy, provides better results, i.e., more cancer cells are being killed. Indeed, the results show that when combined chemoradiotherapy is applied, the number of surviving cancer cells that remain in the tissue is smaller than when only radiotherapy, or only chemotherapy, or no therapy is applied.

Moreover, combined chemoradiotherapy has the best results compared with the three other cases in the number of blood vessels remaining in the tissue. With combined chemoradiotherapy, the number of remaining blood vessels is the smallest, so the possibility for tumor metastasis is the smallest too. It is interesting to study the number of blood vessels because when it is increasing, the chance for tumor metastasis is more considerable than if the number of blood vessels is restricted, so the chance for cancer cells to metastasize is smaller.

Finally, as radiotherapy and chemotherapy have been incorporated into the pre-existing mathematical model, and it has been observed that combined chemoradiotherapy yields the best results for cancer treatment, some combined therapeutic cases were studied. The aforementioned combined chemoradiotherapy is applied concurrently, d=for example chemotherapy and radiotherapy start on the same day ($t_{radio} = 60$, $t_{chemo} = 60$). In the twelve therapeutic cases studied, chemotherapy and radiotherapy were applied on different time instances. For example, radiotherapy starts first, and after one-week chemotherapy starts too ($t_{radio} = 60$, $t_{chemo} = 67$) or vice versa ($t_{chemo} = 60$, $t_{radio} = 67$). So after applying chemotherapy and radiotherapy at different time instances, twelve therapeutic cases were raised. Each therapeutic case has its pros and cons that explained in more detail in the relevant chapter 6.

Shortly, it is worth mentioning that the therapeutic case in which chemotherapy and radiotherapy were applied concurrently, i.e., $t_{radio} = 60$, $t_{chemo} = 60$, had the highest percentage of treatment efficacy 96% right after the last treatment administration (zero months). The therapeutic efficacy levels, up to 80%, persisted two months after the last therapy application. Although the high levels of therapeutic efficacy after six months had decreased by 44%, so the therapeutic efficacy was 52%. Hence, this decrease in therapeutic efficacy was observed to be quite bigger than other therapeutic cases. For the therapeutic case where radiotherapy was applied first and after six weeks chemotherapy was applied, i.e., $t_{radio} = 60$, $t_{chemo} = 102$, the percentage of treatment efficacy was 79% right after the last treatment administration. This percentage is not so high compared with the previous case, but after six months, it decreased only by 20%, so the therapeutic efficacy was 56%.

Another case that worths to be mentioned is the therapeutic case in which chemotherapy is applied first, and after six weeks, radiotherapy starts it application too, i.e., $t_{chemo} = 60$, $t_{radio} = 102$. In this case, the percentage of treatment efficacy was 95% right after the last treatment administration. This percentage is as high as the case of concurrent chemoradiotherapy and, after six months, it decreased by 50%, so the therapeutic efficacy was 45%. Indeed, the concurrent chemoradiotherapy, i.e., $t_{radio} = 60$, $t_{chemo} = 60$, was the therapeutic method that was applied in established

cancer protocols [1] so we wanted and eventually had the most considerable therapeutic efficacy. The other two therapeutic cases, i.e., $t_{radio} = 60$, $t_{chemo} = 102$ and $t_{chemo} = 60$, $t_{radio} = 102$, also had high percentages of therapeutic efficacy which did not differ a lot compared with the concurrent chemoradiotherapy. Indeed, applying different therapeutic cases and having reasonable differences is a good sign because the model responded to our expectations. More modifications are imperative for our simulations to be more accurate and respond better to a real tissue with a growing tumor.

Last but not least, the number of blood vessels was examined for all studied therapeutic cases. In cases where chemotherapy precedes radiotherapy, the number of blood vessels increased at a higher rate, so the probability for tumor metastasis was also higher. On the other hand, in cases where radiotherapy preceded chemotherapy, the number of blood vessels increased at a lower rate, so the probability for tumor metastasis was smaller too.

7.2 Recommendations for Future Research

Some recommendations for future research could be the following. The application of radiotherapy, which in our case is external beam radiation, is the most widely used type of radiation therapy. Other types of radiation therapy could also be used, for example, internal radiation therapy, in which radiation sources are put into or near the area that needs treatment. Moreover, another type of radiation therapy which is interesting to be applied is radiopharmaceuticals, which are drugs that contain radioactive materials called radioisotopes. They can either be put in a vein, taken by mouth, or placed in a body cavity.

Additionally, concerning radiation therapy, in our model, the radiotherapy is applied in fractions; in essence, every fraction is applied once a day, and each fraction includes the same amount of irradiation. A different way radiotherapy can be applied is by hyperfractionated radiation, which divides the daily dose into two treatment sessions without changing the length of the treatment. In this case, the treatment is twice a day. Accelerated radiation is another way that could be applied as an alternative way of radiotherapy, which gives the total dose of radiation in a shorter frequency, i.e., providing more frequent doses (more than once a day) to get the same total dose of radiation. In the end, hypofractionated radiation breaks radiation into fewer doses so that each dose is larger. Sometimes, this could mean that it is provided less often than once a day, which is another method that radiotherapy could be applied.

In addition, a combination of types of radiation therapy could be applied to a therapeutic case. For example, a combination of external with internal radiation. Combining internal and external radiotherapy is a novel promising approach in radiation oncology [92]. A combination of external beam radiation with radiopharmaceuticals is another therapeutic model for the combined treatment [93].

Moreover, adding the impact of radiotherapy to the equation of the healthy cells in the mathematical model will simulate reality better, so the results could be even more robust. Ultimately, we combined radiotherapy with cytotoxic therapy based on a cancer protocol that combines radiotherapy with taxane, as a cytotoxic drug [1]. The combination of radiotherapy with novel targeted

anticancer agents enables patients to receive more targeted doses of radiation on the tumor, with sparing of adjacent normal tissues [94].

Finally, combining radiotherapy with more innovative therapies is recommended for future research, such as hormone therapy and immunotherapy, something that lies beyond the scope of this thesis and is left for future consideration and research. [95].

Bibliography

[1] B.Cancer, "Bc cancer protocol summary for treatment of locally advanced non-small ..." Sep 2015. [Online]. Available: http://www.bccancer.bc.ca/chemotherapy-protocols-site/Documents/Lung/LULACATRT_Protocol.pdf

[2] Z. Liu and C. Yang, "A mathematical model of cancer treatment by radiotherapy," *Computational and mathematical methods in medicine*, vol. 2014, 2014.

[3] H. Schättler and U. Ledzewicz, "Optimal control for mathematical models of cancer therapies," *An application of geometric methods*, 2015.

[4] A. Cancer Society, "Radiation therapy: Radiation treatment for cancer," Dec 2019. [Online]. Available: https://www.cancer.org/treatment/treatments-and-side-effects/treatment-types/radiation.html

[5] V. Cristini and J. Lowengrub, *Multiscale Modeling of Cancer: An Integrated Experimental and Mathematical Modeling Approach*. Cambridge University Press, 2010. [Online]. Available: https://books.google.gr/books?id=sBI1nwEACAAJ

[6] B. Alberts, D. Bray, K. Hopkin, A. Johnson, J. Lewis, M. Raff, K. Roberts, and P. Walter, *Essential Cell Biology*. CRC Press, 2015. [Online]. Available: https://books.google.gr/books?id=Cg4WAgAAQBAJ

[7] G. Dunn, L. Old, and R. Schreiber, "The three es of cancer immunoediting," *Annual review of immunology*, vol. 22, pp. 329–360, 2004.

[8] D. Hanahan and R. Weinberg, "Hallmarks of cancer: The next generation," *Cell*, vol. 144, no. 5, pp. 646–674, 2011. [Online]. Available: https://www.sciencedirect.com/science/article/pii/S0092867411001279

[9] A. R. A. Anderson and M. A. J. Chaplain, "Continuous and discrete mathematical models of tumor-induced angiogenesis - bulletin of mathematical biology." [Online]. Available: https://link.springer.com/article/10.1006/bulm.1998.0042#citeas

[10] M. Marušić, Bajzer, J. P. Freyer, and S. Vuk-Pavlović, "Analysis of growth of multicellular tumour spheroids by mathematical models," *Cell Proliferation*, vol. 27, no. 2, pp. 73–94, 1994. [Online]. Available: https://onlinelibrary.wiley.com/doi/abs/10.1111/j.1365-2184.1994.tb01407.x

[11] S. Chandrasekaran and M. R. King, "Gather round: In vitro tumor spheroids as improved models of in vivo tumors," *Journal of Bioengineering and Biomedical Science*, vol. 2012, 2012.

[12] J. Folkman and M. Klagsbrun, "Angiogenic factors," *Science*, vol. 235, no. 4787, pp. 442–447, 1987. [Online]. Available: https://www.science.org/doi/abs/10.1126/science.2432664

[13] S. Davis and G. D. Yancopoulos, *The Angiopoietins: Yin and Yang in Angiogenesis*. Berlin, Heidelberg: Springer Berlin Heidelberg, 1999, pp. 173–185. [Online]. Available: https://doi.org/10.1007/978-3-642-59953-8_9

[14] R. Padmanabhan, N. Meskin, and A.-E. Al Moustafa, *Mathematical Models of Cancer and Different Therapies*, 11 2020.

[15] L. Preziosi, *Cancer modelling and simulation*. CRC Press, 2003.

[16] V. Cristini and J. Lowengrub, *Multiscale Modeling of Cancer: An Integrated Experimental and Mathematical Modeling Approach*, 01 2010.

[17] P. Carmeliet and R. Jain, "Angiogenesis in cancer and other diseases," *Nature*, vol. 407, no. 6801, p. 249—257, September 2000. [Online]. Available: https://doi.org/10.1038/35025220

[18] J. P. WARD and J. R. KING, "Mathematical modelling of avascular-tumour growth II: Modelling growth saturation," *Mathematical Medicine and Biology: A Journal of the IMA*, vol. 16, no. 2, pp. 171–211, 06 1999. [Online]. Available: https://doi.org/10.1093/imammb/16.2.171

[19] C. J. W. Breward, H. M. Byrne, and C. E. Lewis, "The role of cell-cell interactions in a two-phase model for avascular tumour growth," *Journal of Mathematical Biology*, vol. 45, pp. 125–152, 2002.

[20] C. Breward, H. Byrne, and C. Lewis, "A multiphase model describing vascular tumour growth," *Bull. Math. Biol.*, vol. 65, pp. 609–640, 08 2003.

[21] H. Byrne, J. King, S. Mcelwain, and L. Preziosi, "A two-phase model of solid tumour growth," *Applied Mathematics Letters*, vol. 16, pp. 567–573, 05 2003.

[22] M. Hubbard and H. Byrne, "Multiphase modelling of vascular tumour growth in two spatial dimensions," *Journal of theoretical biology*, vol. 316, pp. 70–89, 2013.

[23] I. Lampropoulos, M. Charoupa, and M. Kavousanakis, "Intra-tumor heterogeneity and its impact on cytotoxic therapy in a two-dimensional vascular tumor growth model," *Chemical Engineering Science*, vol. 259, p. 117792, 2022. [Online]. Available: https://www.sciencedirect.com/science/article/pii/S0009250922003761

[24] A. R. A. Anderson, "A hybrid mathematical model of solid tumour invasion: the importance of cell adhesion," *Mathematical Medicine and Biology: A Journal of the IMA*, vol. 22, no. 2, pp. 163–186, 06 2005. [Online]. Available: https://doi.org/10.1093/imammb/dqi005

[25] A. R. A. Anderson, M. A. J. Chaplain, E. L. Newman, R. J. C. Steele, and A. M. Thompson, "Mathematical modelling of tumour invasion and metastasis," *Journal of Theoretical Medicine*, vol. 2, no. 2, pp. 129–154, 2000. [Online]. Available: https://www.tandfonline.com/doi/abs/10.1080/10273660008833042

[26] D. Mallet and L. De Pillis, "A cellular automata model of tumor–immune system interactions," *Journal of Theoretical Biology*, vol. 239, no. 3, pp. 334–350, 2006. [Online]. Available: https://www.sciencedirect.com/science/article/pii/S0022519305003334

[27] M. E. Kavousanakis, P. Liu, A. G. Boudouvis, J. Lowengrub, and I. G. Kevrekidis, "Efficient coarse simulation of a growing avascular tumor," *Phys. Rev. E*, vol. 85, p. 031912, Mar 2012. [Online]. Available: https://link.aps.org/doi/10.1103/PhysRevE.85.031912

[28] E. L. Bearer, J. S. Lowengrub, H. B. Frieboes, Y.-L. Chuang, F. Jin, S. M. Wise, M. Ferrari, D. B. Agus, and V. Cristini, "Multiparameter Computational Modeling of Tumor Invasion," *Cancer Research*, vol. 69, no. 10, pp. 4493–4501, 05 2009. [Online]. Available: https://doi.org/10.1158/0008-5472.CAN-08-3834

[29] H. B. Frieboes, F. Jin, Y.-L. Chuang, S. M. Wise, J. S. Lowengrub, and V. Cristini, "Three-dimensional multispecies nonlinear tumor growth—ii: Tumor invasion and angiogenesis," *Journal of Theoretical Biology*, vol. 264, no. 4, pp. 1254–1278, 2010. [Online]. Available: https://www.sciencedirect.com/science/article/pii/S0022519310001116

[30] Y. Kim, M. Stolarska, and H. Othmer, "A hybrid model for tumor spheroid growth in vitro i: theoretical development and early results," *Math. Models Methods Appl. Sci.*, vol. 17, pp. 1773–1798, 11 2007.

[31] C. MULTIPHYSICS, "Comsolnbsp;multiphysics® software - understand, predict, and optimize." [Online]. Available: https://www.comsol.com/comsol-multiphysics

[32] W. Hong and G. Zhang, "Simulation analysis for tumor radiotherapy based on three-component mathematical models," *Journal of Applied Clinical Medical Physics*, vol. 20, no. 3, p. 22–26, 2019.

[33] H. McAneney and S. F. C. O'Rourke, "Investigation of various growth mechanisms of solid tumour growth within the linear-quadratic model for radiotherapy," *Physics in Medicine & Biology*, vol. 52, pp. 1039 – 1054, 2007.

[34] R. Syljuåsen, *Cell Cycle Effects in Radiation Oncology*, 10 2019, pp. 1–8.

[35] B. Wouters, "Cell death after irradiation: how, when and why cells die in: Basic clinical radiobiology (eds. joiner m. & van der kogel a.) 27–40," 2009.

[36] H. B. Forrester, C. A. Vidair, N. Albright, C. C. Ling, and W. C. Dewey, "Using computerized video time lapse for quantifying cell death of x-irradiated rat embryo cells transfected with c-myc or c-ha-ras," *Cancer research*, vol. 59, no. 4, pp. 931–939, 1999.

[37] G. Iliakis, Y. Wang, J. Guan, and H. Wang, "Dna damage checkpoint control in cells exposed to ionizing radiation," *Oncogene*, vol. 22, no. 37, pp. 5834–5847, 2003.

[38] A. Di Leonardo, S. P. Linke, K. Clarkin, and G. M. Wahl, "Dna damage triggers a prolonged p53-dependent g1 arrest and long-term induction of cip1 in normal human fibroblasts." *Genes & development*, vol. 8, no. 21, pp. 2540–2551, 1994.

[39] C. S. Sørensen, R. G. Syljuåsen, J. Falck, T. Schroeder, L. Rönnstrand, K. K. Khanna, B.-B. Zhou, J. Bartek, and J. Lukas, "Chk1 regulates the s phase checkpoint by coupling the physiological turnover and ionizing radiation-induced accelerated proteolysis of cdc25a," *Cancer cell*, vol. 3, no. 3, pp. 247–258, 2003.

[40] H. Beck, V. Nähse-Kumpf, M. S. Y. Larsen, K. A. O'Hanlon, S. Patzke, C. Holmberg, J. Mejlvang, A. Groth, O. Nielsen, R. G. Syljuåsen *et al.*, "Cyclin-dependent kinase suppression by wee1 kinase protects the genome through control of replication initiation and nucleotide consumption," *Molecular and cellular biology*, vol. 32, no. 20, pp. 4226–4236, 2012.

[41] Y. Sanchez, C. Wong, R. S. Thoma, R. Richman, Z. Wu, H. Piwnica-Worms, and S. J. Elledge, "Conservation of the chk1 checkpoint pathway in mammals: linkage of dna damage to cdk regulation through cdc25," *Science*, vol. 277, no. 5331, pp. 1497–1501, 1997.

[42] Q. Liu, S. Guntuku, X.-S. Cui, S. Matsuoka, D. Cortez, K. Tamai, G. Luo, S. Carattini-Rivera, F. DeMayo, A. Bradley *et al.*, "Chk1 is an essential kinase that is regulated by atr and required for the g2/m dna damage checkpoint," *Genes & development*, vol. 14, no. 12, pp. 1448–1459, 2000.

[43] H. Zhao and H. Piwnica-Worms, "Atr-mediated checkpoint pathways regulate phosphorylation and activation of human chk1," *Molecular and cellular biology*, vol. 21, no. 13, pp. 4129–4139, 2001.

[44] N. Cancer Institute, "External beam radiation therapy for cancer," May 2018. [Online]. Available: https://www.cancer.gov/about-cancer/treatment/types/radiation-therapy/external-beam

[45] C. Institute, "Brachytherapy for cancer," Feb 2019. [Online]. Available: https://www.cancer.gov/about-cancer/treatment/types/radiation-therapy/brachytherapy

[46] S. Levitt, J. Purdy, C. Perez, and S. Vijayakumar, *Technical Basis of Radiation Therapy: Practical Clinical Applications*, ser. Medical radiology : Diagnostic imaging and radiation oncology. Springer, 2006. [Online]. Available: https://books.google.gr/books?id=Fp5rAAAAMAAJ

[47] Y. Smith, "Radiation therapy dosage," Mar 2021. [Online]. Available: https://www.news-medical.net/health/Radiation-Therapy-Dosage.aspx

[48] C. Research UK, "What is chemotherapy?" Jun 2020. [Online]. Available: https://www.cancerresearchuk.org/about-cancer/treatment/chemotherapy/what-chemotherapy-is

[49] M. M. Moschovi, E. Critselis, O. Cen, M. Adamaki, G. I. Lambrou, G. P. Chrousos, and S. A. Vlahopoulos, "Drugs acting on homeostasis: challenging cancer cell adaptation," *Expert Review of Anticancer Therapy*, vol. 15, pp. 1405 – 1417, 2015.

[50] C. Research UK, "Docetaxel (taxotere)," Aug 2019. [Online]. Available: https://about-cancer.cancerresearchuk.org/about-cancer/treatment/drugs/docetaxel

[51] K. Gelmon, "The taxoids: paclitaxel and docetaxel." *The Lancet*, vol. 344, no. 8932, pp. 1267–1272, 1994.

[52] E. B. Golden, S. C. Formenti, and P. B. Schiff, "Taxanes as radiosensitizers," *Anti-cancer drugs*, vol. 25, no. 5, pp. 502–511, 2014.

[53] M. C. Wani, H. L. Taylor, M. E. Wall, P. Coggon, and A. T. McPhail, "Plant antitumor agents. vi. isolation and structure of taxol, a novel antileukemic and antitumor agent from taxus brevifolia," *Journal of the American Chemical Society*, vol. 93, no. 9, pp. 2325–2327, 1971, pMID: 5553076. [Online]. Available: https://doi.org/10.1021/ja00738a045

[54] R. B. Tishler, P. B. Schiff, C. R. Geard, and E. J. Hall, "Taxol: A novel radiation sensitizer," *International Journal of Radiation Oncology*Biology*Physics*, vol. 22, no. 3, pp. 613–617, 1992, international Conference on Chemical Modifiers of Cancer Treatment. [Online]. Available: https://www.sciencedirect.com/science/article/pii/036030169290888O

[55] E. Rowinsky, L. Cazenave, and R. Donehower, "Taxol: A novel investigational antimicrotubule agent," *Journal of the National Cancer Institute*, vol. 82, no. 15, pp. 1247–1259, Aug. 1990, funding Information: Received March 5, 1990; revised May 8, 1990; accepted May 9, 1990. E. K. Rowinsky is the recipient of an American Cancer Society Career Development Award. E. K. Rowinsky, R. C. Donehower, Division of Pharmacology and Experimental Therapeutics, The Johns Hopkins Oncology Center, Baltimore, Md. L. A. Cazenave, Investigational Drug Branch, Cancer Therapy and Evaluation Program, Division of Cancer Treatment, National Cancer Institute, Bethesda, Md. Correspondence to: Eric K. Rowinsky, M.D., Division of Pharmacology and Experimental Therapeutics, The Johns Hopkins Oncology Center, 600 N. Wolfe St., Baltimore, MD 21205.

[56] F. Gueritte-Voegelein, D. Guenard, F. Lavelle, M. T. Le Goff, L. Mangatal, and P. Potier, "Relationships between the structure of taxol analogs and their antimitotic activity," *Journal of Medicinal Chemistry*, vol. 34, no. 3, pp. 992–998, 1991. [Online]. Available: https://doi.org/10.1021/jm00107a017

[57] M.-C. Bissery, D. Guénard, F. Guéritte-Voegelein, and F. Lavelle, "Experimental Antitumor Activity of Taxotere (RP 56976, NSC 628503), a Taxol Analogue1," *Cancer Research*, vol. 51, no. 18, pp. 4845–4852, 09 1991.

[58] M. Koukourakis, C. Kourousis, M. Kamilaki, S. Koukouraki, A. Giatromanolaki, S. Kakolyris, A. Kotsakis, N. Androulakis, N. Bahlitzanakis, and V. Georgoulias, "Weekly docetaxel and concomitant boost radiotherapy for non-small cell lung cancer. a phase i/ii dose escalation trial," *European Journal of Cancer*, vol. 34, no. 6, pp. 838–844, 1998. [Online]. Available: https://www.sciencedirect.com/science/article/pii/S0959804997101010

[59] P. Lara-Gonzalez, F. Westhorpe, and S. Taylor, "The spindle assembly checkpoint," *Current Biology*, vol. 22, no. 22, pp. R966–R980, 2012. [Online]. Available: https://www.sciencedirect.com/science/article/pii/S096098221201189X

[60] B. A. Weaver, "How taxol/paclitaxel kills cancer cells," *Molecular Biology of the Cell*, vol. 25, no. 18, pp. 2677–2681, 2014, pMID: 25213191. [Online]. Available: https://doi.org/10.1091/mbc.e14-04-0916

[61] R. B. Mokhtari, T. S. Homayouni, N. Baluch, E. Morgatskaya, S. Kumar, B. Das, and H. Yeger, "Combination therapy in combating cancer," *Oncotarget*, vol. 8, no. 23, pp. 38 022–38 043, 2017. [Online]. Available: https://www.oncotarget.com/article/16723/

[62] C. Research UK, "Chemoradiotherapy treatment," Nov 2019. [Online]. Available: https://www.cancerresearchuk.org/about-cancer/lung-cancer/treatment/chemoradiotherapy/having-chemoradiotherapy

[63] L. Milas, M. Milas, and K. Mason, "Combination of taxanes with radiation: preclinical studies." in *Seminars in radiation oncology*, vol. 9, no. 2 Suppl 1, 1999, pp. 12–26.

[64] J. R. Bellon, K. L. Lindsley, G. K. Ellis, J. R. Gralow, R. B. Livingston, and M. M. Austin Seymour, "Concurrent radiation therapy and paclitaxel or docetaxel chemotherapy in high-risk breast cancer," *International Journal of Radiation Oncology*Biology*Physics*, vol. 48, no. 2, pp. 393–397, 2000. [Online]. Available: https://www.sciencedirect.com/science/article/pii/S0360301600006362

[65] H. Choy, "Taxanes in combined modality therapy for solid tumors," *Critical Reviews in Oncology/Hematology*, vol. 37, no. 3, pp. 237–247, 2001. [Online]. Available: https://www.sciencedirect.com/science/article/pii/S1040842800001128

[66] E. S. Kim and F. R. Khuri, "Docetaxel and radiation as combined-modality therapy," *Oncology (Williston Park, N.Y.)*, vol. 16, no. 6 Suppl 6, p. 97—105, June 2002. [Online]. Available: http://europepmc.org/abstract/MED/12108904

[67] H. Onishi, K. Kuriyama, M. Yamaguchi, T. Komiyama, S. Tanaka, T. Araki, K. Nishikawa, and H. Ishihara, "Concurrent two-dimensional radiotherapy and weekly docetaxel in the treatment of stage iii non-small cell lung cancer: a good local response but no good survival due to radiation pneumonitis," *Lung Cancer*, vol. 40, no. 1, pp. 79–84, 2003. [Online]. Available: https://www.sciencedirect.com/science/article/pii/S0169500202005329

[68] B. Cancer, "Bc cancer protocol summary for neoadjuvant treatment of esophageal and ..." Jul 2012. [Online]. Available: http://www.bccancer.bc.ca/chemotherapy-protocols-site/Documents/Gastrointestinal/GIENACTRT_Protocol.pdf

[69] M. Boemo and H. Byrne, "Mathematical modelling of a hypoxia-regulated oncolytic virus delivered by tumour-associated macrophages," *Journal of Theoretical Biology*, vol. 461, 10 2018.

[70] C. Geng, H. Paganetti, and C. Grassberger, "Prediction of treatment response for combined chemo- and radiation therapy for non-small cell lung cancer patients using a bio-mathematical model," *Scientific Reports*, vol. 7, no. 1, 2017.

[71] J. Liu, D. Hormuth, J. Yang, and T. Yankeelov, "A multi-compartment model of glioma response to fractionated radiation therapy parameterized via time-resolved microscopy data," *Frontiers in oncology*, vol. 12, p. 811415, 02 2022.

[72] J. F. Fowler, "The linear-quadratic formula and progress in fractionated radiotherapy," *The British Journal of Radiology*, vol. 62, no. 740, p. 679–694, 1989.

[73] H. Enderling, M. Chaplain, and P. Hahnfeldt, "Quantitative modeling of tumor dynamics and radiotherapy," *Acta biotheoretica*, vol. 58, pp. 341–53, 12 2010.

[74] "Biomarkers of radiation in the environment," Apr 2022. [Online]. Available: https://link.springer.com/book/10.1007/978-94-024-2101-9

[75] M. Williams, J. Denekamp, and J. Fowler, "A review of ratios for experimental tumors: Implications for clinical studies of altered fractionation," *International Journal of Radiation Oncology*Biology*Physics*, vol. 11, no. 1, pp. 87–96, 1985, henry S. Kaplan Memorial Part 1. [Online]. Available: https://www.sciencedirect.com/science/article/pii/0360301685903669

[76] S. J. McMahon and K. M. Prise, "Mechanistic modelling of radiation responses," *Cancers*, vol. 11, no. 2, p. 205, 2019.

[77] G. Barendsen, "Dose fractionation, dose rate and iso-effect relationships for normal tissue responses," *International Journal of Radiation Oncology*Biology*Physics*, vol. 8, no. 11, pp. 1981–1997, 1982. [Online]. Available: https://www.sciencedirect.com/science/article/pii/036030168290459X

[78] K. Higashi, A. C. Clavo, and R. L. Wahl, "In vitro assessment of 2-fluoro-2-deoxy-d glucose, l-methionine and thymidine as agents to monitor the early response of a human adenocarcinoma cell line to radiotherapy," *Journal of Nuclear Medicine*, vol. 34, no. 5, pp. 773–779, 1993. [Online]. Available: https://jnm.snmjournals.org/content/34/5/773

[79] B. Cancer, "Bc cancer protocol summary for combined modality adjuvant therapy for ..." Dec 2007. [Online]. Available: http://www.bccancer.bc.ca/chemotherapy-protocols-site/Documents/Gastrointestinal/GIRINFRT_Protocol.pdf

[80] Cancer, "Bc cancer protocol summary for combined modality adjuvant therapy for ..." Dec 2007. [Online]. Available: http://www.bccancer.bc.ca/chemotherapy-protocols-site/Documents/Gastrointestinal/GIRCRT_Protocol.pdf

[81] C. Multiphysics. [Online]. Available: https://doc.comsol.com/5.6/doc/com.comsol.help.chem/chem_ug_chemsptrans.08.049.html

[82] COMSOL, "Choosing the right linear system solver." [Online]. Available: https://doc.comsol.com/5.5/doc/com.comsol.help.comsol/comsol_ref_solver.27.118.html

[83] [Online]. Available: https://medialab.chemeng.ntua.gr/mde_dpms_ym/

[84] H. Kenmotsu and Y. Tanigawara, "Pharmacokinetics, dynamics and toxicity of docetaxel: Why the japanese dose differs from the western dose," *Cancer Science*, vol. 106, no. 5, pp. 497–504, 2015. [Online]. Available: https://onlinelibrary.wiley.com/doi/abs/10.1111/cas.12647

[85] S. J. Clarke and L. P. Rivory, "Clinical pharmacokinetics of docetaxel," *Clinical Pharmacokinetics*, vol. 36, no. 2, p. 99–114, 1999.

[86] A. Ray, N. Larson, D. B. Pike, M. Gr'Oner, S. Naik, H. Bauer, A. Malugin, K. Greish, and H. Ghandehari, "Comparison of active and passive targeting of docetaxel for prostate cancer therapy by hpma copolymer€"rgdfk conjugates," *Molecular Pharmaceutics*, vol. 8, no. 4, pp. 1090–1099, 2011, pMID: 21599008. [Online]. Available: https://doi.org/10.1021/mp100402n

[87] PubChem, "Oxygen." [Online]. Available: https://pubchem.ncbi.nlm.nih.gov/element/Oxygen

[88] E. Norris, J. King, and H. Byrne, "Modelling the response of spatially structured tumours to chemotherapy: Drug kinetics," *Mathematical and Computer Modelling*, vol. 43, no. 7, pp. 820–837, 2006. [Online]. Available: https://www.sciencedirect.com/science/article/pii/S0895717705005029

[89] D. D. Bois and E. F. D. Bois, "A height-weight formula to estimate the surface area of man," *Proceedings of the Society for Experimental Biology and Medicine*, vol. 13, no. 4, pp. 77–78, 1916. [Online]. Available: https://doi.org/10.3181/00379727-13-45

[90] R. M. Reilly, N. A. Petry, T. M. Quinton, S. W. Schwarz, C. Brown, L. DiBenedetto, and S. Lardner, "The fundamental principles of compartmental pharmacokinetics illustrated by radiopharmaceuticals commonly used in nuclear medicine continuing education for nuclear pharmacists and nuclear medicine professionals," 2013.

[91] J. Turnidge, "Pharmacokinetics and pharmacodynamics of fluoroquinolones," *Drugs*, vol. 58, no. Suppl 2, pp. 29–36, 1999.

[92] A. Dietrich, L. Koi, K. Zöphel, W. Sihver, J. Kotzerke, M. Baumann, and M. Krause, "Improving external beam radiotherapy by combination with internal irradiation," *The British Journal of Radiology*, vol. 88, no. 1051, p. 20150042, 2015, pMID: 25782328. [Online]. Available: https://doi.org/10.1259/bjr.20150042

[93] A. Sarnelli, M. L. Belli, I. Azzali, E. Loi, S. Severi, and L. Strigari, "Alpha-emitter radiopharmaceuticals and external beam radiotherapy: A radiobiological model for the combined treatment," *Cancers*, vol. 14, no. 4, p. 1077, 2022.

[94] S. S. Ahmad, M. R. Crittenden, P. T. Tran, P. G. Kluetz, G. M. Blumenthal, H. Bulbeck, R. D. Baird, K. J. Williams, T. Illidge, S. M. Hahn *et al.*, "Clinical development of novel drug–radiotherapy combinationsclinical development of novel drug–radiotherapy combinations," *Clinical Cancer Research*, vol. 25, no. 5, pp. 1455–1461, 2019.

[95] S. Yu, Y. Wang, P. He, B. Shao, F. Liu, Z. Xiang, T. Yang, Y. Zeng, T. He, J. Ma, X. Wang, and L. Liu, "Effective combinations of immunotherapy and radiotherapy for cancer treatment," *Frontiers in Oncology*, vol. 12, 2022. [Online]. Available: https://www.frontiersin.org/articles/10.3389/fonc.2022.809304